Optical investigations on rubrene in the condensed state

Dissertation

zur

Erlangung des Doktorgrades (Dr. rer. nat.)

der

Mathematisch-Naturwissenschaftlichen Fakultät

der

Rheinischen Friedrich-Wilhelms-Universität Bonn

vorgelegt von

Olga Krylova

aus Kischinjow

Bonn, November 2012

Angefertigt mit Genehmigung der Mathematisch-Naturwissenschaftlichen Fakultät
der Rheinischen Friedrich-Wilhelms-Universität Bonn

1. Gutachter: Prof. Dr. M. Sokolowski
2. Gutachter: Prof. Dr. J. Pflaum

Tag der Promotion: 26.04.2013
Erscheinungsjahr: 2013

to my husband Relja

Contents

1 Introduction

The main objective of the present thesis was the investigation of the optical properties of rubrene.

Rubrene (Rub) received strong international interest, since a surprising high charge mobility was observed for Rub single-crystal organic field effect transistors [1]. It was up to ten times larger in comparison to the mobility of other comparable organic molecules. In addition, Rub is used as a fluorescent dopant in organic light emitting diodes [2] [3] and as a laser dye [4] due to its strong fluorescence. Although Rub has a promising potential for such device applications, the information about the optical properties of this material were only partly known [5] [6] when the project was started.

The interest for the optical properties of Rub also was motivated by a previous investigation [7]. The investigated system was ultra thin tetracene (Tc) films deposited on thin epitaxial films of aluminium oxide (AlO_x) on a $Ni_3Al(111)$ single crystal. For ultra thin films (< 2 monolayers) a luminescence quenching was observed due to a strong overlap of metal and Tc wave functions. A consequence of these experiments was that Tc on thin $AlO_x/Ni_3Al(111)$ does not permit to study the luminescence of molecules on this surface. In order to suppress the charge transfer between the photo-excited molecule and the metal substrate state, Tc was substituted by Rub. Tc and Rub are two prototype fluorescent molecules. Both molecules exhibit the same "fluorescent backbone". In comparison to Tc, Rub has four additional phenyl groups, which act like spacers and keep the "fluorescent backbone" at a larger distance to the surface, thus reducing the wave function overlap between the excited Rub molecules and the metal surface. Hence, Rub is a promising candidate for luminescence investigations of molecules on surfaces. For completeness, the optical properties of Rub in solution and of single crystals of Rub were investigated within the present project prior to the experiments on surfaces.

The present thesis includes eight chapters. After the introduction (Chapter 1), the structural properties of Rub are introduced (Chapter 2). In Chapter 3, the process of samples preparation is reported. Chapter 4 is dedicated to the experimental and theoretical study of absorption and emission properties of Tc and Rub molecules in solution. Using the results of both of these studies, the difference of optical spectra for Tc and Rub are interpreted. In Chapter 5 the properties of Rub thin and ultra thin films are discussed. The influence of the chirality of the Rub backbone on the structural properties, the interesting temperature and thickness behaviour of Rub luminescence spectra are in the centre of the discussion. In addition, the luminescence spectra of suspensions of Tc and Rub nanoaggregates in water are reported.

Fluorescence spectra of Rub single crystals show the interesting temperature dependence. A detailed analysis of the luminescence and absorption results is reported in Chapter 6, followed by a discussion of the excitation relaxation mechanisms. In particular, the temperature evolution of luminescence properties of Rub crystals has been analysed by a model fit of the experimental data, that allows describing successfully the excitation relaxation mechanism in Rub crystals. The radiative and non-radiative constants, as well as the activation energies of the different processes, which are included in the excitation relaxation mechanism, were determined. In Chapter 7, time-resolved investigations of the luminescence of Rub single crystals at different temperatures and at different excitation powers are reported.

Finally, general conclusions and findings concerning the optical properties of Rub are summarized in Chapter 8. The appendix, acknowledgments and references complete the work and provide an overview on scientific and personal inputs which lead to the resulting thesis.

2 Structural properties of Rub

Rub belongs to the class of polyacenes, which exhibit an extended π-electron system. The Rub molecule ($C_{42}H_{28}$), otherwise known as 5,6,11,12-tetraphenylnaphthacen, is an aromatic molecule consisting of a Tc backbone with four additional phenyl groups. Rub is red colored and has a molar mass of 532.42 g/mol. The melting point of Rub is reported to be 334 °C [8]. The sublimation temperature is 180 °C [9].

Rub is synthesized from 1-chlor-1,1,3-triphenyl-propine in two consecutive steps (see Fig. 2.1). The first step is a rearrangement to the allene followed by a separation of HCl. The second step is the Dien-synthesis, where Rub is synthesized from 1-chlor-1,1,3-triphenyl-propine [10].

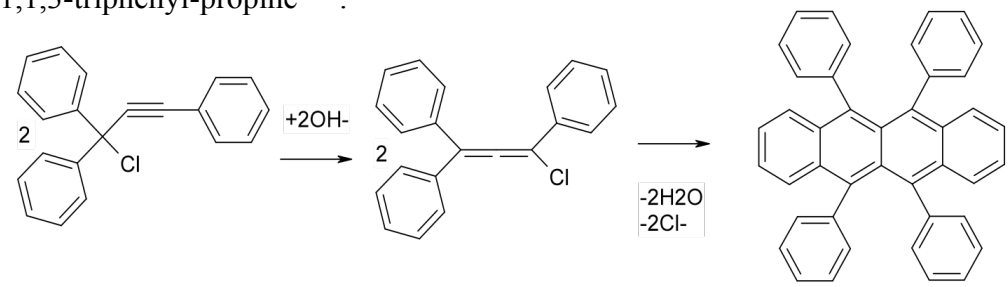

Fig. 2.1 *Representation of the synthesis reaction for Rub. Reproduced from* [10].

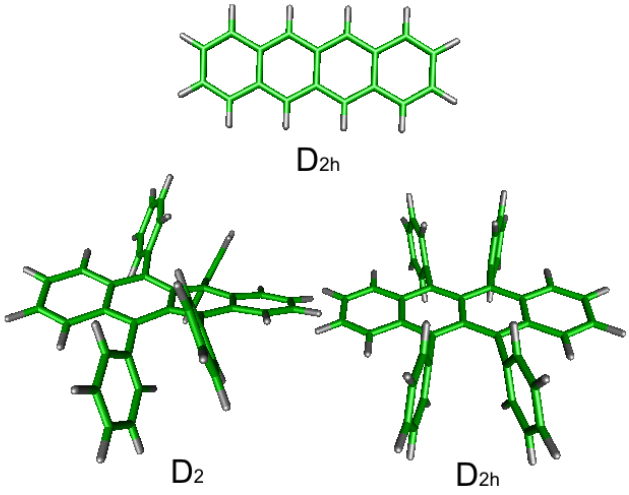

Fig. 2.2 *Geometric structures of Tc-D_{2h} ($C_{18}H_{12}$, above), Rub-D_2 (in the gas phase) and Rub-D_{2h} (in the crystalline phase). Reproduced from* [11].

The density functional theory calculation shows that two different Rub structures are possible (see Fig. 2.2). For free molecules, the twisted Tc backbone is the more stable configuration [11] [12] (Rub-D_2, see Fig. 2.2). The twisting angle is about 42° [12]. In contrast, in the crystal phase, the Tc backbone is planar [6]. In the crystal phase, the energy required

for planarization of the backbone is compensated by the lattice energy, i.e. by the more efficient packing of the planarized Rub molecules in the bulk [13]. The energy difference of both molecular conformations is 0.21eV [12]. As a result, the thermal energy at room temperature is too small to activate the required conformation change by adsorption of Rub on surfaces. This results in a nonplanar conformation of adsorbed Rub molecules [14] [15] [12] and, in consequence, in the formation of amorphous films with on dielectric surface as observed in present work (Rub on glass and Rub on AlO_x surface).

Progress in the growth of ordered Rub thin films has been achieved by employing „hot wall“ deposition [13]. The growth of the well-oriented crystalline films of Rub on silicon dioxide (SiO_2) and gold (Au(111)) substrates by using „hot wall“ deposition has been reported [13]. Conformational changes of Rub molecules involving a loss of chirality upon crystallization become possible at a large vapour pressure and a high temperature.

As observed by scanning tunnelling microscopy, Rub molecules adsorbed on copper surfaces (Cu (100)) have a nonplanar conformation as well, but may self-assemble into one or two highly ordered structures where individual molecules are aligned along the high symmetry directions of the substrate [14].

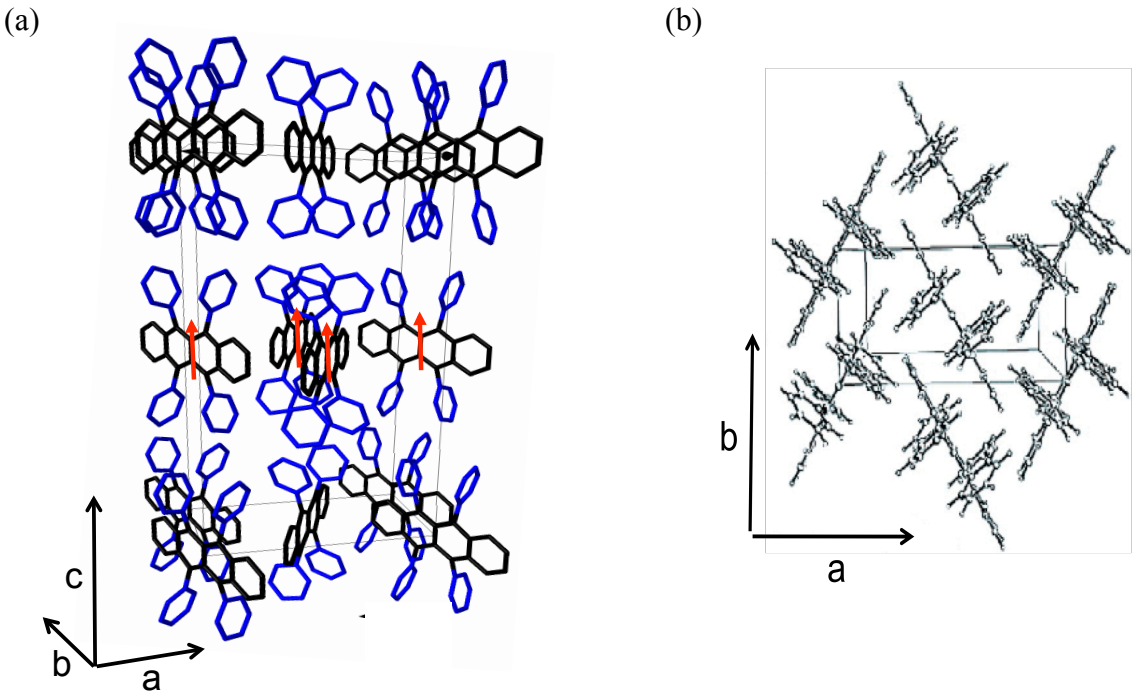

Fig. 2.3 *(a) Crystallographic structure of a Rub crystal, red arrows show the orientation of transition dipol moments for the S_0-S_1 transition. Reproduced from [13] and adapted. (b) Crystallographic structure of a Rub crystal, projection onto the (ab)-plane. Reproduced from [16].*

X-ray diffraction showed that Rub crystals are orthorhombic with the axes a = 14.433 Å, b = 7.184 Å, c = 26.897 Å, V = 2789 Å^3, with 4 molecules per unit cell

(Z = 4) [6]. Rub single crystals have the form of plates with the plate plane being the (ab)-plane (see Fig. 2.3). The transition dipole moment is oriented along the short axis of the Rub molecule and within the plane of the π system for the S_0-S_1 transition [6]. In a Rub crystal, this is the c-direction, which is perpendicular to the (ab)-plane (see Fig. 2.3).

The molecular packing of the Rub crystal shows the enhanced π–π overlap along the b-direction and reduced overlap along the a-direction (see Fig. 2.3) [16]. It was observed that the maximum charge mobility ($\mu = 15$ cm²/Vs) is realized for a hole transport along the b-axis. This is qualitatively consistent with the molecular packing in the Rub crystal, for which one might expect a stronger overlap of the electronic π–orbitals along the b-axis.

3 Sample preparation

3.1 Purification

Rub and Tc were both purchased in powder form from Aldrich with ≥ 98 % purity. The Tc was purified by one and the Rub by two cycles of gradient sublimation. The method of the sublimation purification uses the vapour pressure difference between the materials to separate them. The success of a vacuum sublimation depends significantly on the temperature stability of the used raw materials, the speed of the sublimation, and the temperature gradient. Fig. 3.1 shows the schema of the sublimation apparatus. The sublimation equipment consists mainly of an evacuable sublimation tube. Inside this tube, there are seven small inner tubes, which can be removed from the sublimation tube. All tubes are made of quartz glass. The sublimation tube is 40 cm long, and has an inner diameter of 17 mm. Ohmic heating is achieved by a resistance wire. The temperature gradient is created by a filament, which is wrapped more closely on one side of the inner tube with the powder sample and more loosely on the opposite side. The temperature of the inner tube is measured by using a Chromel/Alumel thermocouple and is controlled by a thermostat. The vacuum (about 10^{-5} mbar) is created by an oil diffusion pump. The pressure is measured by an ionisation gauge. To protect the pump from gas pollution, two cold traps with nitrogen cooling were located between the sublimation tube and the pump.

The temperature of the inner tube with the Rub powder was keep up at 223 °C. After about 41 hours, all of the Rub powder (250 mg) had left the inner source tube due to sublimation. It condenses on the glass and grows into Rub crystallites in the two next attached inner tubes due to the lower local temperature of around 207 - 187 °C (see Fig. 3.2). Rub condenses in the form of amorphous deposits at a temperature around 164 °C. Impurities with higher vapour pressure condense in the impurity precipitate area (two last inner tubes on the right side of Fig. 3.2).

3.2 Growth of crystals

Single Rub crystals obtained during the vacuum sublimation have a maximum diameter of 1 mm and a typical hexagonal geometry (Fig. 3.3 (a)). As can be noted from the time scale, it is possible to observe the growth of the crystals already a few hours after the starting of the heating process of the setup at a temperature of the inner tube with the Rub

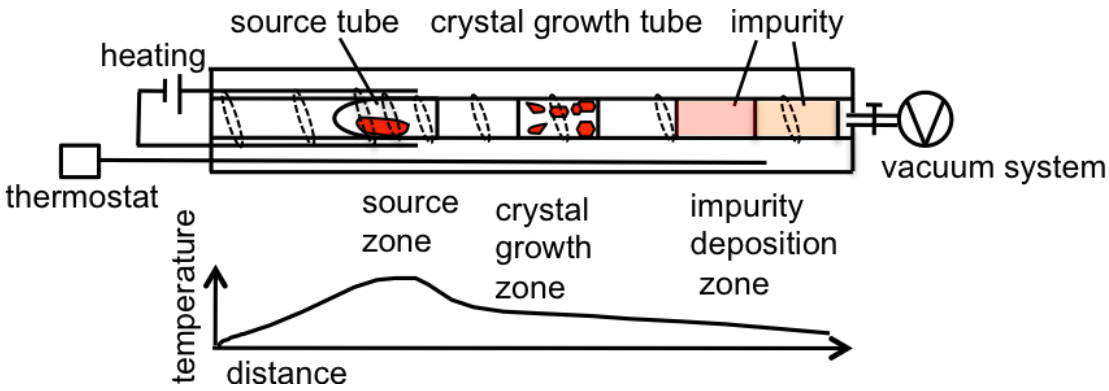

Fig. 3.1 *The upper picture represents the scheme of the sublimation apparatus. The picture below shows the typical temperature gradient profile. Reproduced from* [17] *and adapted.*

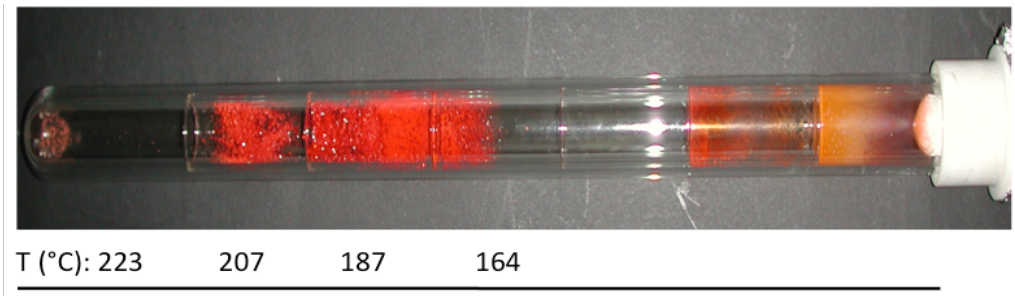

Fig. 3.2 *Photo of the sublimation tube with inner tubes after purification of Rub. The noted temperatures were measured at the centres of the inner tubes. The first inner tube (with the powder sample) was at a temperature of 223 °C. The next three tubes (between 207 °C - 164 °C) contain purified Rub. Biggest Rub crystals are observed in the third inner tube at temperatures between 197 °C - 187 °C. The last two inner tubes (on the right hand side) contain impurities (orange, yellow colours). This picture shows the result of the second cycle of the purification.*

powder at 223 °C. First, a slow growth of single crystals has been observed. Later, the greater concentration of Rub crystals in the growth area causes the coalescence of Rub crystals and therefore structural defects. From the experiment, it is possible to conclude that to obtain bigger single crystals, it is necessary to use a smaller amount of initial Rub powder or/and to stop the process, when the single crystals have reached the necessary size. The size of the crystals, which were grown in the second cycle of purification, increased comparing to that from the first cycle. The majority of the crystals were broken or had some defects or were aggregated with other crystals (see Fig. 3.3 (b)). A schematic cross section of these crystals is presented in Fig. 3.4. The crystal surface consists of layers which cause extraordinary wide terraces. The width of the terraces is not constant, although the majority of them are about 0.039 mm in size. In addition, the microscopic picture shows “furrows” extended parallel to the longer side of the crystal. The space between

the furrows is constant, about 0.01 mm. The nature of the observed terraces and furrows is not completely clear. It is interesting that the wide terraces (of more than a few mikrometers) were observed as well on the very high quality single crystals of Rub by Minato et al. [18]. Frequency modulation atomic force microscopy measurements show that a nearly perfect Rub crystal surface consists of broad terraces separated by monoatomic steps. The step edges are nearly perpendicular to the longer side of the crystal (b-axis), which is in agreement with the direction of stacking of the Rub molecules. This suggests, that the crystal growth takes place preferentially along the direction of the b-axis [18].

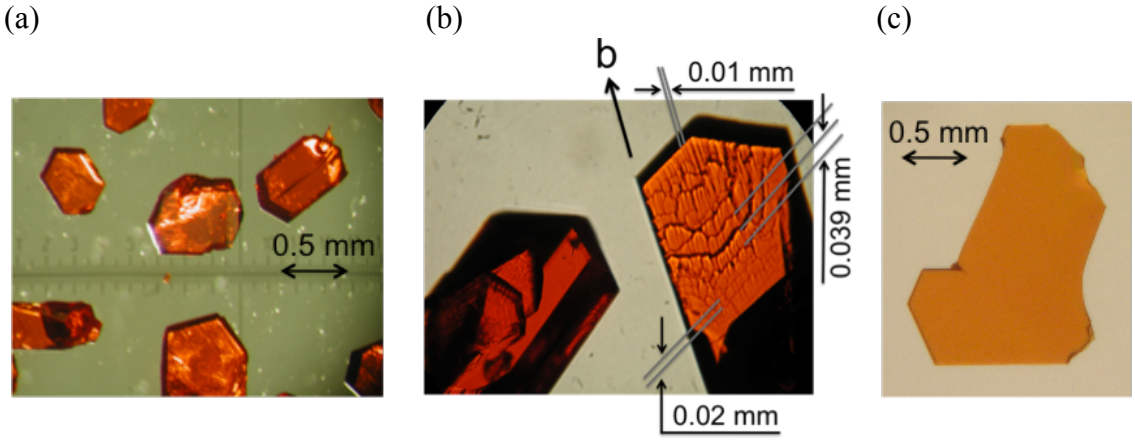

Fig. 3.3 *(a) Microscopic image of single crystals of Rub with their typical hexagonal shape. Present crystals have been grown in the second cycle of vacuum sublimation. The picture is taken by a stereoscopic binocular microscope (MBS-10). (b) The image of typical single crystals of Rub under polarized light. The picture taken by a polarizing microscope shows the differences in colours appear due to the optical anisotropy of the crystals. The majority of the crystals have some defects. (c) Image of typical single crystals grown in the group of Prof. Dr. J. Pflaum by sublimation under streaming hydrogen. This is a high quality crystal that does not show visible defects.*

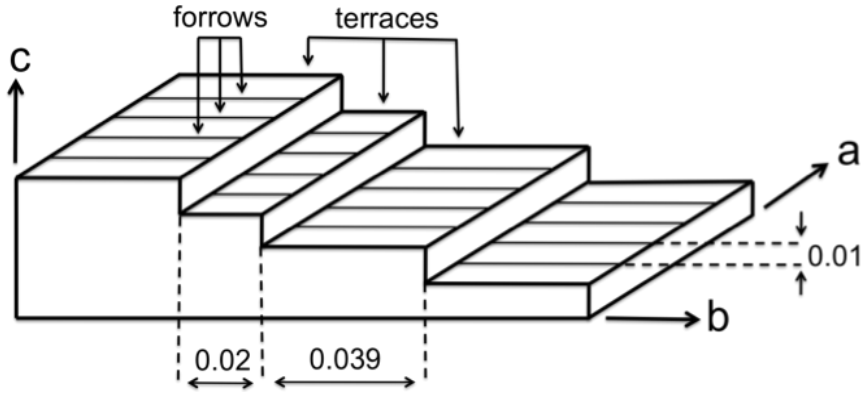

Fig. 3.4 *Schematic cross section of the crystal presented on Fig. 3.3 (b). The crystal surface consists of layers which cause wide terraces. The width of observed terraces is not constant (e.g. 0.039 mm, 0.02 mm). The microscopic image shows the "furrows" extended parallel to the b-axis. The space between the furrows is roughly constant (0.01 mm).*

In general, the growth of high quality single crystals and the control of their size and shape are crucial issues for the study of fundamental physical properties of materials [19]. The quality of the crystals is very important, because defects of crystals change dramatically their electrical and optical properties. In addition, optical characterisation requires thin samples of high quality (i.e., low defect density) for transmission measurements in order to avoid saturation of the signal. Many reliable methods have been proposed for the growth of single crystals of organic materials. For example, conditions for growing vapour-phase crystals of organic materials can be found in the work of Laudise et al. [17]. An alternative to vapour-phase methods is the growth of organic crystals in a solution [20].

It was found that the quality of the crystals, grown under vacuum sublimation, was not good enough for the absorption investigations. It was not possible to obtain satisfactory absorption spectra of the single crystals, since the vibronic bands were not resolved. But, the obtained crystals have been satisfactory used in the photoluminescence investigations. In collaboration with Prof. Dr. J. Pflaum and coworkers from the University of Stuttgart it was possible to obtain high quality single Rub crystals, which were grown by sublimation under streaming hydrogen. Most of those crystals do not show visible defects (see Fig. 3.3 (c)). They are bigger and much thinner comparing to the crystals grown under vacuum sublimation by ourselves. The maximal observed size of these crystals is about 5 mm. Most of them do not show hexagonal geometry, which is probably just a result of the brittleness of the very thin crystals during the transportation. These single crystals with higher quality were successfully used in optical investigations of the absorption properties.

3.3 Preparation of Rub solutions

For measurements of absorption and photoluminescence spectra of the Rub solution, Rub was dissolved in sebacat (see Fig. 3.5), a colourless liquid. The input mass (m_{Rub}) of Rub was:

m_{Rub} = 0.00280 ± 0.00002 g and it was added to sebacat with $m_{sebacat}$ =15.21570 ± 0.0000 g.

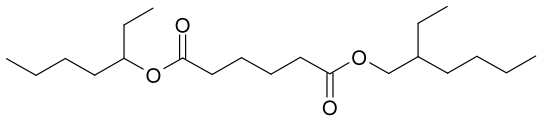

Fig. 3.5 *Chemical structure of Bis(2-ethylhexyl)-sebacat. Reproduced from* [21].

The concentration of Rub c_{Rub} was calculated from the following equation: $c_{Rub} = \frac{n_{Rub}}{V_{Rub} + V_{sebacat}}$ [mol/L], where n_{Rub} is the amount of Rub, V_{Rub} and $V_{sebacat}$ are the volumes of Rub and sebacat. $V_{sebacat}$ can be calculated from the equation:

$V_{sebacat} = \frac{m_{sebacat}}{\rho_{sebacat}}$, where $\rho_{sebacat}$ is the density of sebacat and $\rho_{sebacat}$ = 0.91 g/cm^3 [21]. Thus, the volume of sebacat is $V_{sebacat}$ = 1.672·10^{-2} L. The amount of Rub is equal to: $n_{Rub} = \frac{m_{Rub}}{M_{Rub}}$, where M_{Rub} is the molar mass of Rub and M_{Rub} = 532.42 g/mol, so $n_{Rub} = 5.26 \cdot 10^{-6}$ mol. The volume of Rub V_{Rub} is calculated from the following equation: $V_{Rub} = \frac{m}{\rho_{Rub}}$. The density is calculated from the structure data of the Rub crystal. From the knowledge of the values of the volume of the elementary cell of Rub V_{ec} = 2788.9 Å^3 and the mass of elementary cell

$m_{ec} = 4 \cdot M_{Rub} \cdot m_{atomic} = 4 \cdot 532.42$ [g/mol]·166·10^{-24} [mol] $= 3.5 \cdot 10^{-21}$ g, the density of Rub is calculated: $\rho_{Rub} = \frac{m_{ec}}{V_{ec}} = 1.268$ g/cm^3. So the V_{Rub} is 2.21·10^{-6} L. The volume of Rub is 10^4 times smaller in comparison to the volume of sebacat, so the volume of Rub can be neglected in the present calculations. The concentration of Rub is equal to

$c_{Rub} = 3.14 \cdot 10^{-4}$ mol/L.

3.4 Preparation of Rub films on glass

Thin films of Rub were obtained by depositing Rub on quartz glass substrates. A schematic diagram of the experimental setup is shown in Fig. 3.6. A turbo molecular pump was used to create the vacuum. The vacuum was about 7.3·10^{-6} mbar. The substrate was mounted onto a copper block in the vacuum chamber. The copper block was mounted in a specimen holder in such a way that the sample surface pointed in the direction of the evaporation source. A clean piece of quartz glass (the size of the glass sample was 20x20x0.7 mm^3) was attached to the sample holder. At first, the sample was introduced into the chamber in such a way that it was not positioned above the evaporation cell. Rub was inserted into a small glass crucible and this was introduced into the top part of the evaporation cell (see Fig. 3.7).

The temperature of the carbon-heating element was controlled by a current control. The temperature of the crucible holder was measured using a Ni/NiCr thermo couple contacting the evaporation cell. The shutter of the evaporation cell above the crucible was opened. As soon as the temperature and the rate of the Rub evaporation flow were constant, the sample surface was placed directly above the evaporation cell. The rate of the Rub evaporation flow was controlled by a quartz microbalance placed close to the sample. The deposition rate was 0.7 nm per minute. The Rub was then sublimated on the quartz glass up to a thickness of 150 nm at a temperature of $T_{crucible}$ = 320 °C and a heating current of approximately 3 A. The nominal layer thickness of the evaporated Rub was measured using the quartz microbalance. The reading accuracy of the used device is 0.1 nm.

Since the geometries of the sample and the quartz microbalance in the apparatus are different with respect to the evaporation cell, the quartz microbalance shows a different film thickness compared to that which is actually sublimated on the substrate. The deviation and thickness of the layer are taken into account, using the so-called tooling factor as calculated by M. Voigt and which is equal to 3 [22]. This means that the measured thickness should be multiplied by a factor of 3 in order to obtain the real value for the thickness. The accuracy of the tooling factor is about 20 % [22].

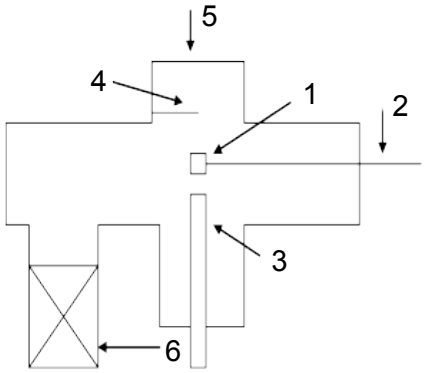

Fig. 3.6 *Schematic diagram of the evaporation apparatus: 1 – sample surface, the quartz glass substrate, 2 – specimen holder, 3 – evaporation cell, 4 – quartz microbalance, 5 - window, 6 – turbo molecular pump (not to scale).*

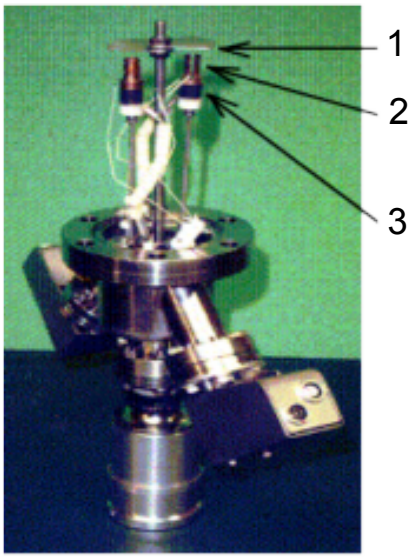

Fig. 3.7 *Photo of the evaporation cell. 1 – Shutter for to control the deposition flux on the sample (can be open and closed). 2 – Glass crucible with purified Rub inside, with thermo couple attached to the crucible for temperature control of an evaporating substance. 3 – Carbon heating element, the temperature can be controlled using a current control.*

During the investigations of the properties of the Rub films on glass, three samples were made. The first sample had a thickness of only 45 nm. It was not stable in time due to

oxidation of the sample. This instability of the sample was easy to see. The sample, which originally had a slightly pink colour, started to be nearly transparent after 20 minutes exposition to air and the absorption spectra of the sample dramatically changed after being removed from the vacuum system. Therefore two further samples were made with larger thickness (150 nm) and they had adequate stability for our spectroscopic and microscopic investigations.

3.5 Preparation of Rub thin films on $AlO_x/Ni_3Al(111)$

The preparations of the sample and following spectroscopic investigation of Rub thin films on AlO_x were made in an ultra high vacuum (UHV) chamber. A schema of the UHV chamber is shown in Fig. 3.8.

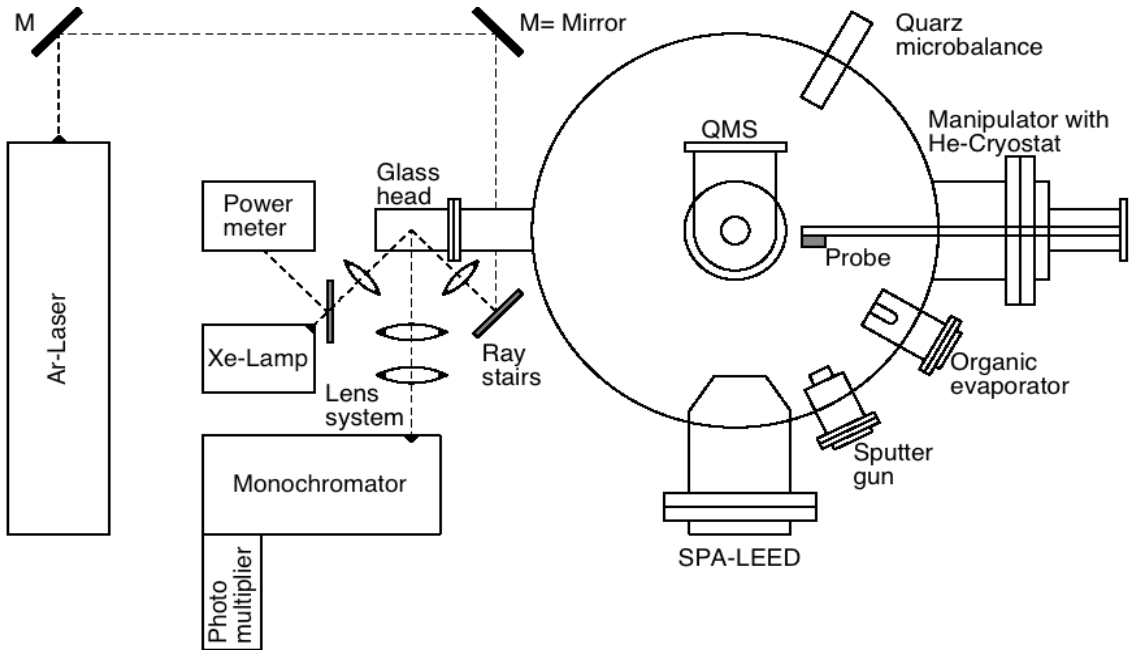

Fig. 3.8 *Schematic diagram of the UHV chamber equipped with organic evaporator (Knudsen cell); manipulator with He cryostat and the $Ni_3Al(111)$ single crystal; sputter gun; spot profile analysis low energy electron diffraction (SPA-LEED) apparatus; a quadrupole mass spectrometer (QMS); glass head - the place where the probe was located for optical measurements. On the left side of the diagram the optical part of the experiment is shown. The xenon (Xe) lamp and the power meter were used for PLE measurements (not to scale).*

UHV chamber

The vacuum in the system was usually about $7 \cdot 10^{-11}$ mbar. Five pump steps were used to achieve UHV. Two primary-pumps, the rotary pump and oil diffusion pump lower the pressure to 10^{-3} mbar. By the following turbo molecular pump a vacuum below 10^{-3} mbar was achieved. An ion pump was used to lower the pressure below 10^{-6} mbar (reaching up to 10^{-11} mbar). Finally, a titanium sublimation pump as an ultra high vacuum pump was used to lower the pressure bellow 10^{-10} mbar.

The sample, a $Ni_3Al(111)$ single crystal, is mounted on the sample manipulator (company VAB). The manipulator is equipped with micrometers, which allow very precise movements of the sample. The sample can be shifted in two horizontal (x, y) and one vertical (z) directions and rotated as well. The manipulator is equiped with a helium (He) cryostat inside. Via the cryostat, liquid He cools the sample down to 40 K. Using the heating element (Tantal filament), which is below the sample and an additional high voltage, the sample can be heated-up to maximal 1350 K. The sample temperature is measured using the thermo couple (Typ K, Chromel/Alumel). The thermostat (Typ Eurotherm 2704) provides the constant temperature within 0.01 K. The evaporation source for deposition of Rub consists of a button heating unit and an attached copper holder. In the holder is a Knudsen cell, which is a glass crucible filled with molecules which are to be deposited. The evaporation source can be drawn out of the UHV chamber and separated by a UHV valve from the chamber. By these means, it is possible to vent and to evacuate the source by a rotation pump and a turbo molecular pump without breaking the UHV of the main chamber. This avoids a ventilation of the main chamber during the exchange of the organic substances.

The preparation of a Rub film on AlO_x consisted of several steps:

1. Preparation of $Ni_3Al(111)$
   - 1.1 Sputtering – cleaning of the substrate
   - 1.2 Annealing
   - 1.3 Control of $Ni_3Al(111)$ substrate quality by means of a SPA-LEED experiment
2. Preparation of AlO_x film on $Ni_3Al(111)$
   - 2.1 Oxidation of $Ni_3Al(111)$ at 1030 K
   - 2.2 Control of AlO_x substrate quality by means of a SPA-LEED experiment
3. Rub film deposition on AlO_x

Before the above steps will be described more detailed, it is necessary to introduce the characteristics of the system AlO_x films on $Ni_3Al(111)$, which are attractive for surface experiments [23]. The oxidation process on $Ni_3Al(111)$ leads to a growth of self terminating

epitaxial films (two monolayers, 0.5 nm) of alumina [24] [25]. These films are highly ordered and commensurate to the $Ni_3Al(111)$ substrate, forming a large superstructure [26]. Finally, this insulator film is supposed to suppress an ultra fast charge transfers between the organic film and the metal substrate, which should allow measuring of PL signals for ultra thin films.

1.1 Sputtering

Even at low pressure, there are many residual gases in the chamber. The surface of the sample would be covered completely in less then one minute at 10^{-5} mbar. At UHV this process takes about one hour. The sputtering removes these contaminants from the surface by bombarding the surface with Argon ions. The sputtering removes the top few layers of the sample together with contaminants. Argon is a noble gas, so it does not adsorb on the sample. The argon gas is ionized inside the sputter gun (from company SPECS, Modell PU-IQE 11/35). Firstly, the $Ni_3Al(111)$ substrate was cleaned by Ar+ ion sputtering at 600 K at an Ar pressure of $5.5 - 6.7 \cdot 10^{-6}$ mbar for about 15 min. In the present experiment, an emission current of 10 mA and a beam voltage of 2500 eV were used.

1.2 Annealing

The sample surface is very rough from the sputtering. By sputtering, especially Al atoms are removed from the surface. In order to enrich the surface again by Al atoms and to get a smooth surface, the sample was heated at 1340 K for about 15 min. During this annealing, the surface almost melts and imperfections smooth out. Finally, the sample was heated at 1000 K for 10 to 15 min to obtain the ideal 3:1 stroichiometry at the surface.

1.3 Control of $Ni_3Al(111)$ substrate quality by means of a SPA-LEED experiment

In the next step, the quality of the prepared $Ni_3Al(111)$ surface has to be checked by spot profile analysis low energy electron diffraction (SPA-LEED). The SPA-LEED apparatus from the company Omicron was used. The electron energy (about 80 eV) determines the amount of the reciprocal space that is visible. The routine of preparation of a clean and ordered $Ni_3Al(111)$ substrate has to be repeated until the diffraction picture shows a good surface quality.

2.1 Oxidation of $Ni_3Al(111)$ at 1030 K

The preparation procedure of AlO_x on the $Ni_3Al(111)$ surface was reproduced according to the description given in Refs. [26] [23]. The epitaxial AlO_x film grows on the cleaned $Ni_3Al(111)$ substrate. The oxydized alumina film was prepared in 3 separate oxydation cycles. In each cycle the following procedure was done:

First, the sample was heated to 1030 K. The alumina films were grown by oxydation of the $Ni_3Al(111)$ substrate at an oxygen pressure of $6.2 \cdot 10^{-8}$ mbar. The amount of oxygen added to the chamber in one cycle is equal to 40 Langmuir. Under this oxygen pressure, the probe was annealed for 15 min at 1030 K. In the last step, the probe was heated for

5 min at 1070 K, in order to improve the crystalline order of the oxidized film.

At the end of the oxidation preparation cycle, the probe was cooled to room temperature (with a rate of about 2 – 3 K/s), and the pressure in the chamber decereased again to $5 \cdot 10^{-10}$ mbar, since the oxygen flow was stopped. The oxidation process was performed two more times to obtain closed and long-range ordered alumina films.

2.2 Control of AlO_x substrate quality by means of a SPA-LEED experiment

After the oxidation cycles the quality of the AlO_x film was controlled by SPA-LEED measurements.

3. Rub film deposition on AlO_x

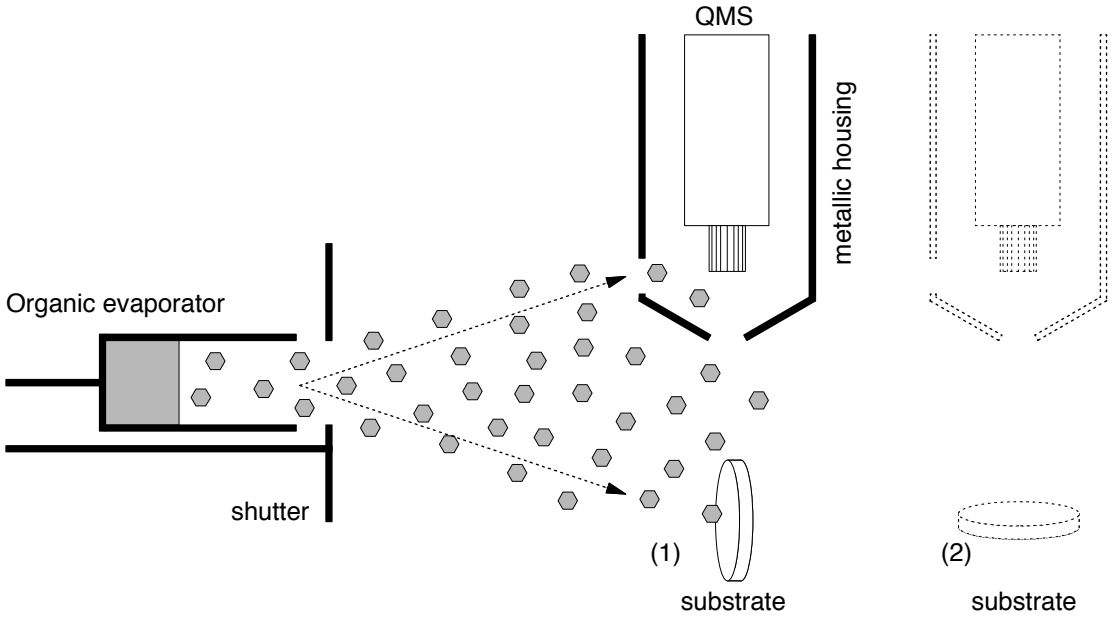

Fig. 3.9 *Schematic diagram of the experimental set-up for determination of the nominal layer thickness during film deposition by measurement of the evaporated dose (1) and determination of the film thickness by the TPD method (2).*

Rub, purified in two cycles, was inserted into a small crucible glass which was introduced into the top part of the evaporation cell. Before the Rub molecules deposition on the surface started, the Knudsen cell was heated for 10 min to a temperature between 525 K and 550 K, in order to reach constant experimental conditions. Then the shutter was opened. The Rub molecules were deposited onto the AlO_x substrate at room temperature. The nominal layer thickness of the evaporated Rub was measured using the quadrupole mass spectrometer equipped with a grid ion source. (QMS, Pfeiffer-Balzers, Modell QMG 433). During the Rub film deposition, the evaporated Rub dose was measured by the QMS (see Fig. 3.9). When the requested film thickness was reached, the shutter was closed. After optical investigations, the film thickness was calibrated using the thermal

programmed desorption (TPD) method. The details of TPD experiments are described in the literature [23] [27].

3.6 Preparation of nanoparticles

Suspensions of Tc and Rub nanoaggregates in water were made using a reprecipitation method, described in the literature [28]. Rub powder (4.5 mg) and Tc powder (2 mg) were separately mixed with tetrahydrofuran (10 mL). The mixtures were held in an ultrasonic bath until the powders were completely dissolved with a resulting concentration of $c_{Rub} = 8.45 \cdot 10^{-4}$ mol/L and $c_{Tc} = 8.76 \cdot 10^{-4}$ mol/L. 100 µL of each solution was injected into 10 mL of distilled water. The solution was covered with aluminium foil to avoid unnecessary exposure to light. Afterwards, the solution was stirred for another 15 min to ensure complete mixing. The preparations were performed at room temperature (298 K). The unnecessary exposition to air was avoided as much as possible.

In order to obtain a reference sample for absorption measurements, a mixture of tetrahydrofuran with distilled water with the same mixing ratio as in the main sample was prepared.

Two additional warm preparations (at 333 K and 353 K) for Rub were made in order to observe eventual thermodynamical effects. 500 µL of this basic solution (Rub in tetrahydrofuran) were warmed to 333 K and stir-added to 10 ml destilled water at the same temperature. The mixture was held in an ultrasonic bath for additional 15 minutes. After cooling down to room temperature, the luminescence and absorption measurements of this solution were made. In addition, 1000 µL of the basic solution were stir-added to destilled water at a temperature of 353 K and held in an ultrasonic bath for 15 minutes at the same temperature. Again, after cooling down to room temperature, the luminescence and absorption measurements of this solution were made. Only freshly prepared solutions were used for PL and absorption measurements.

4 A combined experimental and theoretical study of absorption and emission properties of Rub and Tc in solution

4.1 Introduction

The detailed understanding of the optical properties of fluorescent π conjugated molecules with the help of theoretical calculations has been a big challenge for a long time. Within the present chapter a comparative experimental and theoretical investigation on the two model molecules Tc and Rub is presented. Tc and Rub are two prototype fluorescent molecules. Both molecules exhibit the same "fluorescent backbone". The spectra of Rub and Tc have a common electronic structure origin and are characterized by similar vibrational fine structures. However, significant differences in the optical spectra of both molecules have been observed. In particular, optical spectroscopy of the respective solutions reveals that the $S_0 \rightarrow S_1$ transition in Rub is red-shifted with respect to Tc by ~2000 cm^{-1}, that Rub exhibits a considerably larger Stokes shift, and less resolved vibrational progression.

These differences are a result of the additional four phenyl groups to the Tc backbone in the Rub molecule. The present investigation was motivated by a simple question: What is the influence of the four phenyl groups in Rub on its optical properties? In this context, Tc exhibits the same π conjugated backbone as Rub, but without the four phenyl groups. Due to the additional four phenyl groups, the backbone of Rub is twisted (about 42°) [12], whereas it is planar for Tc.

From very simple empirical rules, two counteracting effects of the phenyl groups can be envisaged. On the one hand, as mentioned, the phenyl groups lead to a twisted Tc backbone in Rub. The twist lowers the total energy by about 200 meV with respect to the planar, untwisted molecule [12]. As a consequence, the conjugation in the π system should be smaller for Rub than for Tc, which is expected to cause a blue shift of the lowest optical transition. On the other hand, the phenyl groups have an inductive effect, which is expected to lead to a red shift. In the present experiments, a red shift of the $S_0 - S_1$ transition is observed, which hence requires an explanation regarding the two mentioned effects. In addition, the role of the phenyl groups on the vibronic structure of the optical spectra is interesting and deserves attention in theoretical and experimental investigations.

The content of this chapter was a part of a general study, which investigates the optical properties of Rub and Tc in a combined experimental and theoretical approach. As such the results were published in The New Journal of Physics [11], wherein

the theoretical part was performed by Dr. Petrenko et al. Since the detailed theoretical analysis has been published, only short overview of theoretical analysis is reported in this chapter.

4.2 Methodology of electronic structure calculations and theoretical analysis of optical spectra

The absorption and fluorescence spectra of Tc and Rub were analyzed in the framework of the independent mode, displaced harmonic oscillator (IMDHO) model and the finite-temperature approximation using the time-dependent technique for the calculation of optical bandshapes [29] [30] [31]. In this method the absorption cross-section $\sigma(E_L)$ and the fluorescence efficiency $A_{k0}(E_R)$ corresponding to emission from the *k*-th electronically excited state to the ground state are given by the following equations [29] [30] [31]:

$$\sigma(E_L) = \frac{4\pi}{3\hbar c} \cdot E_L \cdot \sum_k (D_{ok})^2 \cdot \mathrm{Re} \int_0^8 e^{i(E_L - E_{ok} - \lambda_k/2)t - \Gamma_k t - \frac{1}{2}\Theta_k^2 t^2 - \sum_j \frac{(\Delta_{kj})^2}{2}\left(\left(2\langle n_j\rangle + 1\right)\left(1-\cos w_j t\right) + i \sin w_j t\right)} dt \qquad (4.1)$$

$$A_{k0}(E_R) = \frac{4E_R^3}{3\pi\hbar c} \cdot E_L \cdot \sum_k (D_{ok})^2 \cdot \mathrm{Re} \int_0^8 e^{i(E_L - E_{ok} - \lambda_k/2)t - \Gamma_k t - \frac{1}{2}\Theta_k^2 t^2 - \sum_j \frac{(\Delta_{kj})^2}{2}\left(\left(2\langle n_j\rangle + 1\right)\left(1-\cos w_j t\right) + i \sin w_j t\right)} dt, \qquad (4.2)$$

where E_L denotes the energy of the incident photon, E_R is the energy of the emitted photon, k labels the electronic state (index 0 corresponds to the electronic ground-state); E_{0n} is the adiabatic minima separation energy between states 0 and *k*, λ_k is the corresponding Stokes shift, D_{ok} is the electric transition dipole moment evaluated at the ground-state equilibrium geometry. ω_j is the ground-state vibrational frequency for normal mode j; Γ_k and Θ_k are the homogeneous and inhomogeneous linewidth parameters. Δ_{kj} is the dimensionless origin shift of the k-th excited-state potential energy surface along the j-th normal coordinate. $\langle n_j \rangle = \left[\exp\left(w_j / k_\beta T\right) - 1\right]^{-1}$ is the thermal average occupation number of mode j for temperature T.

The model parameters $\{E_{0k}\}$, $\{\lambda_k\}$, $\{D_{ok}\}$, $\{\Gamma_k\}$, $\{\Theta_k\}$, $\{\omega_j\}$, and $\{\Delta_{kj}\}$ can be determined from the analysis of the optical spectra according to eqs. 4.1 and 4.2. The value of E_{0k} corresponds to the position of the 0-0 vibrational peak, λ_k is related to the separation of the first maxima in absorption and fluorescence. The overall intensity of the absorption cross-section is determined by $|D_{ok}|^2$, while the linewidth and shape of each vibronic

band depends on $\{\Gamma_k\}$ and $\{\Theta_k\}$. Positions and relative intensities of different vibronic bands are entirely specified by $\{\omega_j\}$ and $\{\Delta_{kj}\}$.

Generally, molecules in solutions show unresolved, or like in the present study, partially resolved vibrational structure in absorption and fluorescence spectra. Therefore, from an experimental point of view, the parameterization of optical data in the frame of the independent mode, displaced harmonic oscillator (IMDHO) model is questionable, since entirely different sets of the model parameters may equally well reproduce the spectra. The resonance Raman (rR) technique can be very helpful in resolving such ambiguities [31] [32] [33]. However, it is hardly realizable to obtain rR data for strongly fluorescent molecules like those of the present study. Moreover, the experimental vibrational frequencies of totally symmetric modes for Tc and Rub in a solution are also not available, since conventional Raman spectra are supposed to be strongly dominated by solvent lines. Thus, it was decided to use $\{\omega_j\}$ and $\{\Delta_{kj}\}$ obtained from the calculations using density function theory (DFT) and time depended density function theory (TD-DFT) as the starting point for understanding and fitting of the experimental spectra. Excited-state state energy scan calculations were performed at the BHLYP/TZVP level in conjunction with vibrational frequencies and normal coordinates obtained with the BP86 functional. The purely theoretical parameters were afterwards refined through minimizing the mean weighted absolut difference between the calculated and experimental spectra.

The program ORCA was used for the electronic-structure calculations, spectral simulations and fits [34].

4.3 Experiment

For the optical experiments, both Rub and Tc were dissolved in cyclohexane at room temperature. Photoluminescence (PL) spectra were measured with a Perkin Elmer LS 55 fluorescence spectrometer. The excitation source was a Xe flash tube and the excitation wavelength was selected by a monochromator and could be scanned across the total visible range. The emitted light was detected by a photomultiplier (PM). The emission spectra were corrected regarding the sensitivity of the detector by a factor of λ^2, when going from the wavelength to the wavenumbers axis (see Appendix A.1). However, since the sensitivity of the PM for wavelength above 570 nm is reduced (see Appendix A.4), absolute intensities have to be considered with care. Absorption spectra were recorded on a Perkin Elmer Lambda 35 UV/VIS spectrometer equipped with halogen and deuterium lamps. The spectral resolution of both spectrometers was about 2 nm. A cuvette out of fused silica with an optical path length of 10 mm was used. All measurements were performed at room temperature (about 18° C).

Notably, the maximum of the emission spectra of both molecules systematically shifted to longer wavelengths with an increase of concentrations. This was explained as

"inner filter effect" [4] and will be described in section 4.4.2. Therefore, in order to maximally avoid the distortions of the PL spectra by "inner filter effect", small concentrations of Rub and Tc were chosen, $2.6 \cdot 10^{-6}$ mol/L and $1.7 \cdot 10^{-5}$ mol/L for Rub and Tc, respectively. For these and lower concentrations, the positions of high-energy-maxima of the PL spectra do not shift.

For Rub, the excitation wavelength (λ_{ex}) was varied between 430 and 540 nm. No variations in the shape of the PL spectra were seen. For the data presented below the excitation wavelength λ_{ex} = 440 nm for Tc, and λ_{ex} = 495 nm for Rub was used, respectively.

Since Rub is sensitive to photo-oxidation [5] [35], the optical experiments were performed on freshly prepared solutions, and unnecessary exposure to light was avoided.

4.4 Results and analysis

4.4.1 Experimental spectra

Fig. 4.1 displays the experimental PL and absorption spectra of Tc and Rub in cyclohexane.

In the case of Tc, the emission and absorption spectra both show pronounced effective vibronic progressions that are dominated by 3 and 5 peaks, respectively. The effective vibronic spacing in emission and absorption is ~ 1400 cm^{-1}. The highest energy peak in the PL spectrum (21 190 cm^{-1}) and the lowest energy peak in the absorption (21 270 cm^{-1}) have the highest intensities. These two peaks, which are related to the *zero-phonon* (0-0) transition (*vide infra*), show a small energy difference (the so-called Stokes shift) of 80 cm^{-1}.

In the case of Rub, the progressions in the emission and the absorption spectra are dominated by only 2 and 4 peaks, respectively. The vibronic bands are less resolved compared to Tc, and show a spacing of ~ 1200 cm^{-1} (in emission) and of ~ 1300 cm^{-1} (in absorption). The highest energy peak in the PL spectrum and the lowest energy peak in absorption are found to be at 18 180 cm^{-1} and 19 000 cm^{-1}, respectively. The corresponding energy difference of 820 cm^{-1} is by a factor of 10 larger than in the case of Tc. The spectra of Rub are red-shifted compared to Tc by 3010 cm^{-1} in emission and 2270 cm^{-1} in absorption. It should be noted that, due to the low sensitivity of the photodetector in the wavelength region above 570 nm, the intensity of the PL spectra in this spectral range may be less reliable.

The decadic extinction coefficients at the maxima of the absorption spectra are $(13 \pm 3) \cdot 10^3$ $M^{-1}cm^{-1}$ (at 470 nm) and $(12 \pm 1) \cdot 10^3$ $M^{-1}cm^{-1}$ (at 526 nm) for Tc and Rub, respectively (see Fig. 4.1). The error bars of the extinction coefficients describe the statistic

variation over several measurements. These values are in agreement with those of earlier experiments, which reported values between 9550 $M^{-1}cm^{-1}$ [36] [37] and 14 000 M^{-1} cm^{-1} [38] for Tc, and between 8800 $M^{-1}cm^{-1}$ [4] and 11 500 $M^{-1}cm^{-1}$ [39] for Rub. These differences within the values have been attributed to different solvents, and possible uncontrolled effects due to oxygen which were found to be particularly pronounced in the case of Rub.

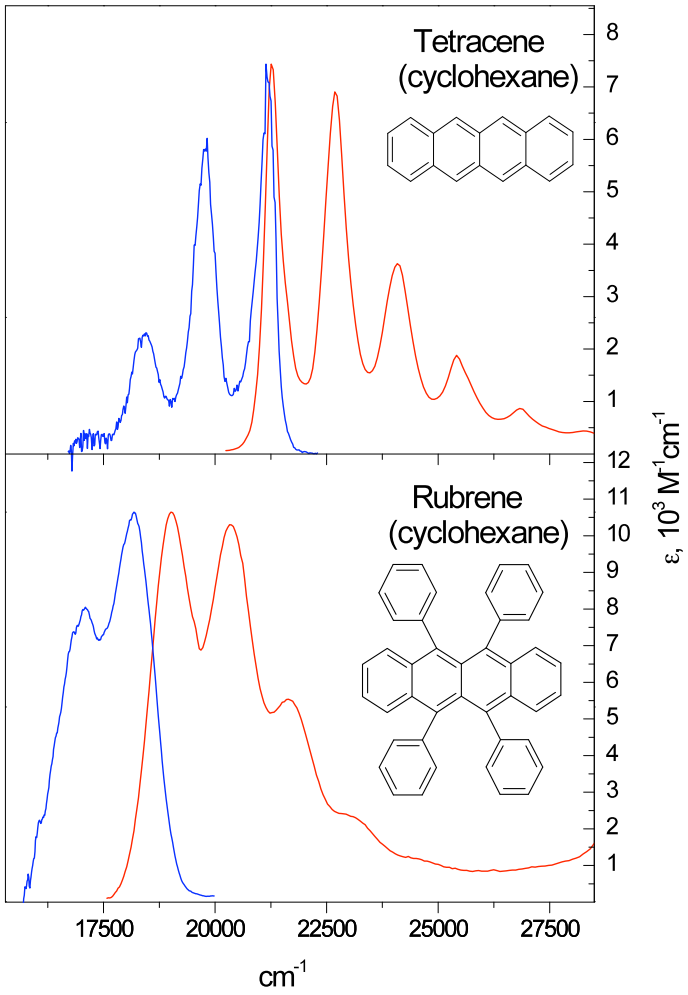

Fig. 4.1 *Normalized absorption (red line) and fluorescence spectra (blue line) of Tc (λ_{ex} = 440 nm) and Rub (λ_{ex} = 495 nm) in cyclohexane at room temperature. The Tc and Rub concentrations were $1.7 \cdot 10^{-5}$ mol/L and $2.6 \cdot 10^{-6}$ mol/L, respectively.*

4.4.2 The inner filter effect

In this paragraph the influence of the concentration of Rub and Tc on the PL spectrum are experimentally illustrated. Afterwards, by a simple calculation, the assumption about the existence of the "inner filter effect" for high concentrations is verified.

As it was already noted, the positions of the high-energy-maxima of emission spectra of Rub and Tc are shifted to longer wavelengths with the increase of the concentration (see Fig. 4.2 and Fig. 4.3). This effect is caused by self-absorption of the fluorescent light ("inner filter effect"), which is due to a partial overlap of the absorption and emission spectra (see Fig. 4.1). The effect was found to become negligible for concentrations below ~ $2.23 \cdot 10^{-6}$ mol/L for Rub and below ~ $3.29 \cdot 10^{-6}$ mol/L for Tc.

(a) Rub (b) Tc

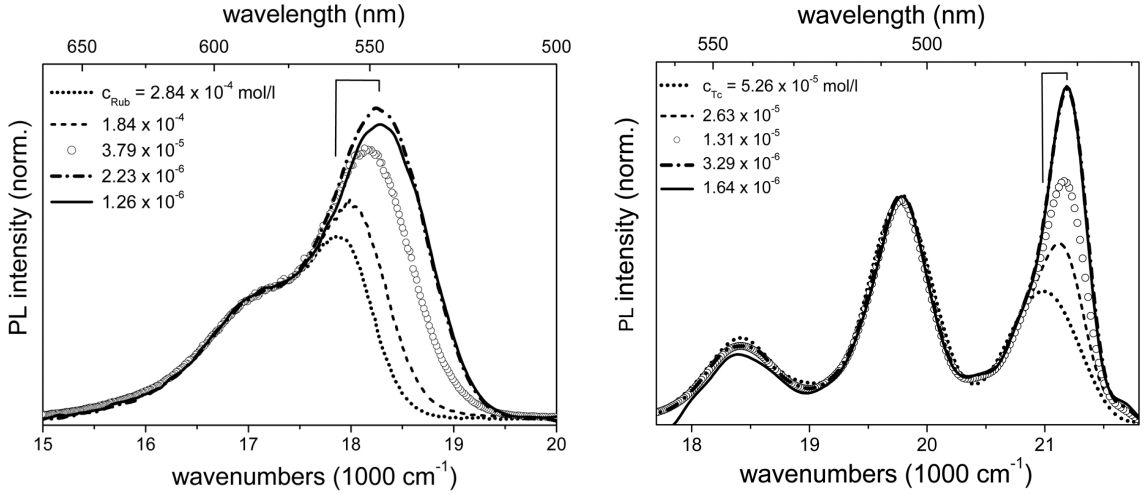

Fig. 4.2 *Fluorescence spectra of Rub (a) and Tc (b) for different concentrations in cyclohexane at room temperature (λ_{ex} = 495 nm for Rub, λ_{ex} = 440 nm for Tc). The spectra were normalized at the positions of the second PL maxima (at 17 100 cm^{-1} for Rub and 19 800 cm^{-1} for Tc) for clarity. Due to the "inner filter effect", the positions of the high-energy-maxima systematically shifted in direction of lower energies with the increase of the concentration. The relative intensity of the high-energy-maxima of the PL spectra decreases with the increase of the concentrations due to the self-absorption. There is no influence of the concentration on the spectral shape for low concentrations, which avoids the effect of self-absorption (see curves marked by compact and dash-dotted lines). The form of the second maximum (at lower energy) in the case of Rub spectra is a bit distorted in comparison to the spectrum in Fig. 4.4. The sensitivity of the detection system is wavelength depended (see Appendix A.4). The correction factor can in principle be taken into account by the software during the recording of optical spectra. Unfortunately, the correction factor was not activated in this set of the measurements, therefore the form of the spectra is a bit distorted. For all other spectra presented in this chapter, the sensitivity of the detection system was taking into account.*

(a) Rub (b) Tc

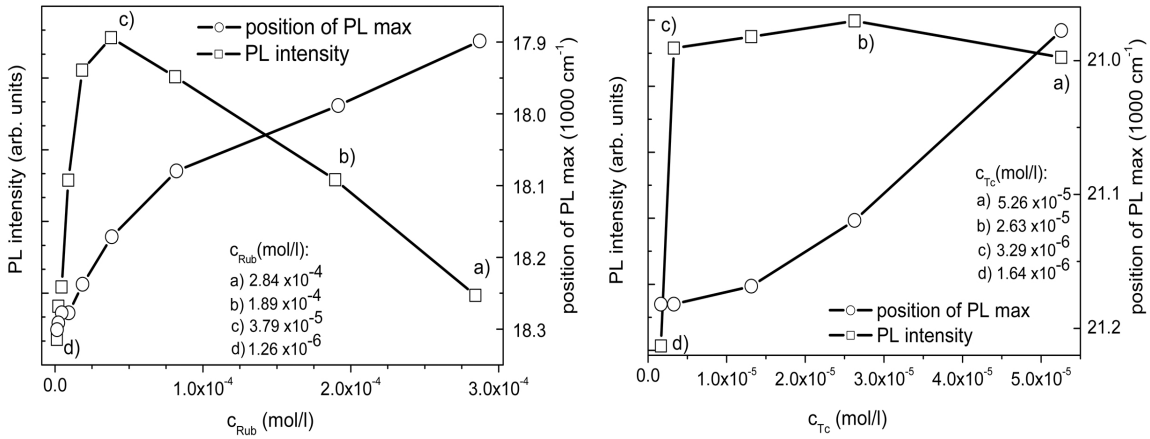

Fig. 4.3 *Curves with squares represent the PL intensity dependence of high-energy-maxima on the concentration of Rub (a) and Tc (b) in cyclohexane at room temperature. Curves with circles represent the dependence of the positions of the high-energy-maxima in the PL spectra on the concentrations.*

In addition, as shown in Figs. 4.3 (a) and (b), the intensities of high-energy-maxima of the PL spectra (marked with squares) increase with the decrease of the concentration down to $3.79 \cdot 10^{-5}$ mol/L for Rub and $2.63 \cdot 10^{-5}$ mol/L for Tc. Upon further decrease of the concentration the PL intensities start to decrease. It was assumed that at higher concentrations (above $3.79 \cdot 10^{-5}$ mol/L for Rub and $2.63 \cdot 10^{-5}$ mol/L for Tc) PL intensities start to increase with the decrease of the concentration due to the decrease of the self-absorption. In other words, some molecules of the sample can "filter" and trap (or absorb) the emission of another excited molecules. Upon low concentrations (below $3.79 \cdot 10^{-5}$ mol/L for Rub and $2.63 \cdot 10^{-5}$ mol/L for Tc), the PL intensities are proportional to the numbers of excited molecules. The PL intensities decrease with the decrease of the concentration.

Figs. 4.3 (a) and (b) show that the maximal values of the concentrations, below which the spectral shifts are not observed and the maximal values of the concentrations, below which the intensities start to be proportional to concentrations, are not the same (Figs. 4.3 (a) and (b), curves with circles and squares, correspondently). For example, for Rub the intensity starts to decrease below $3.79 \cdot 10^{-5}$ mol/L, but there is still the shift in the high-energy-maximum for lower concentrations (until $9 \cdot 10^{-6}$ mol/L, see curves with circles), i.e. the "inner filter effect" still exists. The assumption about the existence of the "inner filter effect" is supported by the calculation of the transmitted intensity I_{tr} for Rub. The transmitted intensity was calculated by using the follow eq. [40]:

$$I_{tr} = I_{PL} \cdot \exp^{-A} = I_{PL} \cdot \exp^{-\varepsilon \cdot l \cdot c}, \tag{4.3}$$

where I_{PL} is the real PL intensity, A is the absorption, ε is the molar extinction coefficient, l is the thickness of the absorbing medium and c is the concentration in the medium. As I_{PL}

we used the experimentally measured PL spectrum for a low concentration ($\sim 9 \cdot 10^{-6}$ mol/L). A low concentration was used in order to avoid distortion of the spectral shape due to the self-absorption effect. The value of the absorption maximum was chosen equal to one for the absorption, which corresponded to experimentally measured PL spectrum (I_{PL} in eq. 4.3) with the concentration $\sim 9 \cdot 10^{-6}$ mol/L. To see the influence of the concentration on the form of the spectra the value of the absorption A was varied. Calculated I_{tr} spectra for different values of the absorption are presented in Fig. 4.4. The influence of the concentration on the calculated I_{tr} spectrum is in a full agreement with the measured dependence (see Fig. 4.2 (a)), that confirms the assumption about the distortion of the spectral shape due to an "inner filter effect" at high concentrations. As note above, the sensitivity of the photomultiplier was not taken into account for the PL spectra in the experimental data sets presented in Fig. 4.2 (a). This explains the deviation of the shape of the PL spectra for wavelength areas above 570 nm in comparison to the shape of the spectra presented in Fig. 4.4. The second maximum of the PL spectra presented in Fig. 4.4 is relatively higher and better pronounced in comparison to the spectra in Fig. 4.2 (a).

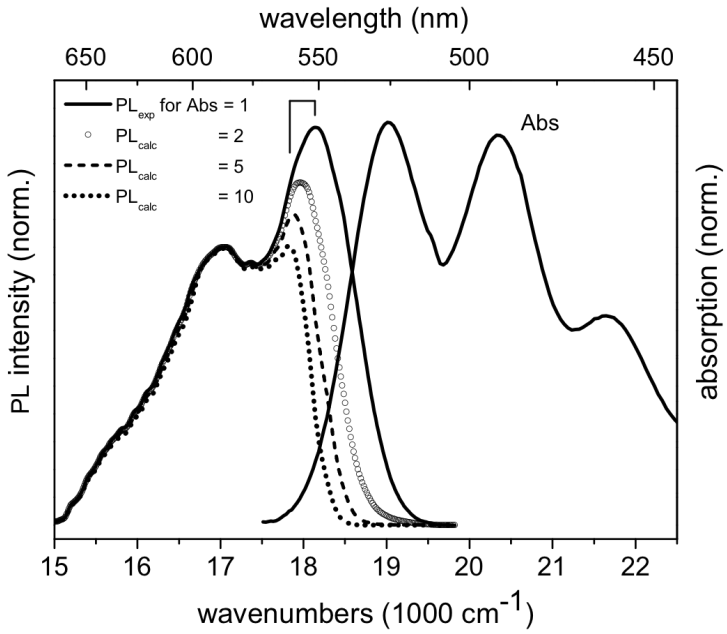

Fig. 4.4 *Measured PL spectrum (PL_{exp}) and absorption (Abs) spectrum of Rub (λ_{ex} = 495 nm) in cyclohexane at room temperature for Rub concentration about $9 \cdot 10^{-6}$ mol/L marked by compact lines. The calculated PL spectra for higher absorptions (higher concentrations) confirm the assumption of a "inner filter effect" at high concentrations.*

4.4.3 Quantum chemical calculations and fit of the Tc spectra

$1^1A_g \rightarrow 1^1B_{2u}$ transition in Tc

The TD-DFT/TDA calculations performed by Dr. Petrenko indicate a single dipole allowed transitions around ~ 20 000 cm^{-1}, which is characterized by an oscillator strength of $f \sim 0.1$ [11]. This excitation is as assigned as a $1^1A_g \rightarrow 1^1B_{2u}$ transition that involves promotion of an electron from the highest doubly occupied a_u molecular orbital (MO) to the lowest unoccupied b_{2g} MO. Therefore, absorption and PL spectra of Tc in the range 17 000-28 000 cm^{-1} were analyzed under the assumption of a single electronic band.

The D_{2h} symmetry of Tc leads to 15 totally symmetric normal modes that are potentially active in the absorption and photoluminescence spectra within the IMDHO model. Tab. 4.1 shows calculated vibrational frequencies and dimensionless normal coordinate displacements corresponding to the $1^1A_g \rightarrow 1^1B_{2u}$ transition in Tc for the totally symmetric modes [11].

Mode	ω (cm^{-1})			Δ			
	BP86	Fit		BP86	BHLYP	Fit	
		T=293 K	T=0 K			T=293 K	T=0 K
1	313	318*	333*	0.73	0.70	0.74*	0.77*
2	619	619	619	0.15	0.27	0.27	0.27
3	749	749	749	0.28	0.22	0.22	0.22
4	849	849	849	0.04	0.10	0.10	0.10
5	997	997	997	0.05	0.14	0.14	0.14
6	1124	1124	1124	0.23	0.26	0.26	0.26
7	1192	1177*	1137*	0.29	0.57	0.67*	0.66*
8	1394	1394	1394	0.08	0.17	0.17	0.17
9	1392	1380*	1379*	0.49	0.93	1.02*	1.04*
10	1426	1426	1426	0.17	0.23	0.23	0.22
11	1514	1513*	1511*	0.38	0.69	0.62*	0.62*
12	1520	1519*	1517*	0.55	0.56	0.50*	0.50*

Tab. 4.1 *Fitted and calculated vibrational frequencies ω and dimensionless normal coordinate displacements Δ for $1^1A_g \rightarrow 1^1B_{2u}$ electronic transition in Tc obtained from the BP86 and BHLYP DFT methods [11]. ω and Δ which were varied in the fit are marked with asterisks. The fitted parameters were obtained in the room temperature approximation (T = 293 K) according to eq. 4.1 and 4.2 and in the zero-temperature approximation (T = 0 K). For more details see Ref. [11].*

Quantum chemically predicted spectra and initial fit

The DFT calculations reveal 12 totally symmetric modes in the range 0-1600 cm^{-1} that are composed of C-C stretching as well as C-C and C-H bending coordinates. As expected, the BP86 frequencies in combination with BHLYP normal coordinate displacements provide a rather consistent prediction of the vibrational structure in the spectra. Hence, the agreement between simulated and experimental bandshapes is already very good if only E_0, λ, Γ and Θ are slightly adjusted. We note that the calculated vibrational frequencies for the totally symmetric modes are in very close agreement with those which can be deduced from the high-resolution emission spectrum of Tc in superfluid helium droplets [41].

One observes that the fitted and experimental spectra are in close agreement, except for the region in the fluorescence spectrum below 17 600 cm^{-1} (see Fig. 4.5). We assume that this mismatch is mainly due to the low sensitivity of the detector in this spectral range.

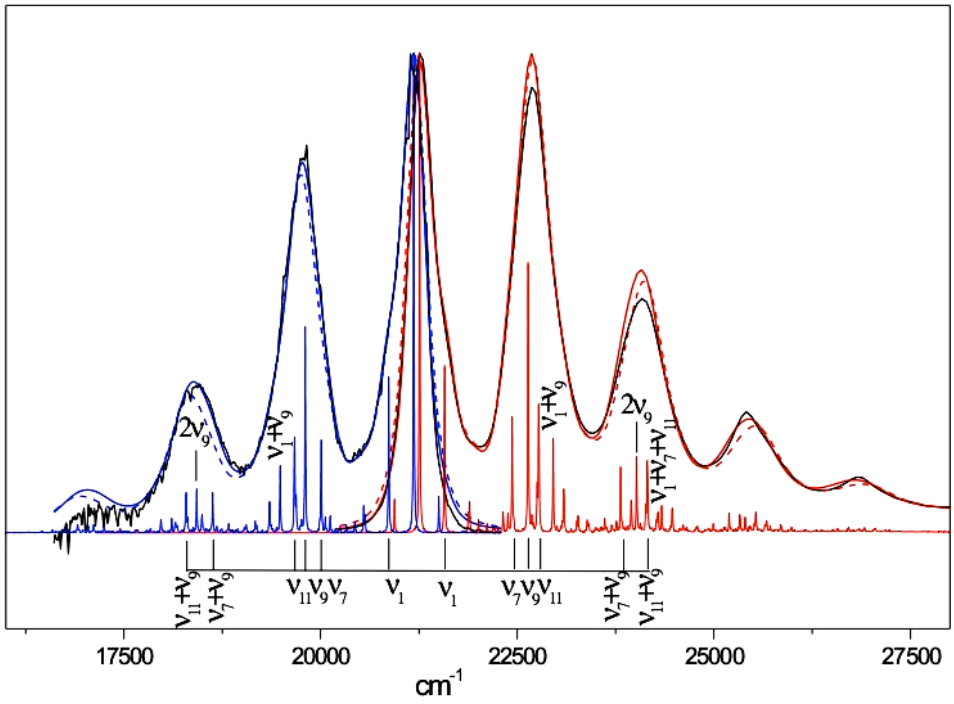

Fig. 4.5 *Experimental (solid black line) and calculated absorption (solid red line) and fluorescence (solid blue line) spectra of Tc in cyclohexane corresponding to the fitted values of dimensionless normal coordinate displacements and vibrational frequencies. The dashed lines represent the fit in which the transition energy, the Stokes shift and the linewidth parameters were varied, while the values of the displacements and vibrational frequencies were fixed to those obtained at the BHLYP and BP86 levels, respectively. The calculated spectra displaying the detailed vibrational structure in the absorption (vertical red lines) and fluorescence (vertical blue lines), including specification of dominant fundamental, overtone and combination transitions, were constructed using the fitted model parameters and reduced values of the linewidth parameters of* $\Gamma = 5\ cm^{-1}$ *and* $\Theta = 0\ cm^{-1}$. *Reproduced from [11].*

Interestingly and importantly, the fitted vibrational frequencies and dimensionless displacements show only small deviations from the quantum-chemically calculated values (see Tab. 4.1). The fit made within the zero-temperature approximation resulted in minor deviations of the adjusted model parameters compared to the case of T = 293 K, thus indicating that temperature effects are not important in the optical spectra of Tc (see Tab. 4.1).

Nature of $1^1A_g \rightarrow 1^1B_{2u}$ Transition and vibronically active modes in Tc

As mentioned above, the $1^1A_g \rightarrow 1^1B_{2u}$ transition in Tc essentially involves promotion of an electron from the highest doubly occupied a_u molecular orbital (MO) to the empty b_{2g} MO (see Fig. 4.6). The donor and acceptor MOs feature rather different bonding character. Accordingly, the difference density plot corresponding to this transition (see Fig. 4.6) indicates 1) a loss of bonding for the C_2—C_3, C_4—C_5, C_6—C_7 and C_8—C_9 bonds, thus leading to their lengthening in the electronically excited state; 2) a gain of bonding for the C_3—C_4, C_3—C_8, C_7—C_8 and C_5—C_6 bonds, resulting in their contraction in the excited state. The totally symmetric normal modes with the largest projections onto this elongation and contraction pattern are expected to show the dominant vibronic activity in the absorption and fluorescence spectra. These criteria are met by modes 1, 7, 9, 11 and 12 (see Fig. 4.6). In particular, mode 9 that features stretching of the C_2—C_3, C_3—C_4, C_4—C_5, C_5—C_6, C_6—C_7, C_7—C_8 and C_8—C_9 bonds with alternating phase along this chain has the largest projection ($\Delta \sim 0.9$).

4.4.4 Quantum chemical calculations and fit of the Rub spectra

$1^1A \rightarrow 1^1B_2$ transition in Rub

The DFT calculations reveal two possible equilibrium structures of Rub that are characterized by D_{2h} and D_2 symmetries. The conformation of D_{2h} symmetry (Rub-D_{2h}) is characterized by a planar structure of the Tc-backbone with the phenyl rings being oriented perpendicular to the aromatic plane (see Fig. 2.2). The D_2 symmetric structure of Rub (Rub-D_2) is characterized by a twisted Tc-backbone (see Fig. 2.2). The twisted configuration Rub-D_2 is more stable than Rub-D_{2h} by 2102 cm^{-1} (BP86) and 2278 cm^{-1} (BHLYP). These numbers are in agreement with the literature [12]. Therefore, the optical spectra of Rub in solution have been analyzed on the basis of TD-DFT calculations for Rub-D_2. The analysis presented below reveals several important differences in the spectra of Rub compared to the case of Tc which are related to the lower symmetry together with electronic effects of the phenyl substituents. The TD-DFT/TDA calculations indicate a single dipole allowed transition in Rub-D_2 and Rub-D_{2h} in the region around ~20 000 cm^{-1}. This excitation is assigned as a $1^1A \rightarrow {}^1B_2$ transition in Rub-D_2 and involves promotion of an electron from the highest doubly occupied a molecular orbital (MO) to the lowest unoccupied b_2 MO (see Fig. 4.7). The donor and acceptor orbitals have spatial distributions similar to those which are involved in the $1^1A_g \rightarrow 1^1B_{2u}$ transition of Tc (see Fig. 4.6). They are mainly localized on the Tc-backbone but with some noticeable delocalization onto the

phenyl rings (see Fig. 4.7) [11]. A similar situation is found for Rub-D_{2h} (here the excitation is assigned as $1^1A_g \rightarrow 1^1B_{2u}$ and is analogous to the $1^1A_g \rightarrow 1^1B_{2u}$ transition in Tc).

It was found that the delocalization of the highest occupied molecular orbital (HOMO) and the lowest unoccupied molecular orbital (LUMO) of Rub onto the phenyl groups results in an increase of the electronic transition dipole moment by by a factor of ~1.4, thus resulting in an oscillator strength for Rub ($f \sim 0.2$) that is larger than that of Tc by about a factor of 2.0 [11].

Upon going from Tc to Rub the number of totally symmetric modes increases because of the possibility for vibrations of Tc-backbone to mix with different types of vibrations of the phenyl groups. There are 26 totally symmetric modes for Rub-D_{2h} (excluding C-H stretching vibrations). The number of totally symmetric vibrations for the Rub-D_2 is larger (45 modes have to be considered) [11]. Calculated vibrational frequencies and dimensionless normal coordinate displacements corresponding to the $1^1A \rightarrow 1^1B_2$ transition in Rub-D_2 for the totally symmetric modes (excluding C-H stretching vibrations, *vide supra*) are published [11].

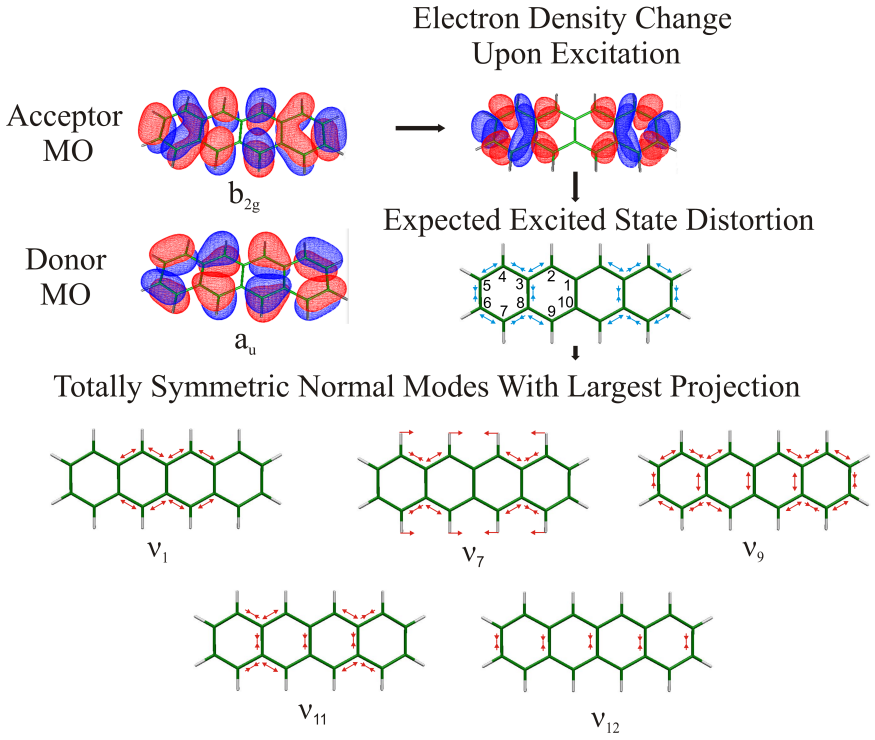

Fig. 4.6 *Normal modes with the largest excited state displacements for the $1^1A_g \rightarrow 1^1B_{2u}$ transition of Tc and their relation to the nature of excitation. Donor and acceptor MOs were obtained from BHLYP DFT calculations. Red and blue colours indicate a decrease and increase of the electronic density in the excited state, respectively. Bond length changes upon excitation are represented by outward arrows (bond elongation) and inward arrows (bond contraction). In the normal mode representation, the length of arrows and archlines roughly designate the relative amplitude of bond stretching and bending, respectively. Internal coordinates vibrating in antiphase are denoted by inward and outward arrows. Reproduced from [11].*

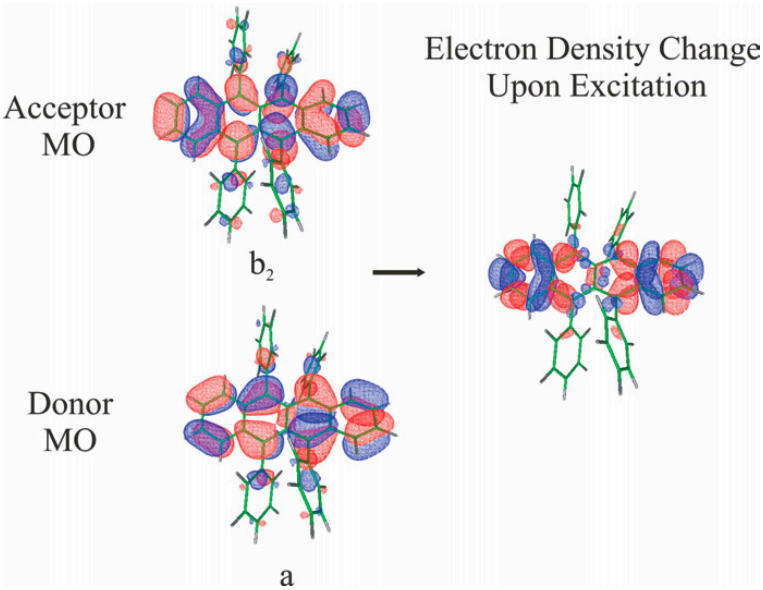

Fig. 4.7 *Donor and acceptor MOs corresponding to $1^1A \rightarrow 1^1B_2$ transition of Rub-D_2 as obtained from BHLYP DFT calculations. Red and blue colours indicate a decrease and increase of the electronic density in the excited state, respectively. Reproduced from [11].*

Obviously, the displacement values and vibrational frequencies for the totally symmetric modes of Tc and their counterparts in Rub-D_2 nicely correlate with each other. Not unexpectedly, this correlation leads to the observed similarities of the vibrational fine structure in the absorption and photoluminescence spectra of Tc and Rub. However, Rub-D_2 additionally features a large number of totally symmetric vibrations with nonzero values of the dimensionless displacements. This results in noticeable broadening of the observed vibronic peaks for Rub-D_2 compared to Tc. While the totally symmetric modes of Tc span the frequency range above 300 cm^{-1}, in the case of Rub-D_2 there are 7 vibronically active modes with frequencies in the range 30-250 cm^{-1} [11]. The low-frequency modes 1, 3, 4 and, 5 have A_u parentage and are not active in the case of Rub-D_{2h}. In particular, mode 1 calculated at 33 cm^{-1} involves twisting of Tc-backbone and rotation of phenyl groups shows a particularly large $\Delta > 2.0$.

(a) T = 293 K

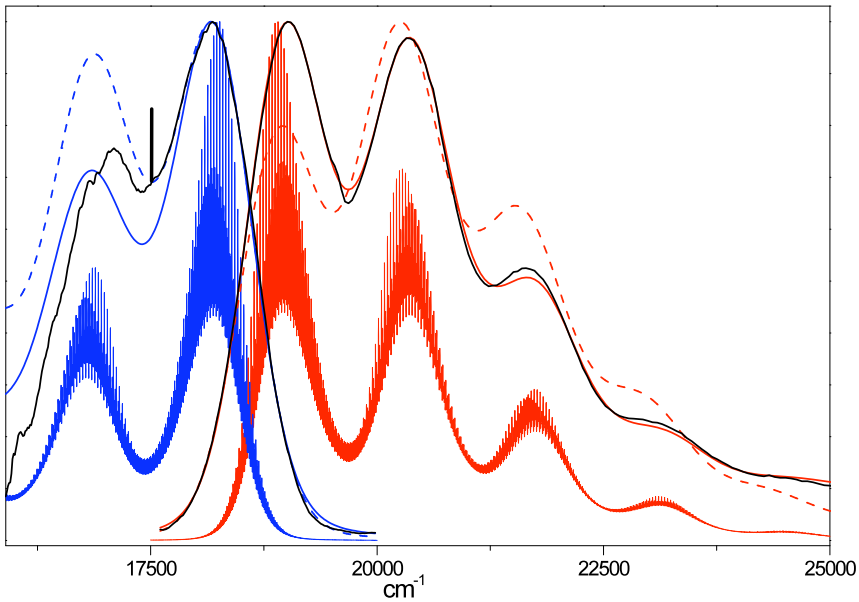

(b) T = 0 K

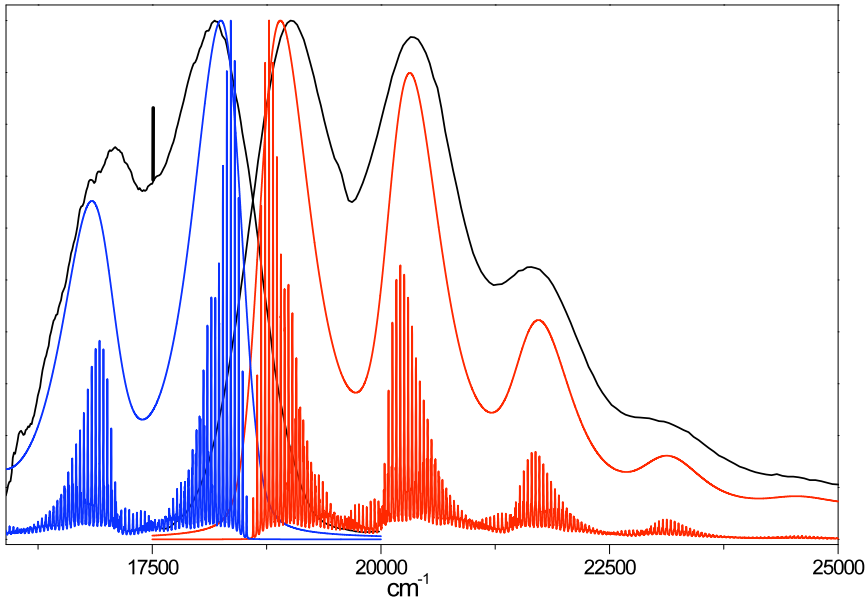

Fig. 4.8 *Experimental (solid black) and calculated absorption (solid red) and fluorescence (solid blue) spectra of Rub-D_2 in cyclohexane corresponding to the fitted parameters ω_{34} = 1373 cm^{-1}, Δ_{34} = 0.87. The small vertical bar designates the low-energy bound of the part of the experimental fluorescence spectrum, which is considered to be less reliable due to the reduced sensitivity of the detector in this range. The dashed lines represent the fit in which transition energy, Stokes shift and linewidth parameters were varied, while the values of the displacements and vibrational frequencies were fixed to those obtained at the BHLYP and BP86 levels, respectively. The spectra presenting detailed vibrational structure (vertical red and blue lines in the absorption and fluorescence, correspondently) were constructed using the fitted model parameters and reducing values of the linewidth parameters to Γ = 2 cm^{-1}, and Θ = 0 cm^{-1}. (a) The fit is calculated for room temperature (293 K) case. (b) The fit is calculated for zero-temperature case. Reproduced from* [11].

Quantum chemically predicted spectra and initial fit

Since the fluorescence data below 17 600 cm^{-1} are less reliable due to the low sensitivity of the detector in this spectral range, the fluorescence spectrum of Rub-D_2 was fitted in the range 17 600-20 000 cm^{-1}. Upon the adjustment of E_0, λ, Γ and Θ (with $\{\omega_j\}$ and $\{\Delta_j\}$ fixed to the values predicted at the BP86 and BHLYP levels, respectively), the agreement between the simulated and experimental spectra (see Figs. 4.8) is not as good as in the case of Tc (see Fig. 4.5). The quality of the fit can be significantly improved upon adjustment of the vibrational frequency and dimensionless displacement for only one mode (mode 34) (see Figs. 4.8, solid blue and red lines). The discrepancy between the calculated and experimental spectra may also be due to the neglect of the Dutschinsky rotations or excited state frequency alterations [42].

4.4.5 Discussion on the Stokes shift and temperature effects

As the optical experiments show, the first resolved vibrational peaks in the absorption and fluorescence spectra of Rub are separated by 820 cm^{-1}. Hereafter this parameter is called effective Stokes shift λ_{eff}. Two contributions to this value can be distinguished:

$$\lambda_{eff} = \lambda + \lambda_V , \tag{4.4}$$

where λ is the Stokes shift that arises from the influence of solvent molecules and λ_V is governed by unresolved vibrational fine structure due to low-frequency modes. As pointed out recently, within the IMDHO model the latter contribution can be aproximated by [31]:

$$\lambda_V = \sum \Delta_f^2 \omega_f . \tag{4.5}$$

Here the index f is confined to the subspace of low-frequency modes (defined as < 600 cm^{-1}), Δ_f is the dimensionless origin shift of the excited-state potential energy surface along the fth normal coordinate, and ω_f is the ground-state vibrational frequency for mode f. The calculated value of λ_V according to eq. 4.5 is 454 cm^{-1}. If we use the value λ = 400 cm^{-1} from the fit to the absorption and fluorescence spectra corresponding to the $1^1A \rightarrow 1^1B_2$ transition of Rub-D_2 (see Fig. 4.8 a) solid red and blue lines) and λ_{eff} = 820 cm^{-1}, than the 'experimental' estimate of $\lambda_V = \lambda_{eff} - \lambda$ = 420 cm^{-1} is in excellent agreement with the calculated value. This indicates that the vibronic activity of the low-frequency modes makes the dominant contribution to the observed effective Stokes shift. Interestingly, it was found out that the modes of A_u parentage made the dominant contribution to λ_V. Moreover, there are good reasons to believe that the fitted value of λ is overestimated. This may be due to the slight underestimation of the quantum

chemically predicted frequencies and dimensionless displacements for certain low-frequency modes which were fixed in the fit. Indeed, it was observed that already a minor increase of Δ_1 by 20% and ω_1 by 10 cm^{-1} (certainly within the accuracy of the DFT method used) will lead to an increase of λ_V by 120 cm^{-1} and a corresponding decrease of λ. In the simplest approximation the parameter λ can be ascribed to the influence of solvent molecules that give rise to low-symmetry distortions of the molecule, thus leading to vibronic activity of the non-totally symmetric modes. In this case the largest excited-state distortions are expected for soft modes that are characterized by low frequencies, and λ is well approximated by eq. 4.5. The quantum-chemically predicted value of this parameter is not available since the solvent molecules were not explicitly included into the DFT calculations. However, presumably, there are no important physical reasons that would account for the substantial differences concerning λ between Rub and Tc ($\lambda = 70$ cm^{-1}). The difference is supposingly due to the low accuracy of the method in determination λ_V.

Finally, Rub-D_2 features large values of dimensionless displacements for low frequency normal modes. Pronounced vibronic activity of the low frequency modes in the case of Rub-D_2 accounts for the large effective Stokes shift of 820 cm^{-1} and significant broadening of the resolved vibronic peaks in the observed spectra. Increased Franck-Condon activity of the low frequency modes is essentially related to the twisted ground-state configuration of the molecule.

While the temperature effects in the spectra of Tc are almost negligible, they are important in the case Rub-D_2 (see Figs. 4.8 (a), (b)). Seven totally symmetric modes in the range 30-250 cm^{-1} are characterized by large occupation numbers (5.7-0.4) at room temperature. This leads to additional broadening of the spectra by a Gaussian form. A detailed discussion of the broadening mechanism and temperature effect is reported in Ref. [11].

4.4.6 Nature of the red shift of the optical transition in Rub

In order to explain the effects of the phenyl groups and the structural twist on the red shift of the optical spectra corresponding to the $1^1A_g \rightarrow 1^1B_{2u}$ transition in Rub-D_2 relative to the case of the $1^1A_g \rightarrow 1^1B_{2u}$ transition in Tc, the TD-DFT/TDA calculations for different idealized geometries of Tc and Rub were performed. The corresponding geometrical structures are designated as follows: Tc-D_{2h}, Rub-D_2 and Rub-D_{2h} denote the equilibrium geometry of Tc and the two equilibrium conformations of Rub described above; Tc-(Rub-D_2) is the Tc molecule with the twisted Tc-backbone of Rub-D_2 (e.g. Rub-D_2 with the phenyl substituents replaced by hydrogens). Rub-D_2-(Tc-D_{2h}) represents the structure of Rub-D_2 in which the geometry of the Tc-backbone is substituted by that of Tc-D_{2h}. For these structures we have explored in detail the differences in the vertical transition energy E_V, the HOMO-LUMO gap, and the corresponding orbital energies.

From Tab. 4.2 it arises that the overall change of the transition energy between Tc-D_{2h} and Rub-D_2 by ~ 2200 cm^{-1} can be partitioned into two contributions: 1) decrease

of E_V by ~ 900 cm^{-1} due to the twisting of Tc backbone; 2) further decrease of E_V by ~ 1300 cm^{-1} upon attachment of phenyl groups (see Fig. 4.9). These transition energy variations closely correlate with the corresponding changes of the HOMO-LUMO gap. The LUMO energies of Tc-D_{2h} and Rub-D_2 actually coincide, and the final transition energy difference of ~ 2200 cm^{-1} is thus mainly due to the destabilization of the HOMO by ~ 2000 cm^{-1}. The HOMO energy always rises upon attachment of the phenyl groups. This destabilization is due to the interaction between the HOMO of Tc and σ-orbitals of the phenyl groups. Thus, the observed red shift in the spectra of Rub is mainly determined by the inductive effect of the phenyl groups.

	E_v cm^{-1}	Δ(HOMO-LUMO) cm^{-1}	ε (HOMO) a.u.	ε (LUMO) a.u.
Tc-D_{2h}	19117	13235	-0.173506	-0.113201
Rub-D_2	16962	11143	-0.163923	-0.11315
Tc-(Rub-D_2)	18216	12352	-0.172903	-0.11662
Rub-D_2-(Tc-D_{2h})	15731	10240	-0.164567	-0.117906
Rub-D_{2h}	18053	12298	-0.165433	-0.109399

Tab. 4.2 *Calculated (BP86/TZVP) vertical transition energy (E_V), HOMO-LUMO gap, and corresponding orbital energies for different geometrical structures of Tc and Rub. Reproduced from [11].*

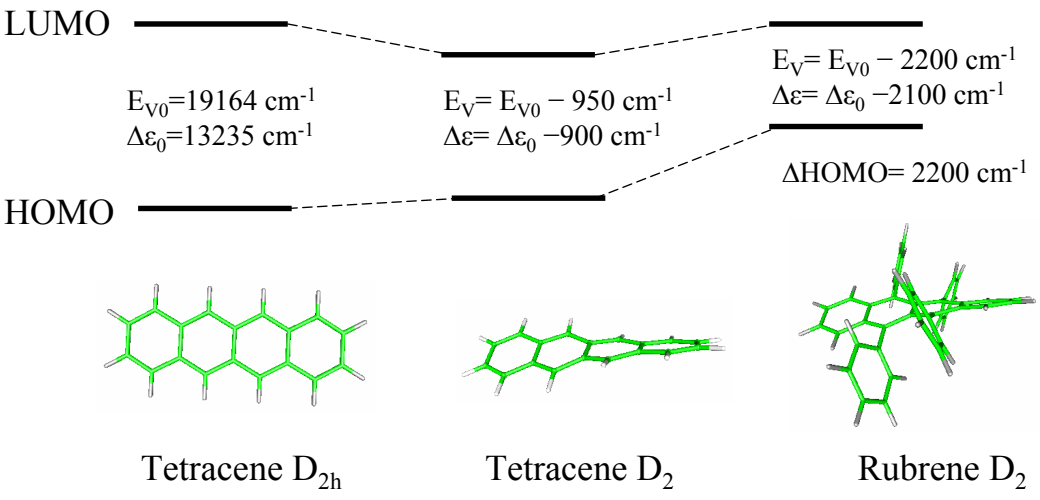

Fig. 4.9 *Schematical illustration of nature of red shift in Rub optical spectra relative to the Tc optical spectra. The observed red shift in the Rub spectra is mainly determined by the inductive effect of the additional phenyl groups, which leads to destabilization of the donor HOMO. Reproduced from [43].*

4.5 Conclusions

An experimental study in combination with a detailed theoretical study of the optical spectra of Tc and Rub yield a picture that describes the experimentally observed differences between the spectra of the two prototype molecules. The phenyl groups lead to a twisted Tc-backbone in Rub, whereas it is planar for Tc. For Rub in comparison to Tc, the number of totally symmetric modes increases (15→45) due to the possibility of vibrations of Tc-backbone to mix with different types of vibrations of the phenyl groups. The larger number of the totally symmetric modes yields a lower resolution of optical spectra of Rub compared to Tc. Noticeable variation of the value of the effective Stokes shift for Tc and Rub originate mainly from the vibronical activity of low frequency modes which is obtained by the twisting of the backbone in Rub and which must be absent for Tc. The analysis reveals that the ~2000 cm^{-1} red shift of 0-0 vibronic band of Rub relative to Tc is mainly caused by the inductive effect of the phenyl substituents that leads to destabilization of the donor MO.

5 Molecules on surfaces as photon emitters

5.1 Introduction

The contents of this chapter was a part of the general study of optical properties of molecules on dielectric surfaces with concomitant control of the structural and morphological parameters. The study intends to investigate the changes in the optical properties upon the condensation of isolated molecules into thin films and to establish the fluorescence signal as a tool to study kinetic processes, e.g., diffusion of molecules. Such a study is important for a fundamental understanding, as well for the development of nanoelectronic devices based on single molecules or self-assembled molecular thin films [44].

Luminescence spectra of individual molecules, diluted molecules, and molecules in small ensembles (e.g., islands, clusters) on surfaces have been of significant interest for the last few years. It has been found that surface bonding potentials can modify the structural properties of the thin molecular films deposited on surfaces, thus leading to optical properties differing from those of the corresponding bulk molecular crystals [45]. The investigation of the luminescence of diluted molecules is trammeled, because at least for metallic underlying substrates there exist some quenching effects, which quench the PL intensity from molecules on the surface. An ultra fast quenching process was found for the first two layers of films of porphorines on the Au(111) surface [46] and was also found for films of quaterthiophene [47] , PTCDA [47] and Tc on the Ag(111) surface [7]. Evidently optical experiments require that the molecules on the surface fluoresce and that the fluorescence process is not totally quenched.

The first investigated system in the frame of the general project was Tc deposited on thin epitaxial films of aluminium oxide (AlO_x) [48] [7] [23]. The oxide films were grown by a self-terminating oxidation process of a $Ni_3Al(111)$ single crystal in an oxygen atmosphere. Such AlO_x films are highly ordered and smooth. Since the AlO_x film is very thin, the surfaces could be characterized by a low energy electron diffraction, which was performed with a SPA-LEED instrument. The deposition of Tc molecules at low temperatures leads to disordered films. However, after an annealing cycle to about 240 K, ordered films of "standing" Tc molecules can be obtained (see Figs. 5.1 b) and c)). Interestingly, the disordered films were found to be non-luminescent. However, after the annealing and ordering of the films, luminescence spectra were observed (see Fig. 5.1 a)). The observed spectra correspond to those of Tc single crystals. The details are described in the literature [48][23]. The explanation for this result is based on the small thickness of AlO_x films. This small thickness causes that states of the underlying $Ni_3Al(111)$ substrate extend into

the Tc film. The "transparency" of the AlO_x film was also observed by scanning tunnelling spectroscopy on this surface. It allows charge transfer from the photo-excited molecules to the substrate, i.e., luminescence quenching. This transfer appears with high probability for

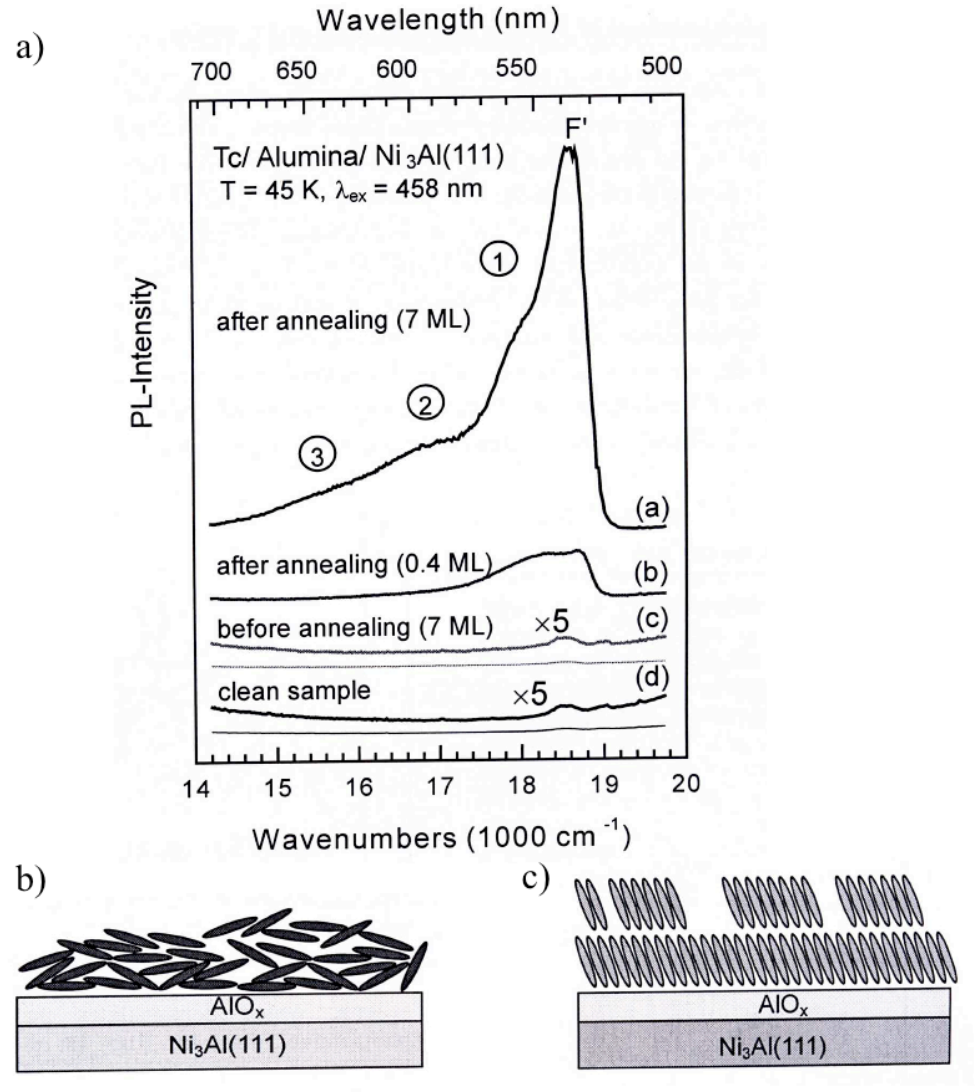

Fig. 5.1 *a) PL spectra of a thin Tc films on the alumina surface. (d) is the spectrum of the clean AlO_x surface for comparison. (c) is the spectrum after deposition of nominally 7 monolayers (ML) of flat lying Tc molecules at 45 K. (b) and (a) are spectra of Tc films with a nominal thickness of 0.4 ML and 7 ML after annealing (an additional slow warming cycle to 240 K with about 1 K/min). All spectra were measured at 45 K under ultra high vacuum. The excitation wavelength was 458 nm. The small peak at about 18 500 cm^{-1} in the magnified spectra (d) and (c) is an artefact, likely from luminescence, excited from scattered laser light of the longpass filter in front of the spectrometer. The spectra are vertically shifted against each other for clarity. b) and c) schematic sketches of the geometric arrangement of the molecules on the substrate before b) and after c) annealing. The darker molecules indicate molecules which do not luminesce, the brighter molecules are those molecules which luminesce after annealing. Reproduced from [23].*

the as-deposited, mainly flat-lying molecules due to a higher overlap of the metal and Tc wave functions. The transition dipole moment for the S_0-S_1 transition in Tc is oriented parallel to the short axis of the Tc molecule. In the case of post annealing, the upright orientation of the Tc molecules yields a smaller overlap of the metal and Tc wave functions, hence suppressing the charge transfer effectively and allowing luminescence.

In order to suppress the charge transfer between the photo-excited molecules and metal substrate states, Tc was substituted by Rub. Rub exhibits the same π-conjugated backbone as Tc with additional four phenyl groups which act like spacers and keep the backbone at a larger distance to the AlO_x surface, thus reducing the overlap of metal and Rub wave functions. Hence, Rub is one of a promising material for the observation of luminescence of surface adsorbed molecules.

5.2 Experiment

Rub films (of 150 nm thickness) on glass were fabricated under a vacuum with the substrate at room temperature (see details in the Chapter 3). After that the sample was exposed to air for about one hour. This was the time necessary to move the sample from the evaporation apparatus to the vacuum system for the spectroscopic measurements. Since Rub films were found to be sensitive to photo oxidation [49] [50], the unnecessary exposition to the air was to be avoided as much as possible.

The argon laser (made by Coherent, Innova Sabre R Ion laser, model DBW 25) was used as the light excitation source (λ_{ex} = 488 nm or 514 nm) in PL measurements. PL spectra were recorded with a Czerny-Turner-Grating monochromator (made by Jobin Yvon, grating 1800 grooves/mm, resolution 0.9 Å). The luminescence was imaged on the entrance slit (0.2 mm) by the lens 1 (silicate lens, focus f = 100 mm, diameter ∅ = 50.8 mm) and lens 2 (silicate lens, focus f = 300 mm, diameter ∅ = 50.8 mm). The optical signal was recorded by means of a photomultiplier. To reduce the intensity of the laser light coming to the sample a grey filter (transparency T = 0.05) was positioned in front of it. In the case of using the laser excitation of 514 nm an additional yellow filter (OG515) was positioned between the lens 2 and the entrance slit to protect the photomultiplier. Absorption spectra were measured with DU Series 7000 spectrometer. The optical measurements were performed under a vacuum of 10^{-5} Torr.

The samples of the Rub films (30 nm) on the $AlO_x/Ni_3Al(111)$ surface were prepared by vapour deposition under UHV at room temperature of the samples. The film deposition and the optical measurements were performed in the same chamber and fully under vacuum. Therefore the any chemical reaction with the air is completely avoided. PL spectra were recorded with a SpectraPro 2300i spectrometer. As a light excitation source the light of an argon laser (Ar-laser) was used as in the case of the investigation of the PL

properties of the Rub films on glass. The schematic diagram of the experimental set-up used for the PL measurements is given in Fig. 3.8.

For temperature depended measurements, the Rub films on glass and on the $AlO_x/Ni_3Al(111)$ surface were cooled with liquid He. In the case of the temperature depended measurements on Rub films on glass the cooling rate equal to 10 K pro minute was used. After the desired temperature was established, we waited always 10 min in order to maintain the same time interval between measurements and to have the same influence of the temperature changes in every measurement step. The temperature controller was keeping the temperature constant within 1 K. PL spectra were measured in the temperature interval from 300 K to 10 K with temperature steps of 10 K.

The procedure of the preparation of Tc and Rub nanoparticals is reported in Chapter 3. The resulting solutions of Tc and Rub are clear, pale yellow and a clear, pale orange, respectively. PL and absorption spectra of of Tc and Rub nanoparticals were measured with a Perkin Elmer LS 55 fluorescence spectrometer and a Perkin Elmer Lambda 35 UV/VIS spectrometer, respectively.

5.3 Results and Analysis

5.3.1 Amorphous structure of the Rub films

Rub films vacuum deposited at room temperature of the substrates (quartz glass, $AlO_x/Ni_3Al(111)$ can only have an amorphous structure or amorphous structure with small crystallities on top as it was observed in the present work (see Fig. 6.2) and as it is in agreement with the results published in the literature [12]. Fig. 5.2 shows the images of an Rub film (150 nm) on glass, which were obtained with a polarisation microscope. The main part of the film is amorphous with islands of small crystallities on top of it. The islands of the Rub film on glass with typical thread-like borders are quite similar to the islands on gold and SiO_2 [13] [51]. Note that the Fig. 5.2 c) and d) show a „corona“ between islands and the amorphous film, although in the literature was no remark about the existence of such a “corona”. It is possible, that the “corona” formation is the result of the oxidation of the sample. The “corona” formation could be also due to the difference in the packing density of the molecules in the amorphous and crystalline structures, since in amorphous structures molecules have more space between each other due to their disorganised packing. So, the molecules from amorphous regions of the film, which are close to the crystalline islands, move to the islands. As a consequence, the crystalline islands grow with time and the “corona” is formed.

Interestingly, Rub films on SiO_2 fabricated with similar procedure as in the present experiment show an amorphous structure with crystalline disks on it. In the amorphous part of the film, the current-voltage characteristics show no mobility. The disk-shape area

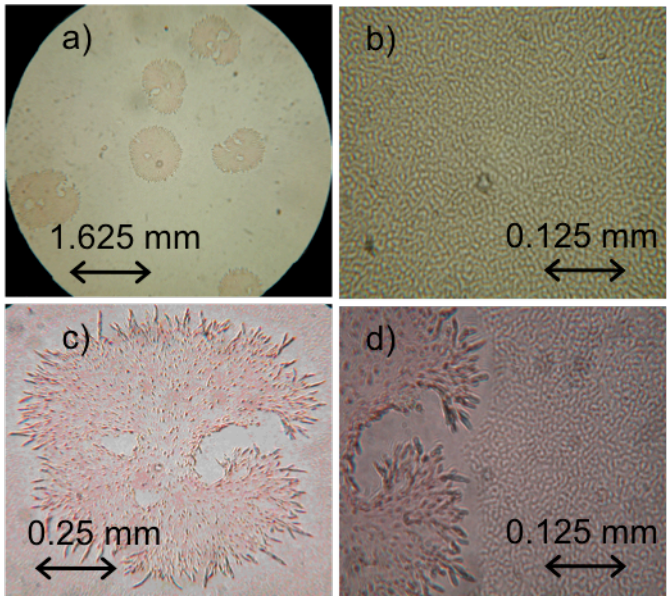

Fig. 5.2 *Rub film (with a thickness of 150 nm) on a quartz glass grown at room temperature. The images are obtained by a polarisation microscope. The images a) shows the typical morphology of the Rub film, which has an amorphous structure and small islands (typical size 1 mm) of crystallites on it. The images b), c) and d) are magnifications of the different parts of the image a). The images c) and d) are different magnifications of the same crystallitie. The islands have a distinctive form with thread-like borders. The images c) and d) show a „corona" between islands and the amorphous film.*

showed good mobility ($1.23 \cdot 10^{-4}$ $cm^2/V\ s$) [51]. These observations corroborate the assumption of a crystalline structure of the disks. Since in common sense the field-effect mobility increases with the size of the crystalline disks, the growth of disks of bigger size is an essential matter to realize Rub field effect transistors with higher mobility.

Due to the chirality of the Rub backbone in the gas phase, it is necessary to have some additional conditions as a higher temperature of the sample and a large vapour pressure to planarize the Rub backbone and to obtain well-oriented crystalline films of Rub, otherwise only rather amorphous films or poly-crystalline dendritic networks could be formed. Progress in the growth of ordered Rub thin films has been achieved by employing „hot wall" deposition [13]. As reported in Ref. [13], well-oriented, chemically stable crystalline Rub films were obtained by employing "hot wall" deposition. In that case, due to the high vapour pressure inside the hot wall evaporator a large number of many body collisions can occur which may assist a conformational change and therefore together with the higher mobility of the molecular entities allow a crystalline growth with long range ordering and a loss of chirality.

As expected SPA-LEED measurements on Rub films on $AlO_x/Ni_3Al(111)$ do not show reflections. That confirms the amorphous surface.

The comparison of the PL spectrum of Rub film (Rub (150 nm)/glass) with the PL spectrum of Rub in solution yields an additional confirmation of the statement about an amorphous structure of the investigated Rub films. As shown in the Fig. 5.3, the PL and absorption spectra of Rub film are nearly identical to the corresponding spectra of Rub in solution. There is a small (320 cm^{-1}) red-shift of the PL and absorption film spectra with respect to the spectra of Rub in solution. This shift is quite small in comparison to the corresponding shift in Tc film spectra with respect to the Tc solution spectra, which is equal to 2400 cm^{-1}. This, so called, "solvent-to-solid shift" has been calculated from a comparison of the Tc spectrum in solution from the present work (see Fig. 4.1) and the PL spectrum of the Tc film from Ref. [52]. The large red solid shift in the Tc case is due to a closer arrangement of molecules and therefore stronger molecular interactions in the solid state. As it was mention before (see Chapter 4), the Tc backbone plays the main role in the spectrum of the S_0-S_1 transition of Rub. From the obtained similarity of Rub film spectra with Rub spectra in solution (see Fig. 5.3) the author supposes that there is no strong resonance coupling between molecules in Rub film due to chirality of the Rub backbone and therefore the amorphous form of the Rub film is confirmed.

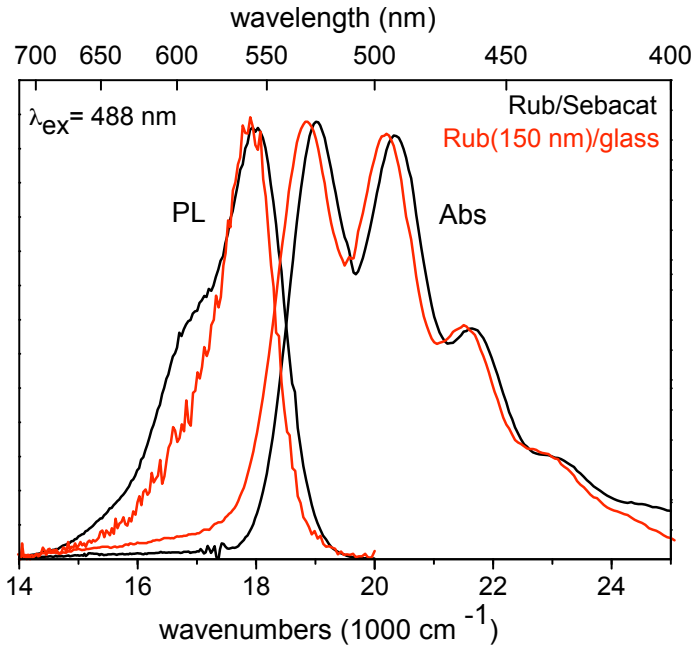

Fig. 5.3 *Normalized absorption (Abs) and PL spectra of Rub in sebacat (black lines) and Rub film on glass (red lines) at room temperature. The input of Ag laser power was 0.08 W in the PL measurements. The spectra of Rub film are nearly identical to the spectra of Rub in liquid.*

5.3.2 Temperature dependency of the PL of thin Rub films

The temperature depended PL spectra of the Rub film (150 nm) on the quartz glass and the Rub film (30 nm) on the $AlO_x/Ni_3Al(111)$ surface have been measured and are presented in Figs. 5.4 (a) and (b). As Figs. 5.4 (a) and (b) show, both spectra data look quite similar.

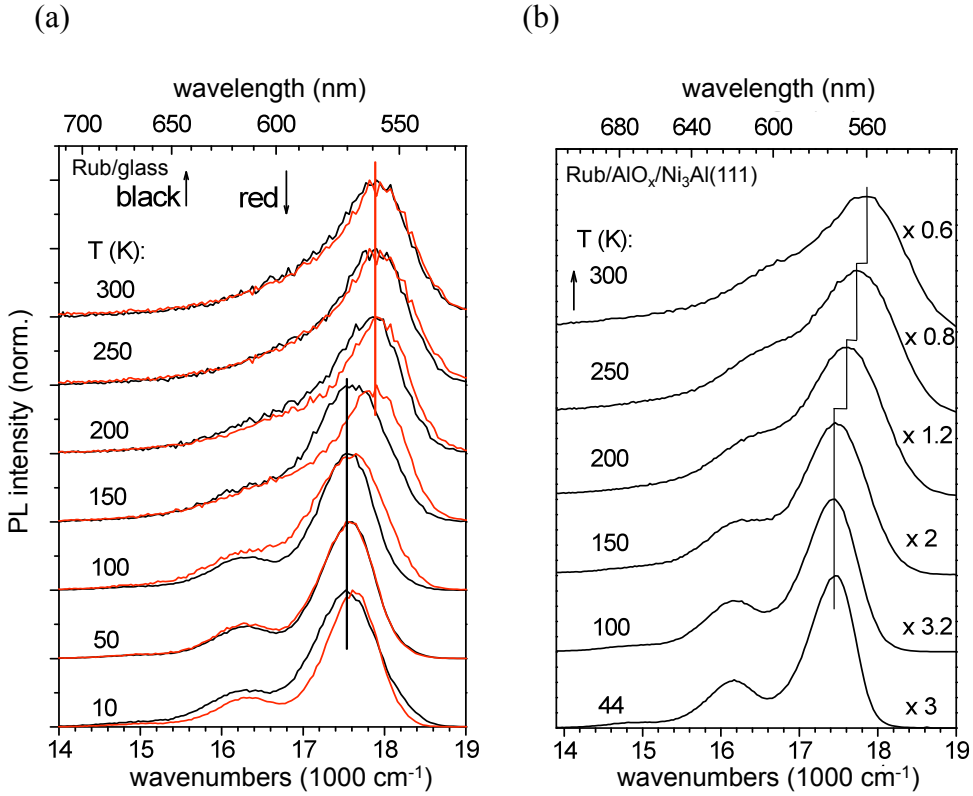

Fig. 5.4 *Normalized PL spectra of thin Rub films as a function of temperature. (a) Rub film (150 nm) on quartz glass. (b) Rub film (30 nm) on the $AlO_x/Ni_3Al(111)$ surface. The spectra show the low energy shift and the appearance of a pronounced vibronic replica with cooling of the samples. The excitation wavelength was 488 nm in both cases. The input of the Ar laser power was 0.08 W. The experiments were performed under high vacuum. The spectra were shifted vertically against each other for clarity.*

The emission spectra of the Rub film (150 nm) on the quartz glass show a dominant peak at 17 860 cm^{-1} at 300 K, which is related to the *zero-phonon* (0-0) transition. Temperature dependent PL spectra show a red shift (about 290 cm^{-1}) of the (0-0) peak to lower energy during the cooling of the sample. The (0-0) peak at low temperatures is observed at about 17 570 cm^{-1}. At low temperatures the PL spectra show partly resolved vibronic progression with a peak separation of 1280 cm^{-1}. We suggest that the additional two peaks (16 290 cm^{-1} and 15 010 cm^{-1}) belong to the same optical transition and its weaker vibronic side-bands.

In a first set of temperature depended measurements, the PL spectra of the Rub film (150 nm) on glass were measured in temperature steps of 50 K (Fig. 5.4 (a)). The sample was heated up from 10 K to 300 K (black curve) and afterwards cooled down (red curve). The spectral shift has been observed at about 150 K from this data set. The spectra are reversible. Only the spectra taken at 150 K and 10 K are exceptional. Apparently, this is related to the slow "reactivity" of the sample during the change of the temperature.

Fig. 5.5 shows PL spectra of the Rub film on glass measured in another set of measurements with smaller temperature steps (10 K). This set of measurements allows one to see that the spectral shift, "phase transition", occurs gradually in temperature intervals from 110 K to 190 K.

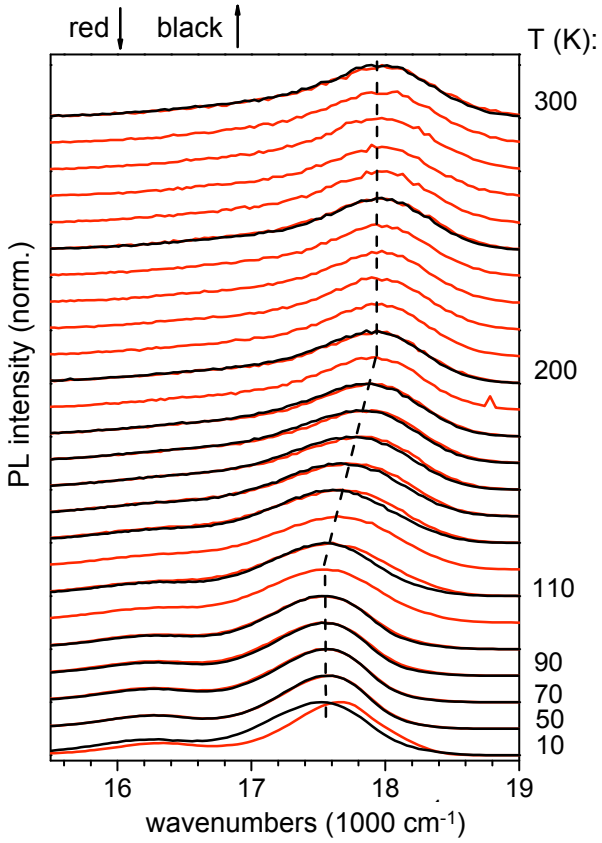

Fig. 5.5 *Normalized PL spectra of the Rub film (150 nm) on glass as a function of temperature. The experimental set was done with temperature steps of 10 K. Spectra are reversible and the "phase transition" occurs gradually in the temperature intervals from 110 K to 190 K. The spectra were shifted vertically against each other for clarity.*

The emission spectra of the Rub film (30 nm) on the $AlO_x/Ni_3Al(111)$ surface show a dominant (0-0) transition at 17 840 cm^{-1} at 300 K. For temperatures from 300 K to 150 K, the position of the (0-0) transition is also gradually shifted (about 390 cm^{-1}) to lower energy. The first luminescence band is located at 17 450 cm^{-1} for low temperatures (150 K - 44 K) (see Fig. 5.4 (b)). At low temperatures, the PL spectra show partly resolved

vibronic progression with the peak separation of about 1300 cm^{-1}. Two additional weaker vibronic bands are observed at 16 150 cm^{-1} and 14 840 cm^{-1}.

The origin of the observed "phase transition" is not clear yet, since the Rub films are amorphous. It might be related to a conformation change of molecules, e.g. a flatting of the twisted backbone at lower temperatures and therefore an increase of a molecule-molecule interaction and as result red shift of the position of the (0-0) transition. Interestingly, similar phase transitions were observed for Tc films [7]. The phase transition for a Tc film on Ag(111) occurs at a temperature of 150 K. The position of the maximum of the (0-0) transition is red shifted (219 cm^{-1}) for low temperatures as well. The origin of this observed similarity in the temperature dependcy of the PL spectra of the amorphous Rub and the cristalline Tc films might have to do with the common electronic structure origin of both molecules (see Chapter 4).

As it was observed from the temperature depended measurements, the cooling of the sample from 300 K to 10 K results in an intensive increase of the photoluminescence of Rub films by a factor of 16 (see Fig. 5.6). Generally, a decrease of the temperature results in an increase the fluorescence quantum yield and the radiative lifetime because the non-radiative processes related to thermal deexcitation channels (intramolecular vibrations and rotations, etc.) are more efficient at higher temperatures. The time-resolved measurements of PL spectra of Rub films show a strong increase of the radiative time upon cooling (see Figs. 5.7 (a) and (b)). This observation explains a strong increase of the PL intensity upon cooling. Details about the time-resolved PL experiments are reported in Chapter 7.

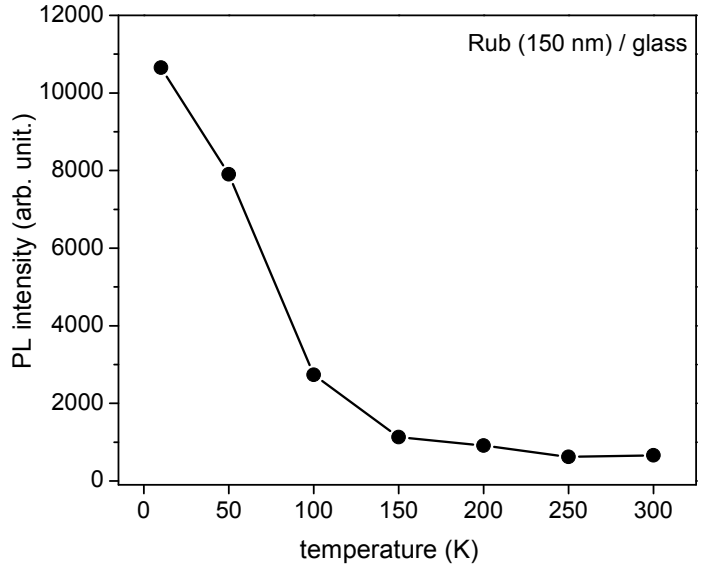

Fig. 5.6 *PL intensity of the maximum of the PL spectrum as a function of temperature for Rub film (150 nm) on glass.*

In addition, it is necessary to notice that the shape of the PL spectrum of a Rub film is very similar to the shape of PL spectrum of Rub single crystals at low temperatures (see Fig. 5.16), although is quite different at room temperature.

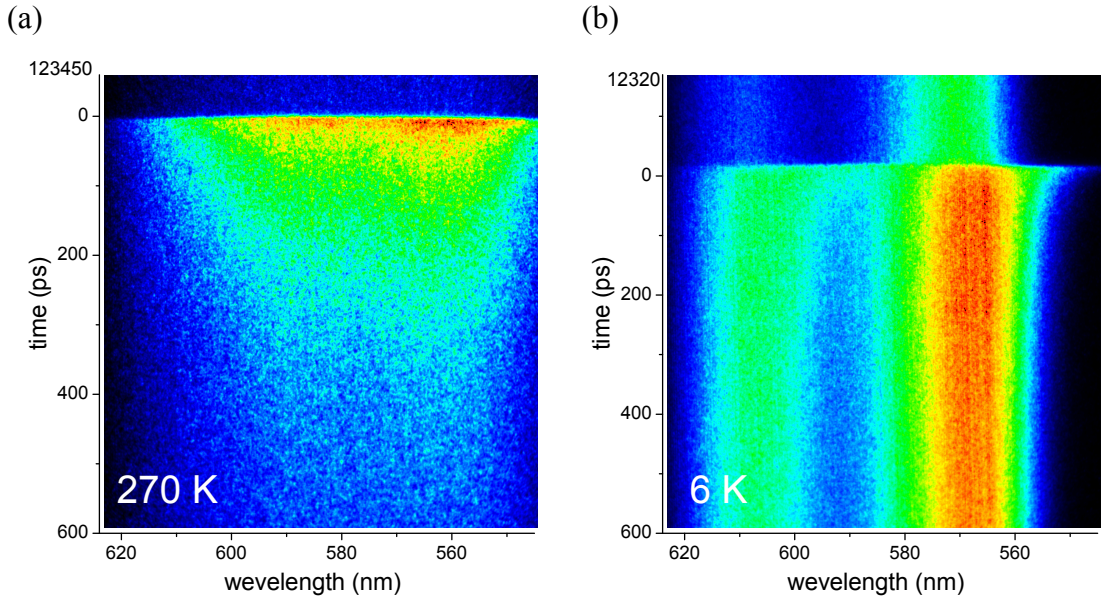

Fig. 5.7 *(a) 2D steak camera PL image of the Rub film (150 nm) on guartz glass taken at 270 K. (b) 2D steak camera PL image taken at 6 K. The horizontal profile represents the PL spectra as a function of wavelength. Vertical profile represents emission decay spectra. The 0 ps was set to the moment of optical excitation pulse. The signal above 0 ps is the spectra at the end of the repetition cycle of the detection. The repetition rate was 12.5 ns. The wavelength of the laser excitation was 440 nm. The input laser power was 87 μW.*

The very strong increase of the PL intensity and the strong increase of the radiative time by cooling have been observed for Rub crystal as well (see Chapter 6 and 7).

Finally, the influence of the input power on the spectrum of Rub film (150 nm) on glass was studied. The power was varied from 0.25 mW to 20 mW. For the measurements we used an Ar laser with excitation wavelength λ_{ex} = 488 nm. The temperature of the sample was 20 K. With increasing power the photoluminescence increases. It should be noted that we did not observe any shift of the PL spectra upon changing the laser power, and the shape of the spectra did not change also. Although, a blue shift of PL spectrum was observed in the case of ordered Tc films upon increase of the input power [7].

5.3.3 Photoluminescence of ultra thin Rub films

The luminescence of very thin films of Rub on the AlO_x surface was investigated in the context of our project by M. Müller [27] [53] (see Figs. 5.8 and 5.9 (a), (b)). In order to obtain immobile molecules, the deposition and the measurements were performed at a sample temperature of 40 K. The nominal film thickness was determined from the inte-

grated thermal desorption spectra, which were calibrated by thickness measurements with a quartz microbalance. The smallest film thickness for which it was possible to obtain reasonable photoluminescence spectra was 0.6 Å. That is at about 1/6 of the ML (see Fig. 5.8). The thickness of one ML (1 ML = 3.7 Å) was calculated from the crystallographic structure of Rub according to Ref. [54]. Due to the amorphous conformation of Rub, in the films studied in this work, the real size of ML might deviate from the value calculated from the crystallographic structure.

The decrease of PL yield with decreasing film thickness is shown in Fig. 5.9 (a)). The doubly logarithmic diagram clearly shows two regions with different slopes of the decrease. For the films, whose thickness is smaller than 30 Å, the dependence of PL yield from the film thickness has a linear character. For the films with a thickness higher than 30 Å, the dependence is cubic.

According to the classical theory of Chance, Prock and Silbey (CPS theory) [55], the decrease of PL yield for thin films is due to an energy transfer from the excited molecule to the image dipole in the metal substrate. Note that, in comparison to the thin Tc films, in case of Rub it was possible to observe luminescence for ultra thin Rub films as well. So, our assumption that the additional phenyl groups keep the backbone at a distance to AlO_x surface and prevent the ultrafast luminescence quenching by metallic substrate is confirmed.

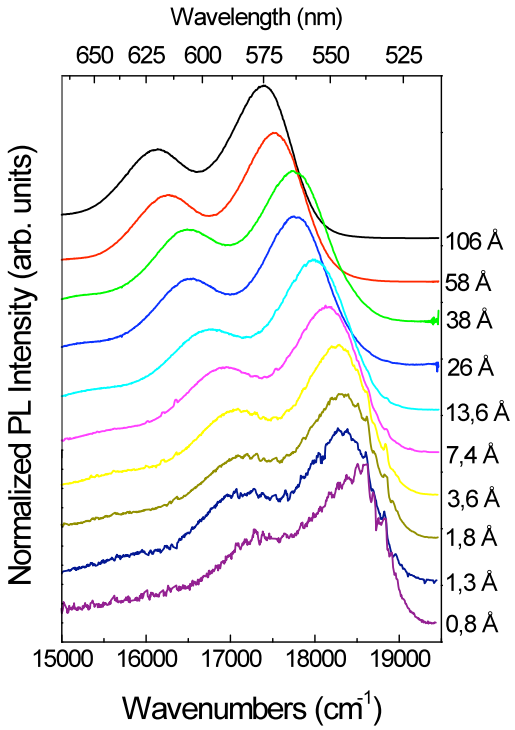

Fig. 5.8 *PL intensity of ultra thin Rub films on the AlO_x/$Ni_3Al(111)$ surface as a function of the film thickness. The spectra show the film thickness dependent shift. The spectra were measured at 40 K. The spectra were normalized and shifted vertically against each other for clarity. λ_{ex} = 496.5 nm. No temperature dependent measurements have been done in this experimental set. Reproduced from [53].*

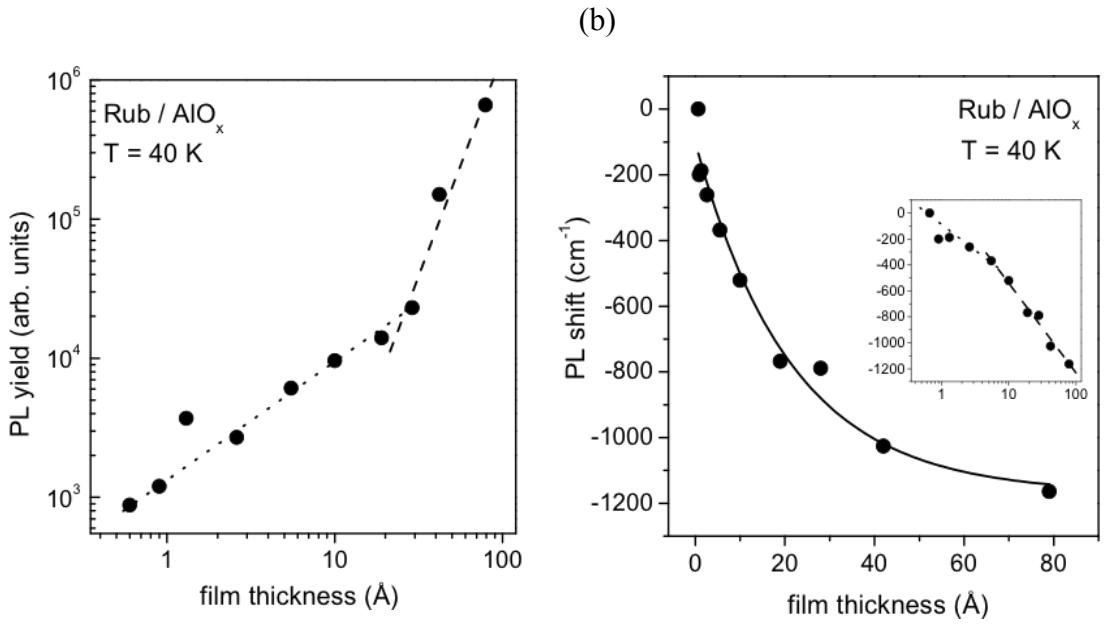

Fig. 5.9 *(a) Logarithmic PL yields (PL yield = intensity (arb. units) / thickness) as a function of the logarithmic nominal film thickness. (b) The film thickness dependent shift of PL spectra. The spectra shows systematically shift to high energies with decreasing film thickness. The data are from Ref. [27]. PL shift equal zero corresponds to the PL of Rub film of 0.8 Å thickness and the value of the high-energy PL maximum is 18 535 cm^{-1}.*

As mentioned above, the SPA-LEED measurements show that the Rub films are amorphous. At 5.5 Å (~1.5 ML) there are almost no substrate spots in LEED. That could be a sign of a layer-by-layer growth (Frank-Van der Merwe or Stranski-Krastanov growth mode). However, in a case of layer-by-layer growth, the PL yield is expected to be constant until the first monolayer is completed (Chance, Prock and Silbey) theory. This is not in agreement with the observed experimental results, which clearly show that the PL yield increases with increasing thickness of the sub monolayer. The increase of the PL yield of the sub monolayer could be explained by clusters growing on the surface (e.g. Volmer-Weber growth mode). These clusters should have a small size with a high surface coverage (pyramidal) to be in an agreement with the LEED results (no substrate reflection already for ~1.5 ML).

Based on the CPS theory, for small distances from a metal substrate, the luminescence yield is proportional to the nominal layer thickness in the case of pyramidal clusters growing [27]. This model successfully describes experimental results for nominal film thickness below 30 Å (Fig. 5.9 (a)). The PL between 30 Å and 80 Å cubically depend from the nominal film thickness. It could be explained by strong changes in morphology of the Rub film that emerge at about 30 Å. A theoretical model to explain this dependence is not found yet. Fig. 5.8 and Fig. 5.9 (b) show that the PL spectra continuously shift to lower energies with increasing film thickness. The low energy shift with increasing film thickness could be explained by increased coupling between the Rub mol-

ecules. For the amorphous films, the coupling has to be considered as mean-field like. The PL red shift dependence on the film thickness can be well described by exponential decay [27]. We suppose that the low energy shift with increasing film thickness has the same origin as the low energy shift with the cooling observed in the temperature depended measurements for Rub thin films in the present work. As mention above, the temperature depended shift was related to an increase of the dipole-dipole coupling between the molecules in the films due to a conformation change of molecules during the cooling, e.g. a flatting of the twisted backbone at lower temperatures.

The value of the high-energy PL maximum of Rub films on the $AlO_x/Ni_3Al(111)$ surface with 30 nm thickness (at low temperatures) is 17 450 cm^{-1} and fits to the exponential described ultra thin film thickness dependence reported in Ref. [27]. The value of the high-energy PL maximum of the Rub film on the glass surface investigated in the present work with 150 nm thickness at low temperatures is 17 570 cm^{-1}. The higher value of the maximum for a 150 nm Rub film on glass could be due to structural changes which could have occurred because of the different substrates. In addition, it might be caused due to errors in the determination of the real values of wavenumbers in different spectrometers which were used in optical measurements of Rub films on glass and Rub films on the $AlO_x/Ni_3Al(111)$ surface (see section 5.2)

5.3.4 Photoluminescence of Rub and Tc nanoaggregates

In addition, the experimental results on the optical characteristic of nanoaggregates of Tc and Rub have to be mentioned. The analysis of Rub nanoaggregates could help to interpret the thickness depended low energy shift in ultra thin Rub films. The three types of samples were studied: monomeric Rub diluted in sebacat, nanoaggregates, and thin films.

A. Tc

Early optical studies of Tc nanoaggregates (≡ nanocrystals) are reported in Ref. [28] [56]. Figs. 5.10 (red lines) present the fluorescence and absorption spectra of the Tc nanocrystals prepared in the present work. Both spectra are in very good agreement with the spectra from the literature [56] of Tc aggregates (~ 60 nm diameter) suspended in water. As shown, the Tc nanocrystals and the thin solid films have similar optical properties [56].

The PL spectrum of the nanocrystals shows a 60 nm (2320 cm^{-1}) red shift of the high energetic maximum and no resolved vibronic progression compared to the spectrum of Tc molecules in solution (see Fig. 5.10 (a)). The highest maximum of the absorption spectra of nanocrystals is red shifted by 49 nm (2125 cm^{-1}) (see Fig. 5.10 (b)). The second upper Davydov splitting component is observed in absorption spectrum of the nanocrystals. It can be found at about 505 nm (19 810 cm^{-1}) and appears as a higher energy shoulder on the lowest energy absorption peak. The measured value of

the Davydov splitting is 600 cm^{-1} and it is in agreement with the reported values for Tc films [57] [58]. For a detailed discussion of optical properties of Tc nanocrystals see Ref. [56].

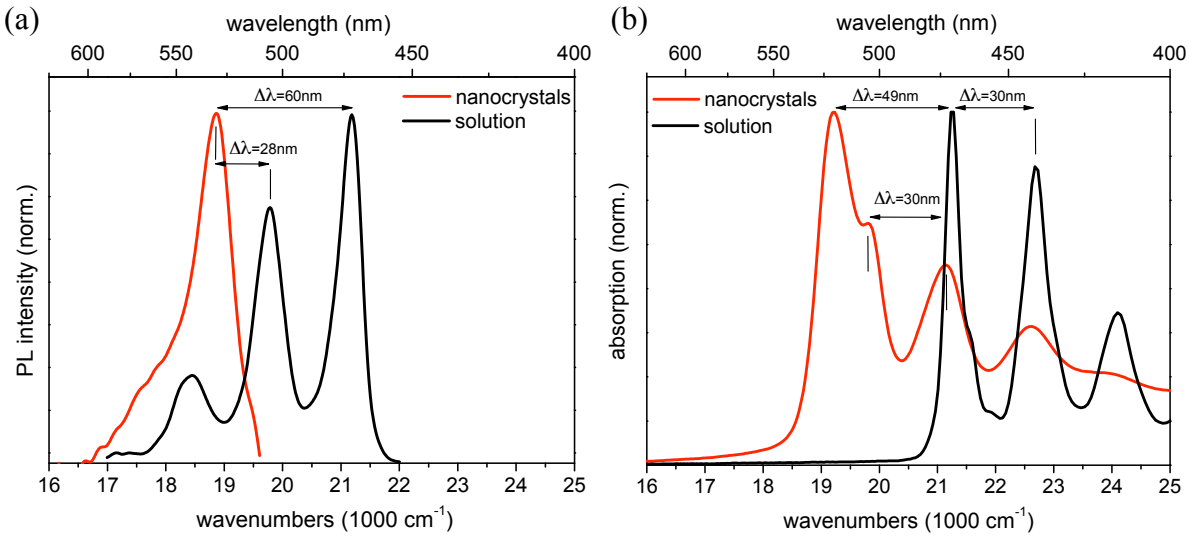

Fig. 5.10 *(a) Fluorescence spectra of dilute Tc in sebacat (black line) at a concentration of $c_{Tc} = 1.3 \cdot 10^{-5}$ mol/L and Tc nanocrystals in aqueous solution (red line) at $c_{Tc} = 8.8 \cdot 10^{-6}$ mol/L (λ_{ex} = 440 nm). The difference in the maximum positions of the spectra of the solution and the nanocrystals is 60 nm (2320 cm^{-1}). (b) Absorption spectra for the same samples as in (a). The difference in the maximal position for spectra in solution and nanocrystals is 49 nm (2040 cm^{-1}). All data were measured at room temperature and normalized.*

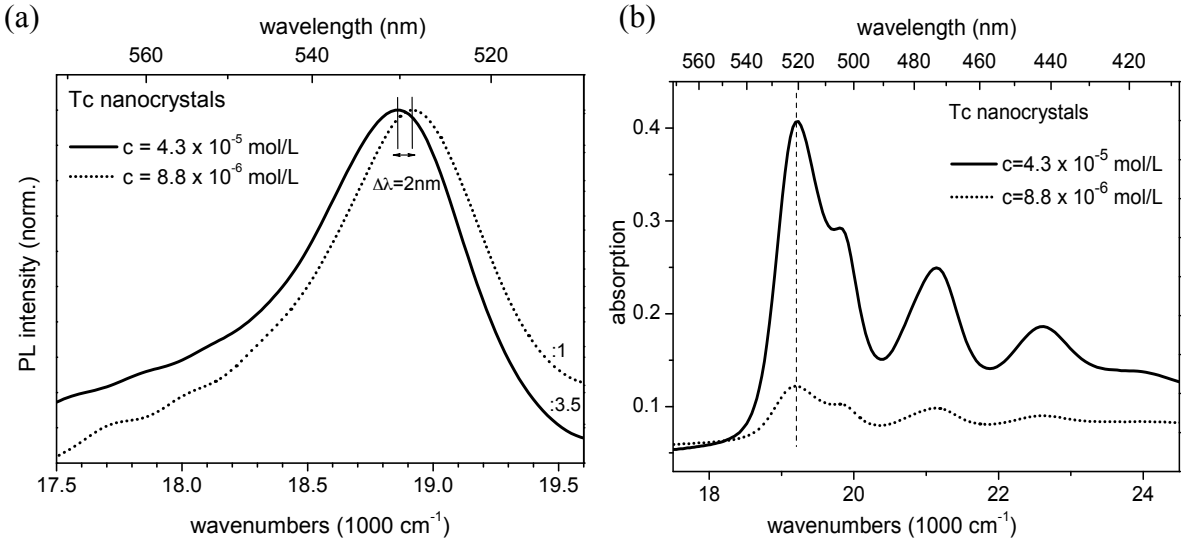

Fig. 5.11 *(a) PL spectra and (b) absorption spectra of Tc nanocrystals in aqueous solution for different concentrations. PL spectra were normalized for clarity (λ_{ex} = 440 nm).*

Fig. 5.11 (a) shows two emission spectra of Tc nanocrystals in aqueous solution prepared for two different Tc concentrations. The figure shows the shift of the maximum of the PL spectra to lower energies and an increase in the emission with an increase of the Tc concentration.

A higher concentration is assumed to result in an increase of the number of nanocrystals and it could also cause the growth of the nanocrystals of bigger size. The increase of the number of nanocrystals can result in the "inner filter effect". As a consequence, the red shift of the PL spectra for higher concentrations can be observed, as it was shown for Tc and Rub diluted in solutions (see Fig. 4.2). The author supposes that there is no influence of the "inner filter effect" in emission spectra of Tc nanocrystals due to the same factor (~ 3.5 times) on the increase in the emission and in the absorption intensities with the increase of concentration (~ 5 times) (see Figs. 5.11 (a) and (b)). However, it is not possible to completely exclude the effect of reabsorption due to partly overlapping of the absorption and PL spectra. If one excludes the influence of an "inner filter effect", then the shift of the PL spectra to lower energies with increasing Tc concentration can be attributed to the increase of the size of the Tc nanocrystals. The increase of the size of nanocrystals might be accompanied by an increase of the coupling between the molecules in nanocrystals. As a result, the shift towards lower energy levels occurs.

Notably, the low-energy-maxima of the absorption spectra do not show the shift with an increase of Tc concentration (Fig. 5.11 (b)).

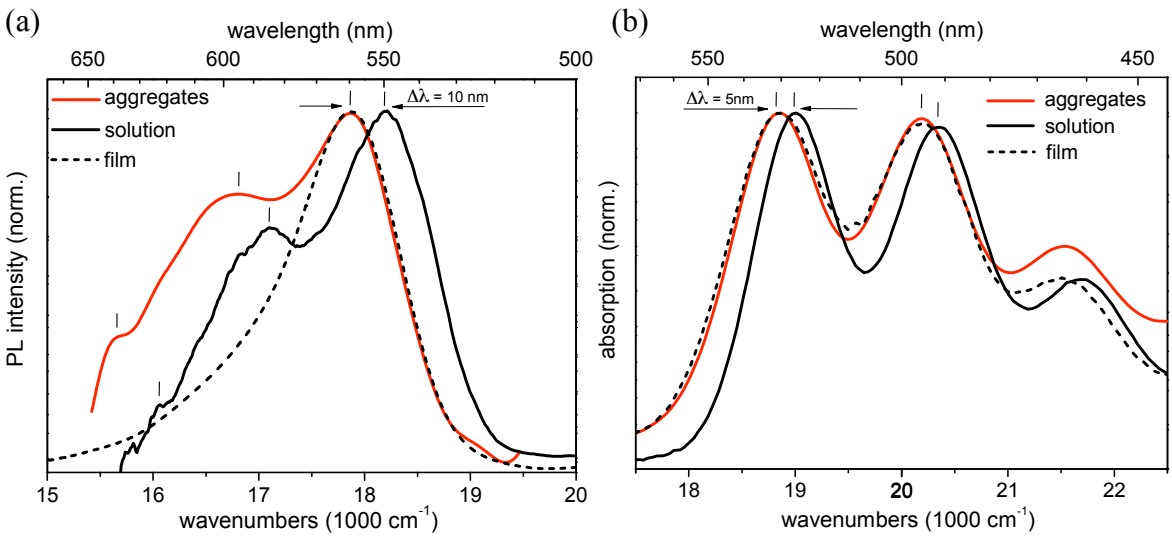

Fig. 5.12 *(a) Fluorescence spectra of dilute Rub in sebacat (black line) at a concentration of $c_{Rub} = 2.6 \cdot 10^{-6}$ mol/L ($\lambda_{ex} = 495$ nm), Rub nanoaggregates in aqueous solution (red line) at $c_{Rub} = 4.2 \cdot 10^{-5}$ mol/L ($\lambda_{ex} = 500$ nm), and a Rub film (150 nm) on the quartz glass ($\lambda_{ex} = 488$ nm). The difference in the maximum positions of the spectra of the solution and the nanoaggregates is 10 nm (340 cm^{-1}) (b) Absorption spectra for the same samples as in (a). The difference in the maximum positions of the spectra in solution and the nanoaggregates is 5 nm (150 cm^{-1}). All data were measured at room temperature and normalized.*

B. Rub

The same procedure of the nanoaggregates preparation as for Tc was applied for Rub. Figs. 5.12 (a) and (b) show the fluorescence and absorption spectra of Rub nanoaggregates suspended in water in comparison with the spectra of a monomeric Rub in solution and a Rub thin film (150 nm) on the glass. The PL spectrum of Rub nanoaggregates shows a partly resolved vibronic progression. The dominant (0-0) transition is observed at 17 860 cm^{-1}. The lower-energy peaks (16 800 cm^{-1} and 15 650 cm^{-1}) are attributed to the same optical transition. The PL spectrum of the nanoaggregates shows a 10 nm (340 cm^{-1}) red shift with respect to the PL spectrum of Rub in solution (Fig. 5.12 (a)). The absorption spectrum of nanoaggregates shows a 5 nm (150 cm^{-1}) red shift (Fig. 5.12 (b)).

The position of the high-energy maximum in the PL and the low-energy maximum in the absorption is the same for nanoaggregates and the solid film. As mentioned above, due to chirality of the Rub backbone in the gas phase, only amorphous films can grow and thus the film on glass is amourphous. In analogy, for nanoaggregates formed from Rub in solution the chirality of the Rub backbone is important, as well. It is likely that the prepared nanoaggregates are small solid molecular ensembles without structural order, similar to the amorphous thin films. This assumption well explains the same position of the high-energy maximum in PL and the low-energy maximum in absorption of the agreggate spectra and the amorphous film spectra.

As mentioned above (see section 5.3.1), by applying additional conditions such as a higher tempeature of the sample and large vapour pressure it is possible to obtain nanocrystalline films of Rub. Based on this assumption, the preparation temperature was increased in order to give to the system additional energy for planarisation of the twisted Rub backbone (see details in section 3.6). Fig. 5.13 (a) shows PL spectra for two different preparation temperatures (298 K and 333 K). The spectra show a 2 nm shift in direction of low energies for preparation at a higher temperature (333 K). A follow-up increase of the preparation temperature by 20 K results in an additional 2 nm shift in lower energy direction of the PL emission peak (see Fig. 5.14). Further increase of the preparation temperature was not possible due to the low boiling point of the solution.

The red shift of the spectra with increasing preparation temperature has been attributed to reduction of the chirality of the Rub backbone, which leads to an increasing interaction between the neighbour molecules (so-called “solvent shift” [38]). Note that the absorption spectrum is shifted in lower energy direction in case of higher preparation temperatures as well (Fig. 5.13 (b)).

In addition, a comparison of PL spectra of Rub nonoaggregates in aqueous solution for two different concentrations shows a red shift (~ 1 nm) of the PL spectrum with an increase of the Rub concentration (see Fig. 5.15) similar as in the case of Tc aggregates (see Fig 5.11 (a)).

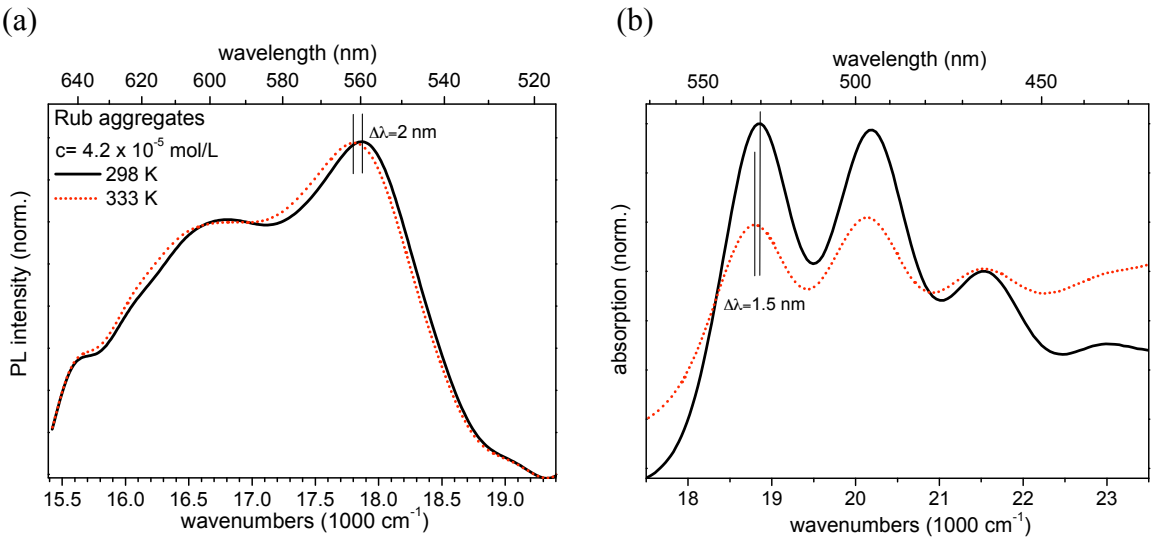

Fig. 5.13 *Influence the preparation temperature on the spectral properties of Rub nanoaggregates in aqueous solution at a concentration of c_{Rub} = 4.2·10^{-5} mol/L. (a) PL spectra (λ_{ex} = 500 nm) and (b) absorption spectra of Rub nanoaggregates in aqueous solution. The black solid lines are the spectra at 298 K preparation temperature. The red dashed lines are the spectra at 333 K preparation temperature. The spectra were normalized.*

As in the Tc case, if one excludes the influence of the "inner filter effect", the shift to lower energies with increasing Rub concentration can be attributed to the increase of the size of the Rub nanoaggregates. The increase of aggregates size is accompanied by an increase of interaction between the molecules in aggregates, which results in a red shift of the spectra. If one excludes the influence of the "inner filter effect", it is supposed that this shift has the same origin as the red shift of PL spectra with the increase of the Rub film thickness (see section 5.3.3). The influence of size of Rub nanoagreggates on the fluorescence yield was reported in the literature (see detail in Ref. [60]). The size of Rub nanocrystals was varied between 25 nm and 800 nm. Here, the PL spectra of Rub nanoaggregates of different sizes do not show a shift of the position of the PL maximum as it was observed in our study (see Fig. 5.15). Unfortunately the sizes of Rub nanoagreggates investigated in our experiments were not measured due to technical reasons. Therefore future spectral measurements of Rub nanoaggregates prepared in different Rub concentrations might be helpful to clear the origin of the shift observed in this study.

The PL spectrum of Rub single crystals at low temperature does not show the expected red shift in comparison to the spectrum of amorphous Rub film (see Fig. 5.16). This observation is explained by the different conformations of the Rub molecules in the amorphous and the crystal phase with a twisted and a planar structure of the Tc-backbone, respectively. A detail discussion about the effect of different molecular conformations on the HOMO-LUMO gap is presented in section 4.4.6.

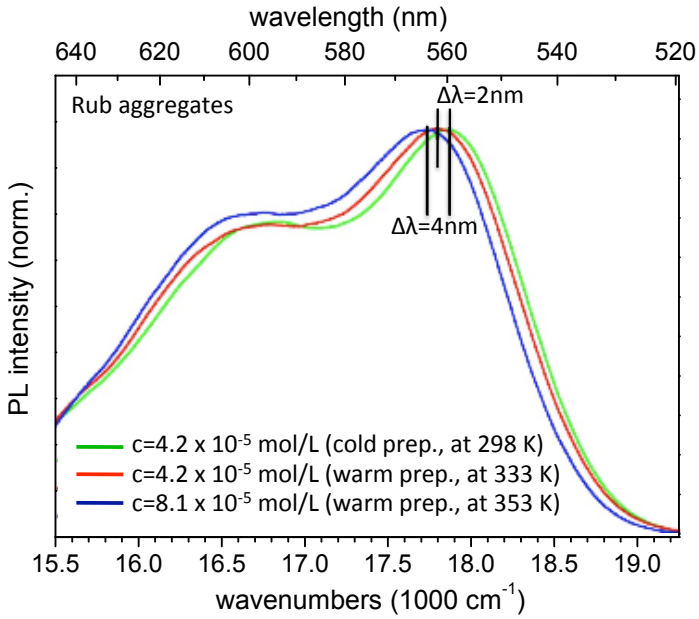

Fig. 5.14 *Influence of the preparation temperature on the spectral properties of Rub nanoaggregates in aqueous solution [59]. Rub concentrations and preparation temperature were varied. The green line shows the PL spectrum of the sample at 298 K preparation temperature (cold pr.) and at concentration* $c_{Rub} = 4.2 \cdot 10^{-5}$ *mol/L* ($\lambda_{ex} = 500$ *nm). The red line shows the spectrum of the sample at 333 K preparation temperature (warm pr.) and at* $c_{Rub} = 4.2 \cdot 10^{-5}$ *mol/L* ($\lambda_{ex} = 500$ *nm). The blue line shows the spectrum of the sample at 353 K preparation temperature (warm pr.) and at* $c_{Rub} = 8.1 \cdot 10^{-5}$ *mol/L* ($\lambda_{ex} = 500$ *nm). The spectra were normalized.*

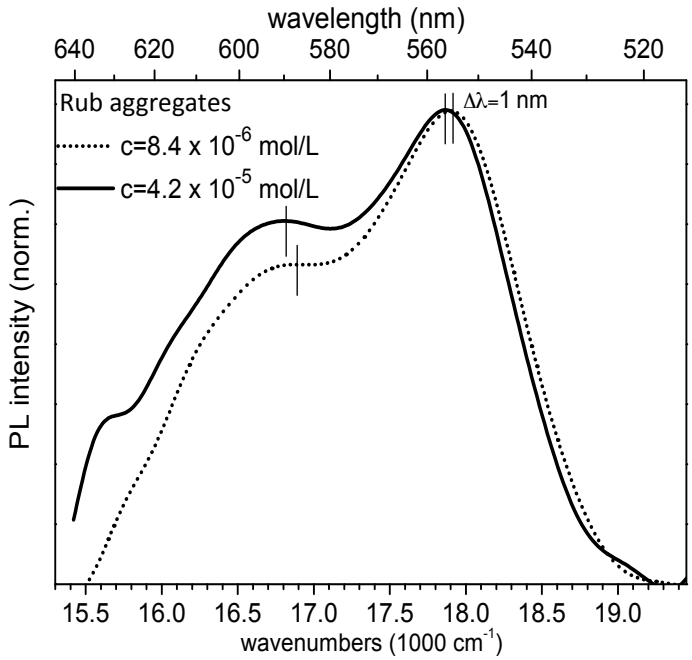

Fig. 5.15 *Fluorescence spectra of Rub nanoaggregates in aqueous solution for different concentrations. The author does not have any information about the size of investigated Rub nanoagreggates. The spectra were normalized.*

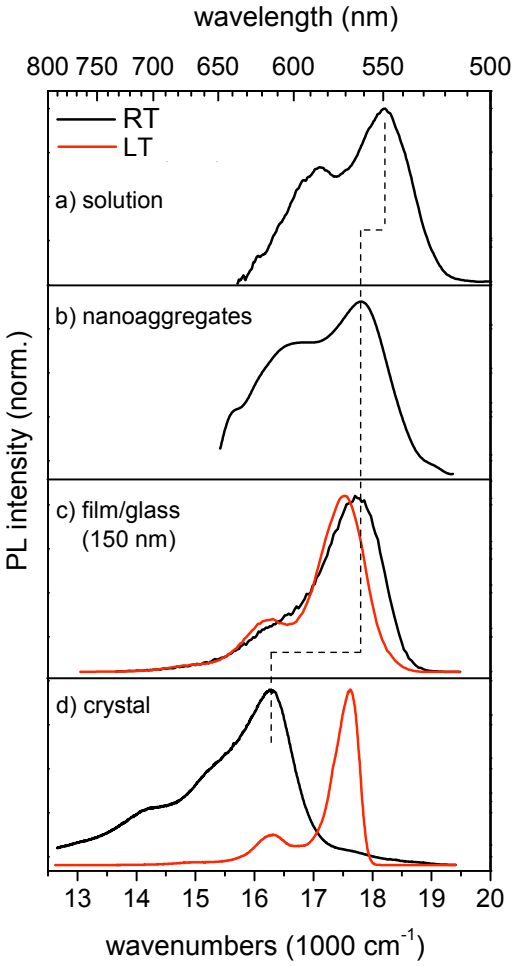

Fig. 5.16 *PL spectra of a) Rub in solution with $c_{Rub} = 2.6 \cdot 10^{-6}$ mol/L ($\lambda_{ex} = 495$ nm) at room temperature (RT), b) nanoaggregates $c_{Rub} = 4.2 \cdot 10^{-5}$ mol/L at 333 K ($\lambda_{ex} = 500$ nm), c) Rub film (150 nm) on glass ($\lambda_{ex} = 488$ nm) at room temperature (RT, 291 K, black line) and at low temperature (LT, 10 K, red line), d) Rub single crystal ($\lambda_{ex} = 450$ nm) at RT (black line) and LT (red line). The spectra were normalized.*

5.4 Conclusions

It was observed that vacuum deposited Rub films on quartz glass or $AlO_x/Ni_3Al(111)$ are only amorphous. A red shift of the PL spectra of Rub film at low temperatures may indicate a phase transition or a conformational change of the Rub molecules. In contrast to thin Tc films, the ultrathin Rub films on the epitaxial AlO_x show PL down to the monolayer range. This observation indicates that the assumption that the additional phenyl groups inhibit the ultrafast quenching by charge transfer to metal states is correct. The luminescence spectra shift gradually to lower energies with increase of the film thickness. This is likely related to an increased coupling between the Rub molecules with film thickness. In addition, the influence of the preparation temperature and concentration on the spectral properties of Rub nanoaggregates in aqueous solution has

been studied. The same procedure of the nanoaggregate preparation as for Tc was applied for Rub as well. Due to the chirality of the Rub backbone, the prepared nanoaggregates are small solid molecular ensembles, without long range order in the structure, similar to the amorphous thin films. The red shift of the spectra with increasing preparation temperature has been attributed to a reduction of the chirality of the Rub backbone, which leads to an increase of the coupling between the Rub molecules. In addition, a comparison of PL spectra of Rub nanoaggregates in different concentrations shows the red shift of the PL spectrum with an increase of the Rub concentration (see Fig. 5.15) as well as in the Tc aggregates case. The shift to lower energies with increasing Rub concentration can be attributed to the increase of the size of the Rub nanoaggregates. The increase of aggregate size is accompanied by the increase of the interaction between the molecules in aggregates, which results in a red shift of the spectra. This shift, as assumed, has the same origin as the red shift of PL spectra with the increasing thickness of the Rub film.

6 Optical investigations of Rub single crystals

6.1 Introduction

As mentioned above, several years ago, single crystals of Rub were found to exhibit a high charge carrier mobility in organic field effect transistors [1]. At that time, the origin of the surprising high charge mobility was not clear. This motivated worldwide large scientific interest in the subject. Additionally, the detailed optical properties of Rub crystals were not known at that time. This motivated an investigation of the optical properties of Rub in our lab, as well as several investigations in other scientific groups [49] [50] [61] [62] [63].

In particular, we observed for the first time that the fluorescence spectra of Rub single crystals show an interesting temperature dependence. Understanding the nature of the observed strong variation of the Rub crystal fluorescence could help to comprehend more fully the optical properties of Rub as a material, which is interesting from fundamental as well as applied aspects. This motivated us to perform additional investigations by time-resolved (see Chapter 7) and excitation photoluminescence measurements (see section 6.6 of this Chapter).

6.2 Overview on PL, absorption, and photoluminescence excitations measurements

PL and absorption measurements

The experimental set-up for continuous wave (cw) photoluminescence and absorption measurements on crystals consisted of a cryostat with the sample under vacuum, a blue light emitting diode (LED, 0.4 A, 8 V) with an emission maximum at about 450 nm as the excitation light source for photoluminescence measurements, and a halogen lamp (12 V) as incident light for absorption measurements (see Fig. 6.1). The spectra were recorded with a 0.3 m-spectrometer (SpectraPro 2300i) equipped with a liquid-nitrogen-cooled CCD camera (T = -100 °C). A grating with 300 grooves mm^{-1} was used. The spectral resolution of the spectrometer is 0.63 nm.

For the optical measurements, a Rub single crystal was mounted on a copper plate in front of a small circular aperture. The single crystal was fixe with a very tiny amount of grease such that the crystal covered the aperture (diameter ø = 1.2 mm) completely. It was mounted as freely as possible (at one point of a small area) to minimize the strain, which occurs during changes of the temperature of the sample. An additional aperture of the same

size was used for the measurements of the incident intensity in the absorption experiment. Then the cooper plate was fixed in the sample holder and installed into the cryostat (vacuum about 10^{-5} Torr). The sample holder was made of electrolytic copper and could be cooled with liquid He to 5 K via a cryostat heat exchanger.

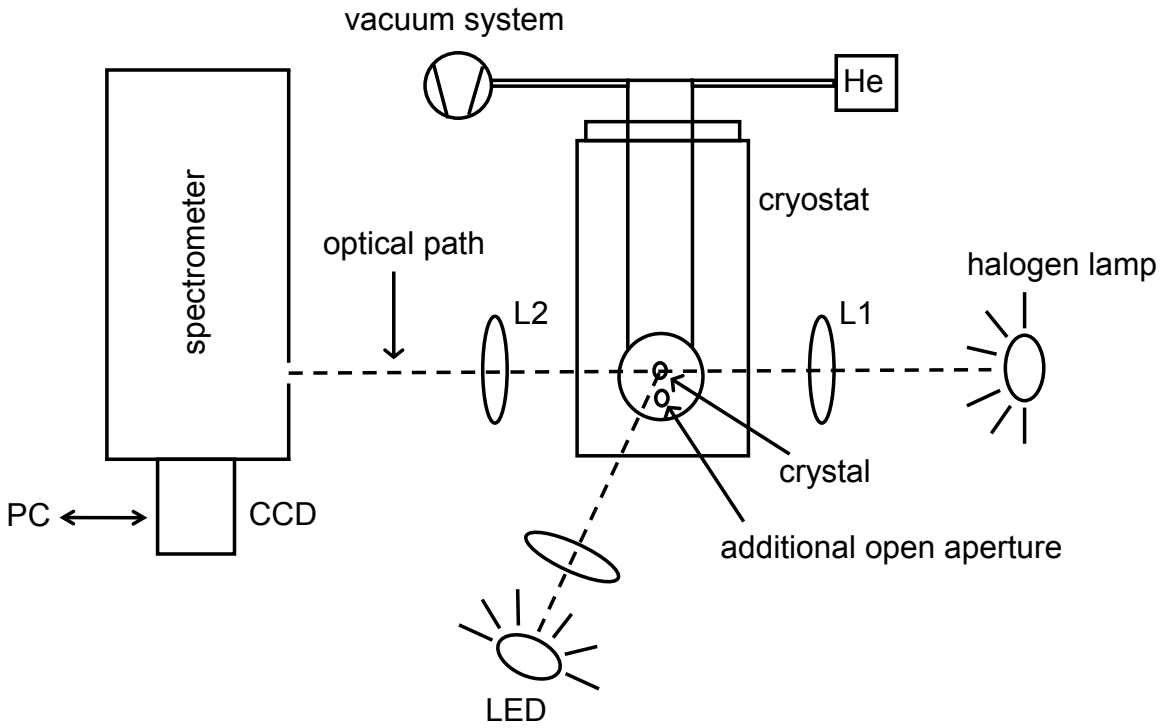

Fig. 6.1 *Schematic diagram of the optical experimental set-up for cw photoluminescence and absorption measurements on Rub crystals.*

The velocity of the cooling of the sample was 1 K per minute. After the desired temperature was reached, we always waited 10 minutes in order to maintain the same time interval between measurements and in order to have the same influence of the temperature change in every measurement step. The temperature control system worked with an accuracy of about 0.5 K. A constant temperature was maintained by a combination of electrical heating the sample holder and cooling by He flow.

With the lens L1 (silicate lens, focus f = 100 mm,) the incident light of the halogen lamp was imaged onto the sample. With the lens L2 (silicate lens, focus f = 100 mm) the luminescence light was imaged on the entrance slit (size = 20 μm) of the spectrometer (see Fig. 6.1). The optical equipment (system of lenses and the sample) has been installed in such a way that the image of the crystal on the entrance slit had a size of about 5 times lager than the real crystal. The size of the circular aperture with Rub crystal on it was 1.2 mm and the image size was about 5 mm as a result of that magnification. Due to the thermal contraction of the sample holder during temperature dependent measurements, the image of the crystal on the entrance slit slightly shifted. It was necessary to readjust

the position of the sample while looking at the image of the sample on the entrance slit. This adjustment was easier to do with the obtained bigger image size on the entrance slit.

An yellow filter (WP 545, no transmission below 500 nm) in front of the entrance slit of the spectrometer was used for the fluorescence measurements to protect the CCD camera from an emission of LED.

The spectra were obtained in the form of intensity per wavelength interval. To present optical spectra on the wavenumbers scale, the required intensity correction was made (see Appendix 4.1). The spectrometer wavelength calibration was done by a Xe pin lamp spectrum. The spectrum of the Xe lamp and a correlation between measured and real spectral positions is presented in Appendix A.2. Some small deviations in the spectral positions of the maxima of the PL spectra measured in the different sets of our measurements and also in the literature have been observed (see Appendix A.3). Those deviations we attributed to experimental artefacts in wavelength calibrations of the optical detectors. The intensity calibration of the PL measured spectra due to the sensitivity of the detection system is described in Appendix A.4.

Photoluminescence excitations (PLE) measurements

The schematic diagram of the experimental set up used for the PLE measurement is presented in Fig. 3.8

The PLE experiment includes measurements of the PL spectra by scanning the excitation wavelength with 2.5 nm steps. Selectively excited PL spectra were obtained using the Xe short arc lamp (1000 W) with the excitation monochromator set at a particular wavelengths. The excitation wavelength was scanned between 400 nm and 600 nm, i.e. in the spectral region where the absorption spectrum of Rub crystal was observed. PLE spectra were received by analyzing the PL signal as a function of the excitation wavelength at a fixed detection wavelength with the Spectra2 program package [64]. All the PLE spectra were corrected for the output intensity of the Xe lamp. The incident intensity calibration was done with the Optical Power Meter System PM 20. The spectra were recorded with the spectrometer SpectraPro 2300i. A yellow glass filter (OG-525, transmission range > 525 nm) for excitation wavelengths from 400 to 515 nm and a grey glass filter (transmission = 0.005) for excitation wavelengths above 515 nm were positioned in front of the entrance slit of the spectrometer to decrease the intensity of the incident light and to protect CCD camera. A violet glass filter (transmission range > 334 nm) for excitation wavelengths from 400 to 470 nm was positioned in the optical path directly after the Xe lamp to sort out emission lines of different spectral orders from the light source.

Rub single crystals were fixed on the substrate (Ni_3Al) in the glass head in the UHV chamber. The PL light of the sample was imaged on the entrance slit of the spectrometer by the lens 1 (L1, silicate lens, f = 100 mm, ø = 50.8 mm) and the lens 2 (L2, silicate lens, f = 300 mm, ø = 50.8 mm).

6.3 Overview on the temperature evolution of the optical characteristics

PL, PLE, and polarized and angle-resolved absorption spectra were measured as functions of the crystal temperature. The spectra were measured in temperature intervals from 300 K to 5 K with steps of 10 K. Normalized time-integrated fluorescence and absorption spectra of Rub single crystals as functions of temperature are displayed in Fig. 6.2. The Rub crystal shows partially resolved vibrational structure in the absorption and fluorescence spectra.

Photoluminescence

As presented in Fig. 6.2 the luminescence spectrum of the Rub crystal shows distinct reversible variations with temperature. These are accompanied by a very strong (about 6 500 fold) increase of the luminescence intensity during the cooling of the sample from room temperature to 5 K (see Fig. 6.5).

In the temperature range above 200 K the maximum emission occurs at wavenumbers around 16 370 cm^{-1} and is denoted on Fig. 6.2 as peak **c**. The highest energy PL transition is represented as a small shoulder in the PL spectrum. As the single-components-fit shows, this shoulder includes two single components at 17 720 cm^{-1} and 17 140 cm^{-1}. They are denoted by **a** and b_1 (or b_2 for low temperatures), correspondingly (see section 6.4, Fig. 6.3).

In the literature [49], peak **c** is attributed to a kind of self-trapped state. The high-energy shoulder is attributed to the free exciton emission [49]. However the presence of two single components in the shoulder and the existence of a gap between the excitation energy and the luminescence (see section 6.9) make this interpretation of high-energy shoulder questionable. Based on the different optical analysis two possibilities to describe the relaxation mechanism in Rub crystals will be discussed (see section 6.6).

The emission spectrum shows several additional partly resolved maxima at lower energies, at about 15 540 cm^{-1} (peak **e**) and at about 14 180 cm^{-1} (peak **f**). The components **e** and **f** are attributed to the vibrational sidebands of the **c** band due to the same temperature dependence (see Fig. 6.5).

As Fig. 6.2 shows, the ratio between spectral maxima changes during the cooling. At temperatures above 150 K, the component **b** is just slightly notable and is marked as b_1. But at temperatures below 150 K the peak of the component **b** starts to be well resolved, and is marked as b_2. Below 80 K, the component b_2 starts to play a dominant role in the emission. Two maxima at 5 K (peak b_2 at 17 520 cm^{-1} and peak **d** at 16 160 cm^{-1}, see Fig. 6.2) are attributed to the same family of vibronic levels due to the same temperature dependence (see Fig. 6.5).

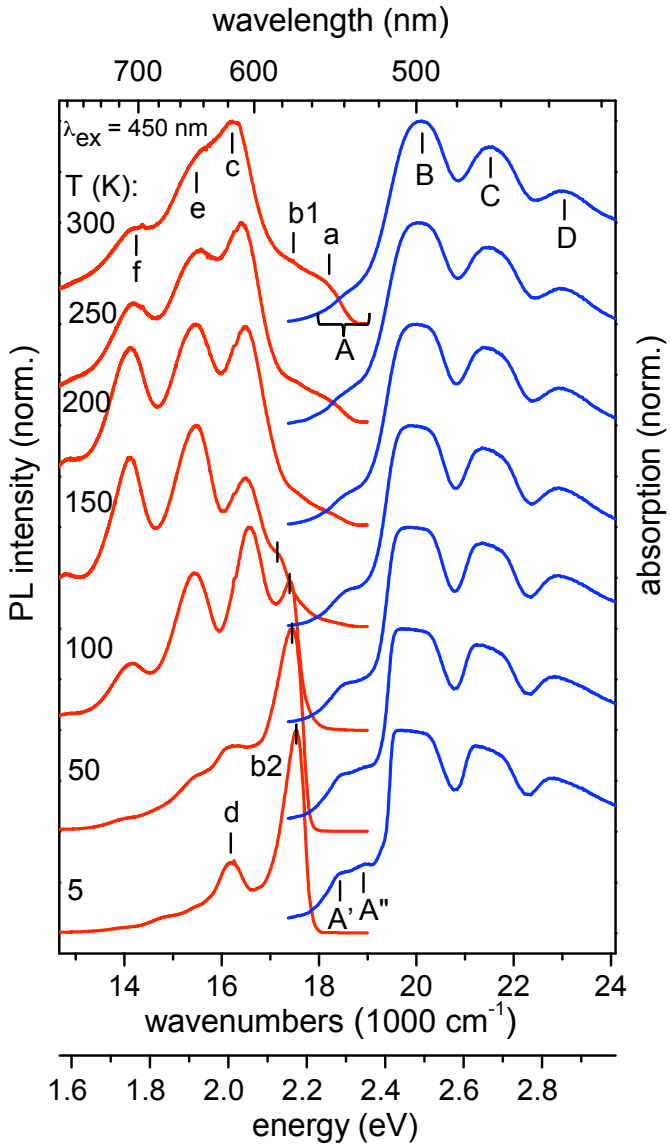

Fig. 6.2 *PL spectra (red lines) and absorption spectra (blue lines) of a Rub crystal at different temperatures. The absorption spectra were recorded at normal incidence with unpolarized light. The spectra were normalized and shifted vertically against each other for clarity. Seven different temperatures between 300 K and 5 K are presented. The light source for the PL measurements was a LED with maximum emission at 450 nm. For the absorption measurements, a halogen lamp was used as a source of the continuous spectrum in the visible range. The absorption (see eq. 6.1)* $A_{B\ at\ 300\ K} = 1.32$ *at maximum B in the absorption spectrum for 300 K.* $A_{B\ at\ 5\ K} = 1.6$ *at maximum B in the absorption spectrum for 5 K.* $A'_{A'\ at\ 300\ K} = 0.18$ *at maximum A' in absorption spectrum for 300 K.* $A_{A'\ at\ 5\ K} = 0.45$ *at maximum A' in absorption spectrum for 5 K.*

Absorption

The absorption spectrum shows partly resolved vibronic progression with main peaks at 20 080 cm^{-1} (2.49 eV), 21 500 cm^{-1} (2.67 eV), 23 000 cm^{-1} (2.85 eV) and a weak shoulder at 18 550 cm^{-1} (2.3 eV) at high temperatures (see Fig. 6.2, peaks B, C, D and A,

correspondingly). The low-energy shoulder (peak A) is attributed to the zero-phonon (0-0) transition. In comparison to the emission spectrum, the absorption spectrum as a function of temperature shows only some small changes. In particular, the intensity of the absorption slightly increases at low temperatures (see details in the caption of Fig. 6.2). Fig. 6.2 shows an obvious increase of the intensity of the low-energy shoulder (peak A) during the cooling of the sample. At temperatures below 100 K, it is possible to see that the shoulder consists of two components, which are denoted as A' and A''. In addition, the absorption progression has a more pronounced shape at low temperatures.

The increase of the absorption explains the inaccuracy in the shape of the highest maximum B (about 20 080 cm^{-1}), which starts to be slightly flat at temperatures from 150 K to 5 K. This "flat" maximum is an effect of a full absorption of the incident light of the halogen lamp in the wavelength area, where the absorption is maximal. I.e. the intensity of the incident light of the halogen lamp was too small. As a result, the light was fully absorbed in some wavelength intervals. The absorption was calculated from eq. 6.1 [40]:

$$A = \log\left(\frac{I_0}{I}\right), \tag{6.1}$$

where A is the absorption, I_0 is the measured incident light intensity and I is the measured transmitted intensity, which passed through the sample.

Generally, the absorption mechanism stays independent of the temperature, but the emission mechanism shows to be strongly dependent on the sample temperature.

6.4 Single components fit of PL spectra at different temperatures

For the separation and analysis of the included components in the PL spectrum a single-components-fit of the spectrum (CasaXPS program) was used. The fit for different temperatures is shown in Fig. 6.3. Symmetrical Voigt functions (convolution of Lorentzian and Gaussian functions) have been used to describe all individual components, except the component b. The high-energy-maximum (component b) in the PL spectrum at low temperatures can be successfully fitted by two symmetrical Voigt functions or by one asymmetrical Voigt function. Therefore, an asymmetrical Voigt function was chosen for the single component analysis. The fit was done with the minimal variation of the single component positions. Input fit parameters, as the height and the full width at half maximum (FWHM) of the single components, were varied.

At room temperature, the most suitable fit of the PL spectra includes six single components. Components a and b are creating the high-energy shoulder in the PL spec-

trum. Component c is responsible for the highest maximum in the luminescence at high temperatures. Components d, f and g are further components at lower energies. During the cooling process the integral intensities of the single components change. Some of them disappear, e.g., component a. Some of them appear, e.g., components d (at 170 K), and h (at 230 K). During the cooling, the intensity of component b strongly increases and at temperatures below 100 K, this component plays a dominant role in the luminescence (see Fig. 6.3).

The positions of single components on the energetic scale and variations of them for different temperatures are presented in Fig. 6.4. As shown there, the central positions of some components undergo small changes with temperature, e.g. component b. Component b has been split into the two components (b_1 and b_2) due to the difference in their temperature dependent behaviour. Component b_1 in the temperature interval from 300 K to 160 K does not show an energetic shift. Component b_2 in the temperature interval from 150 K to 10 K slightly shifts to higher energies during the cooling. Component c shows a small shift in its position as well. For the component c a shift to higher energies upon cooling in the region from 300 K to 230 K is observed, whereas its position is a constant for lower temperatures.

Fig. 6.5 shows the temperature evolution of the emission intensities of the single components. The intensity values are represented on a logarithmic scale. As shown in Fig. 6.5 the emission rate of the components increases with cooling of the sample. In addition, it is possible to see that the temperature dependent intensity behaviour is the same for some of the components (see Fig. 6.5). Based on this observation, three groups of components can be distinguished. The first group (I) includes the components a and b_1, which are only visible above 150 K. The second group (II) includes the components b_2 and d, which are only visible below 150 K. Finally, the third group (III) includes the components c, e, f, and g. These components can be seen in a wide temperature region. The component c is visible in the region from 300 K to 30 K, the component e is visible in the region from 300 K to 10 K, the component f is visible in the region from 300 K to 50 K and the component g is visible in the region from 300 K to 100 K.

The components of the first group show an increase of intensities during the cooling. Both components of the first group have a quite weak intensity, which results in errors in the precision of the fit. The second group shows the strongest increase of the intensity during the cooling in comparison to the other groups. From 50 K, the rate of emission increase slows down with some “saturation” between 20 K to 10 K, where the intensity ceases to increase. The third group, except component g, shows a strong increase of intensity down to 70 K with a following decrease of intensity during the cooling.

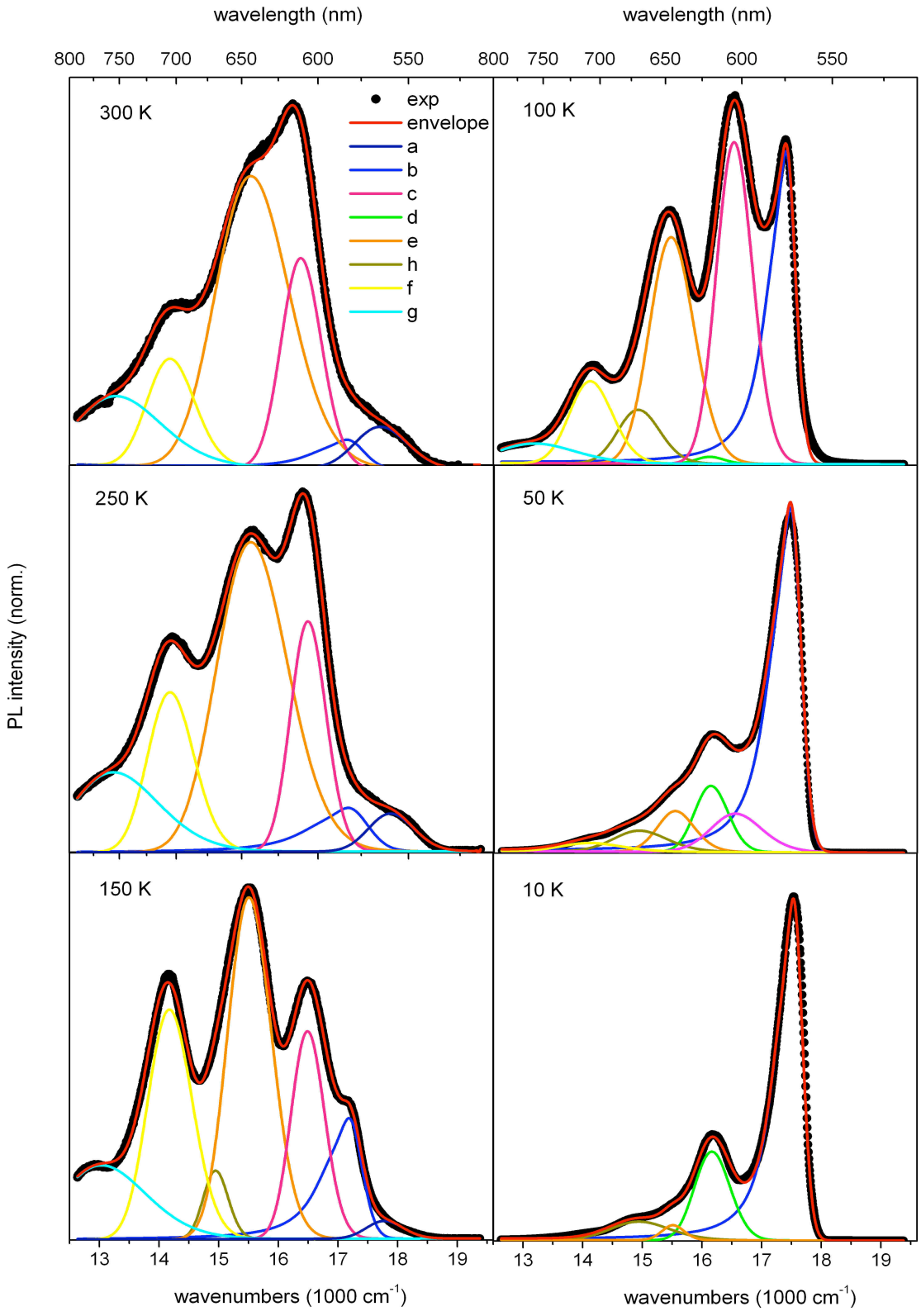

Fig. 6.3 *Fit of PL spectra at different temperatures with single components (Crystal A). The black dots mark the experimental spectra, the red curves mark the envelope of the single components. The spectra were normalized. The wavelengths of the central positions of the single components were allowed to vary slightly at different temperatures (see Fig. 6.4).*

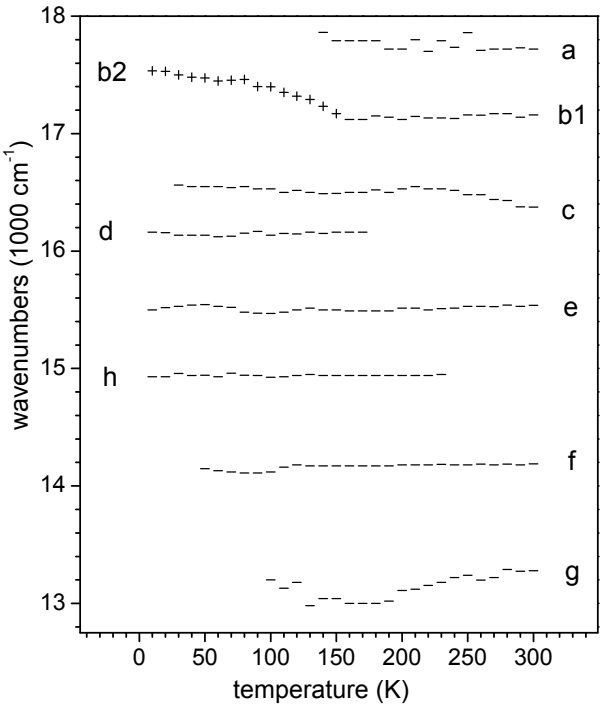

Fig. 6.4 *Variation of the positions of the single components at different temperatures for the fits shown in Fig. 6.3.*

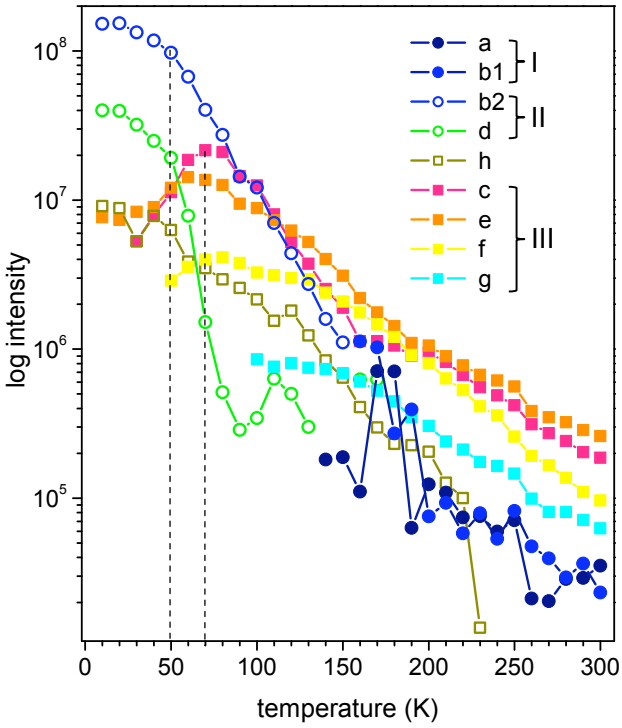

Fig. 6.5 *Temperature dependency of logarithmic integral intensity of the single components. Three groups of components can be distinguished based on the similarity in the temperature dependent intensity behaviours. Additionally, two dotted lines mark the similarity for group II and for group III in the observation.*

The components with the same temperature dependent PL intensity behaviour presumably have a similar origin of the luminescence. The luminescence transition nature of the classified groups will be discussed later, in Chapters 6 and 7.

6.5 General mechanism of excitation relaxation in the system with strong exciton-phonon coupling

The emission is a result of the competition between the intrinsic de-excitation processes (e.g, non-radiative relaxation), different channels of self-trapping of the excitation with following emission (e.g, due to excimer formation, defects, or self-trapping), and the emission from a molecular excited state (e.g, free exciton emission). The probabilities of these processes are strongly dependent on the sample temperature. In this section different kinds of relaxation processes in dependence of the temperature of the sample are described. To describe the temperature evolution of luminescence properties of Rub crystals, models based on the assumption that a Rub crystal is a system with strong exciton-phonon interaction are discussed. This assumption is in agreement with a suggestion of strong exciton-phonon coupling in Rub crystal reported in the literature [75]. In a system with strong exciton-phonon coupling, excitons can be trapped by lattice distortions produced by the excitons themselves [65]. Those trapped excitons are called self-trapped excitons (STE). The adiabatic potential energy curve applicable to a system with strong exciton-phonon interaction has two minima corresponding to the free exciton state and the self-trapped excited state [65] as shown schematically in Fig. 6.6.

After excitation with photon energies higher than the energy of the first exited state, excitons are generated above the free exciton band bottom. The photoexcited excitons relax via one of the following channels, as presented in Fig. 6.6:

Channel 1 is the vibrational relaxation to the lowest vibrational level of the excited state. Channel 2 indicates the direct relaxation of excited excitons towards the self-trapped exciton state.

After vibrational relaxation to the band bottom F of the exciton state (channel 1), there are several follow-up energy relaxation channels. Channels 3 and 4 represent indirect trapping processes, a non-radiative climbing process over the barrier and a tunnelling process through the barrier. Excitons that have climbed over the self-trapping barrier and have passed through the barrier, slip down along the potential curve of the ST state.

Channels 5 and 6 represent radiative decay process of free excitons and self-trapped excitons, respectively.

Channels 7 and 8 are non-radiative relaxation channels to the ground state.

In this system, the dominant loss of the excitation at higher temperatures is due to the emission from the self-trapped (ST) state and non-radiative recombination. The mechanism of the excitonic processes can be explained on the basis of several assumptions. In aromatic molecular crystals with strong exciton-phonon coupling two channels of self-trapping of excitons exist – a direct self-trapping and an indirect self-trapping [66]. It was found that the direct self-trapping rate is high at high temperatures (channel 2) [66]. At the same time, some of the excitons relax to the free exciton band bottom. At high temperatures, the thermal energy is high enough to overcome the potential barrier between the free and the self-trapped state. The necessary energy is represented by E_B as the self-trapping potential barrier. After the climbing process the excitons get to the lowest vibrational level of the self-trapped state due to a fast vibrational relaxation. Finally, they loose the exitation energy by emission from the ST state or due to the non-radiative recombination (channels 6 and 8, see Fig. 6.6). The reverse process needs the higher activation energy. This energy is equal to the sum of E_B and E_{ST}.

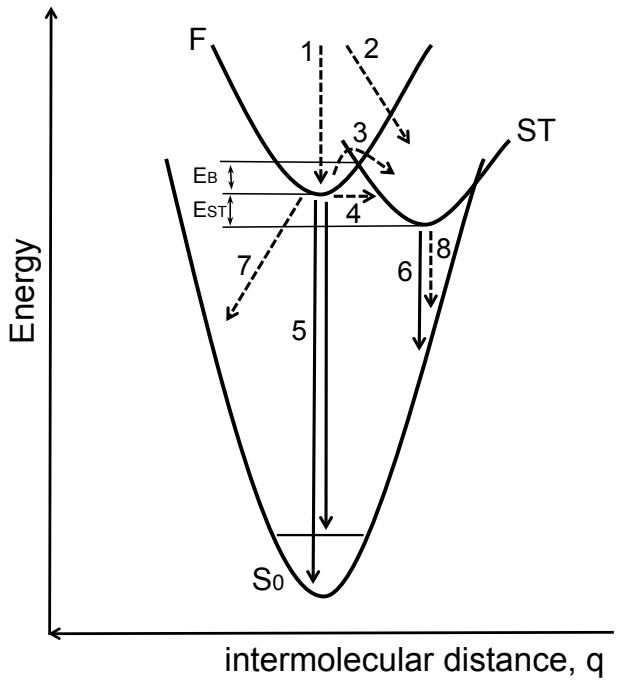

Fig. 6.6 *Schematic potential energy diagrams of the free exciton (F), self-trapped (ST) states and ground (S_0) state in aromatic molecular crystals with strong exciton-phonon coupling (based on Ref. [65]). E_B represents the height of the self-trapping potential barrier between the free exciton state and the self-trapped state, E_{ST} is the self-trapping depth. Channel 1 is vibrational relaxation to the lowest vibrational level of excited state. Channel 2 is a direct self-trapping process. Channel 3 represents a climbing process over the barrier between potential curves of free and self-trapped states. Channel 4 represents the tunnelling process through the barrier. Channels denoted as 5 and 6 indicate a radiative decay process of free excitons and of self-trapped excitons, respectively. Channels 7 and 8 represent non-radiative decay processes from free exciton and self-trapped states to the ground state.*

Matsui showed that in crystals with a strong exciton-phonon coupling the direct self-trapping rate decreases as the temperature is reduced [66]. This means, that at lower temperatures the number of excitons reaching the band bottom of the exciton band increases. From another point of view, the temperature of the sample reaches a point during the cooling, where the thermal energy is no more large enough to activate free excitons to cross the potential barrier between the free exciton state and the self-trapped state. This means, that at low temperatures most exciton relaxations occur from the free exciton state (channel 5 and 7).

Additionally, Matsui [65] suggests that in strong exciton-phonon coupling systems, the free exciton state is a metastable excited state and the self-trapped excited state is a stable excited state. Therefore, it can be concluded that the excitons from the metastable F state relax with high probability into the more stable ST state. Hence, only the ST state will be occupied. This suggestion is in agreement with our interpretation of the PL spectra of Rub crystal at room temperature (see detail in section 6.6)

6.6 Interpretation of the temperature dependency of PL spectra

In this section the temperature depending competition between two transitions are analysed - the single component b (b_1 and b_2) (at about 570 nm) as the strongest component of the PL spectrum at low temperatures and the single component c (at about 610 nm) as the strongest component of the PL spectrum at high temperatures.

Experimental data

Fig. 6.7 shows the experimental temperature dependency of the integrated intensity of the single component b, which is assigned to the emission from state F' (=F) (see schematic energy diagrams in Fig. 6.9 and discussion below). The intensity of the component strongly increases with decreasing temperature.

Fig. 6.8 shows the experimental temperature dependent intensity of the single component c, which is assigned to the emission from ST state (see schematic energy diagrams in Fig. 6.9). The emission from the self-trapped state increases by cooling at temperatures from 300 K to 80 K. By further cooling (from 80 K to 30 K), the intensity of the ST emission decreases.

Models

To simplify the fit model and therefore the number of variable fit parameters, the temperature dependent competition between only these two components has been considered. Fig. 6.9 represents two models of excitation relaxation mechanisms in Rub crystals, which were developed in the frame of this study. In both models the excitation relaxation mechanism is based on the assumption that the Rub crystal is a system with a strong

exciton-phonon interaction (see section 6.5), where excitons can be self-trapped by a lattice distortion produced by the excitation itself. In the system with strong exciton-phonon interaction the self-trapped state is below the free exciton state and there is a barrier between the potential curves of the free and the self-trapped states. In both models, the excitation relaxation mechanism at high temperatures is dominated by non-radiative recombinations and the emission from the self-trapped state. The principal difference between the models is in an interpretation of the low temperatures emission:

Model 1

We attributed the component b (b$_1$ and b$_2$) in the PL spectra of the Rub crystals to the free exciton emission, which occurs upon excitation of first excited state S_1 (see Fig. 6.9, Model 1). As mentioned in Chapter 2, the optical HOMO-LOMO transition in Rub crystals is dipole-allowed and is oriented along the short axes of the Rub molecules. The transition dipole moments are all parallel to the c direction and perpendicular to the ab plate of the crystal (Fig. 2.3). Upon excitation, the strong c-polarized emission propagates in all direction parallel to the ab surface [67]. Therefore, the amount of the c-polarized PL light detected in the direction perpendicular to the ab surface of the crystal is quite small, as it was observed for PL spectra of the Rub crystals at high temperatures (component b$_1$, see Fig. 6.2). The observation of the c-polarized PL light in the direction perpendicular to the ab surface was explained by possible experimental effects, such as a small deviation of the acceptance of the detection from the perpendicular direction or surface defects. These surface imperfections can cause scattering of the c-polarized light leading to a redirection of the light into the detection system [67].

As mentioned above, the component c is assigned to the emission from the ST state. As the temperature is reduced, the direct self-trapping rate decreases. In addition, at low temperatures, the thermal energy is not high enough to activate excitons to cross the potential barrier between the free exciton state and the self-trapped state. We explained the very strong increase of the luminescence of both components below 175 K (see Fig. 6.7) by a decrease of the non-radiative recombination rate.

In addition, the very strong increase of the luminescence of component b below 175 K can be explained by a possible phase transition (F→F'). Model 1 describes the high and low temperature phases of Rub, which have different dynamic evolutions after excitation (F = free exciton state at high temperatures and F' = free exciton state at low temperatures). A signature of the phase transition at 175 K is associated to a closer molecular stacking at lower temperatures [54]. That might be a reason for changes in the energy transfer mechanism, since the electronic coupling varies with the molecular packing.

Another possible explanation for the strong increase of the PL intensity of components b below 175 K is based on the assumption that the cooling of the sample can cause an increase of surface defects. The increase of those surface defects can cause an increase of the scattering of the c-polarized light. This increase of the redirection of the c-polarized

light rises the emission of component b_2 detected in the direction perpendicular to the ab surface. A similar effect of the increase of PL intensity with an increase of surface defects of Rub crystals was observed in the Ref. [67] at room temperature.

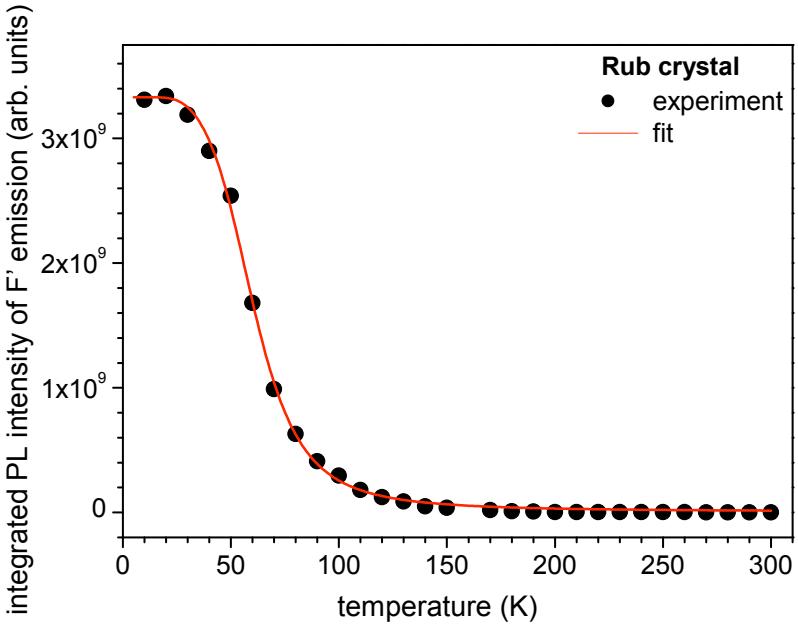

Fig. 6.7 *Integrated PL intensity of F' emission (component b in the single component fit, see Fig. 6.3) as a function of temperature for a Rub crystal. F' is equal to F in the case of model 1. The black circles are the measured values. The red curve is the fit by eq. 6.10. The PL at 5 K is about 6 500 times higher than at 300 K.*

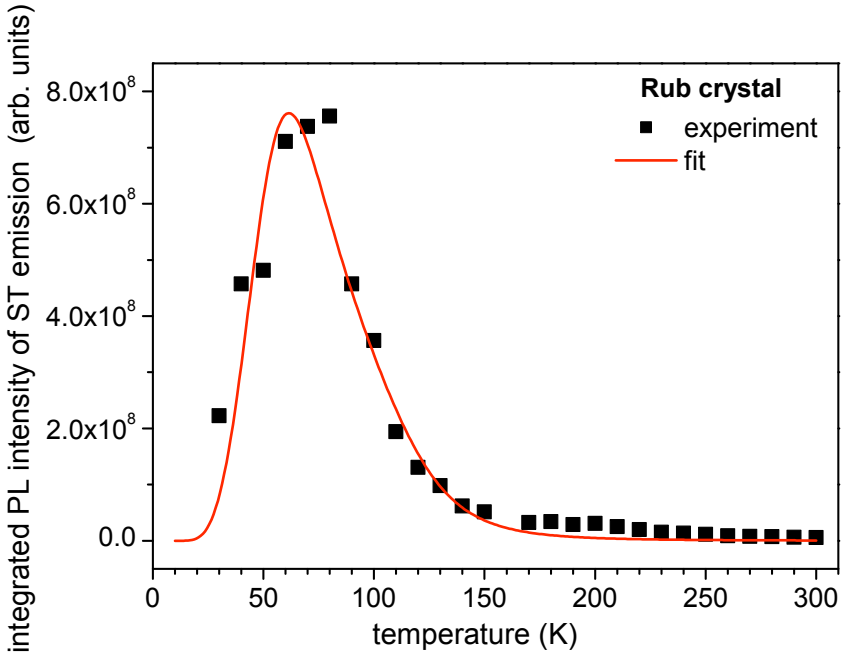

Fig. 6.8 *Integrated intensity of the self-trapped luminescence emission 'ST' (component c in the single component fit, see Fig. 6.3). Filled squares are the measured values. The red curve is the fit by eq. 6.11.*

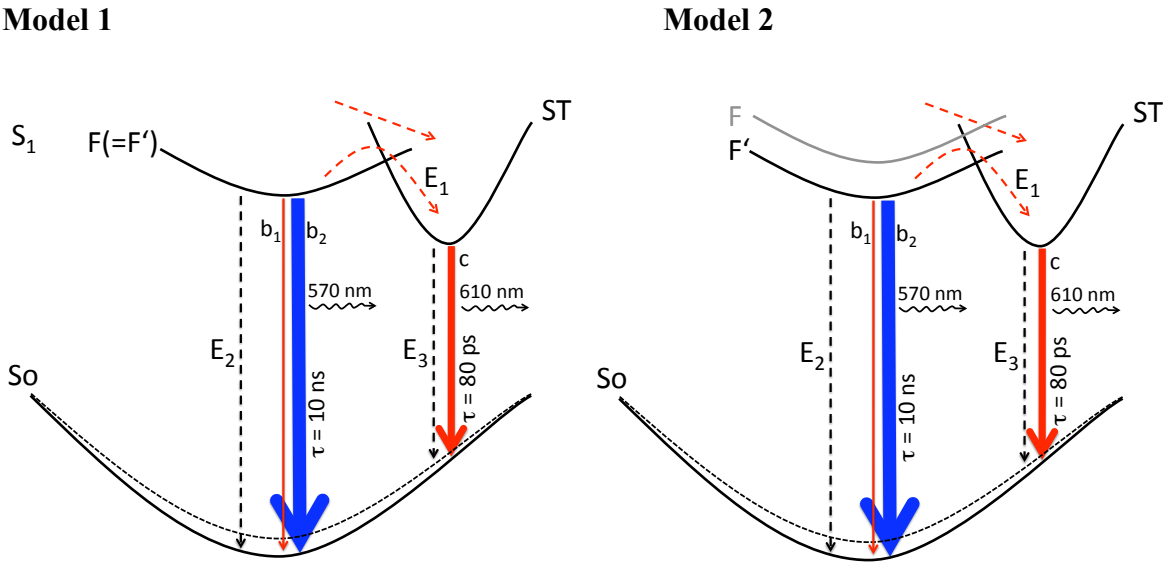

Fig. 6.9 *Schematic potential energy diagrams of the models used in the fit of experimental dependency of the PL intensity of the Rub crystal as a function of temperature. ST denotes the self-trapped state and S_o the ground state in both models. In the model 1, F and F'denote free exciton states for the high and low temperature phases. In model 2, F denotes the free exciton state and F' denotes the trapped state. E_1 represents the height of the self-trapping potential barrier between the F' (or F state at high temperature in model 1) state and ST state. E_2 and E_3 are activation energies for the non-radiative decay from the F' (or F state at high temperature in model 1) state and the ST state, respectively. b_1 denotes the emission from the F state or from the F' state at high temperatures in model 1 and 2, respectively. b_2 denotes the emission from the F' state at low temperatures. c denotes the emission from the ST state. τ is the emission decay time.*

The observation of the sharp lines with energies above the F' state in the case of intense optical excitation (see section 7.4) make the application of the model 1 questionable. On the basis of this observation the other model (model 2, see below) was developed, were the F' state is the emitting state below the free exciton state F.

Model 2

Component b (b_1 and b_2) reproduces de-excitation processes from a kind of trapped state (F' state, see Fig. 6.9). This state is formed due to defect formation or self-trapping and is below the free exciton state (F state).

At high temperatures, after excitation ($S_0 \rightarrow$F transition) the exciton directly relaxes to the self-trapped ST state or first relaxes to the F' state and subsequently relaxes to the ST state by crossing the energy barrier (E_1). At very low temperatures, the activation energy is not high enough to overcome the potential barrier between F (or between the trapped F') state and the self-trapped ST state. In this case the excitons from free exciton state F relax to the trapped state F' with following emission.

Fit

To characterize the underlying microscopic processes, the fit of experimental data represented in Fig. 6.7 and Fig. 6.8 have been summarized in a theoretical model.

1. The fluorescence intensity of the F' state $I_{F'}$ is proportional to the radiative rate constant $k_{radF'}$ and the concentration of excited state $N_{F'}$ [68] :

$$I_{F'} = k_{radF'} N_{F'}. \tag{6.2}$$

Under continuous illumination, the concentration $N_{F'}$ is in a steady state:

$$\frac{dN_{F'}}{dt} = 0, \tag{6.3}$$

where $dN_{F'}$ *is* the change of concentration and *dt is* the change of time.
Thus the relationship between the population rate k_0 and the depopulation rate due to radiative and non-radiative processes is described by the following equation:

$$k_0 = N_{F'}\left(k_{nr1}\exp\left(-\frac{E_1}{k_B T}\right) + k_{nr2}\exp\left(-\frac{E_2}{k_B T}\right) + k_{radF'}\right), \tag{6.4}$$

where k_{nr1} denotes the non-radiative rate of the transition between the F' and ST states; E_1 is the activation energy necessary to overcome the potential barrier between the F' and ST states; k_{nr2} denotes the non-radiative decay rate from F' state with the activation energy E_2. Using eq. 6.2 and eq. 6.4 the dependence of the fluorescence intensity of the F' state from the temperature can be described as

$$I_{F'}(T) = \frac{k_0 k_{radF'}}{k_{nr1}\exp\left(-\frac{E_1}{k_B T}\right) + k_{nr2}\exp\left(-\frac{E_2}{k_B T}\right) + k_{radF'}}. \tag{6.5}$$

2. In analogy to the F' state (see eq. 6.2), the fluorescence intensity I_{ST} of the ST state is given by

$$I_{ST} = k_{radST} N_{ST}, \tag{6.6}$$

where k_{radST} is the radiative rate constant of the fluorescence from the ST state; N_{ST} is the concentration of the ST state.

For the ST state the relation between the population rate k_{nr1} and the depopulation radiative and non-radiative rates can be given by follow eq.:

$$\frac{dN_{ST}}{dt} = N_{F'}k_{nr1}\exp\left(-\frac{E_1}{k_BT}\right) - N_{ST}k_{radST} - N_{ST}k_{nr3}\exp\left(-\frac{E_3}{k_BT}\right). \tag{6.7}$$

In the steady state, the concentration N_{ST} does not change with time. According to this, eq. 6.7 can be rewritten as

$$N_{ST} = \frac{N_{F'}k_{nr1}\exp\left(-\frac{E_1}{k_BT}\right)}{k_{radST} + k_{nr3}\exp\left(-\frac{E_3}{k_BT}\right)}. \tag{6.8}$$

Using eq. 6.5, 6.6 and eq. 6.8 the dependence of the fluorescence intensity of the ST state from the temperature can be described as

$$I_{ST}(T) = \frac{k_{radST}k_0k_{nr1}\exp\left(-\frac{E_1}{k_BT}\right)}{\left(k_{nr1}\exp\left(-\frac{E_1}{k_BT}\right) + k_{nr2}\exp\left(-\frac{E_2}{k_BT}\right) + k_{radF'}\right)\left(k_{radST} + k_{nr3}\exp\left(-\frac{E_3}{k_BT}\right)\right)}. \tag{6.9}$$

To decrease the number of the free parameters in the fits to the experimental data (circles in Fig. 6.7 and squares in Fig. 6.8) the eq. 6.5 and eq. 6.9 were rewritten as:

$$I_{F'}(T) = \frac{k_0}{a\exp\left(-\frac{E_1}{k_BT}\right) + b\exp\left(-\frac{E_2}{k_BT}\right) + 1} \tag{6.10}$$

and

$$I_{ST}(T) = \frac{k_0a\exp\left(-\frac{E_1}{k_BT}\right)}{\left(a\exp\left(-\frac{E_1}{k_BT}\right) + b\exp\left(-\frac{E_2}{k_BT}\right) + 1\right)\left(1 + c\exp\left(-\frac{E_3}{k_BT}\right)\right)}, \tag{6.11}$$

where

$$a = \frac{k_{nr1}}{k_{radF'}},\ b = \frac{k_{nr2}}{k_{radF'}},\ c = \frac{k_{nr3}}{k_{radST}}. \tag{6.12}$$

The experimental temperature dependency of the integrated PL intensities of the F' and the ST states has been fitted simultaneously by one set of parameters by eq. 6.10 and

eq. 6.11 (red lines in Fig. 6.7 and Fig. 6.8, correspondently). The parameter R^2 obtained from the fit in Origin 7 describes the quality of the fit. The R^2 is a value between 0 and 1. If it is close to 1, the relationship between experimental and fit curves will be regarded as very strong and we can have a high degree of confidence in our fit. The fit of the experimental data by eq. 6.10 results in $R^2_{F'}$= 0.999. The fit of the experimental data by eq. 6.11 results in R^2_{ST} = 0.944. Therefore, the calculated curves are in very good agreement with the experimental data. This indicates the validity of the proposed models.

The curves calculated accordingly to eq. 6.10 and eq. 6.11 yield the activation energy necessary to overcome the potential barrier E_1 = 15.0 ± 0.5 meV and the activation energies of the non-radiative decay of the F' and the ST states, E_2 = 39 ± 1 meV and E_3 = 90 ± 5 meV, correspondingly. From the fits the constants a = 8, b = 965, and c = 3 915 have been determined. The errors in the activation energies have been determined under the constraint that constants a, b and c were fixed in the fit.

From the fit of temperature dependent photoluminescence decay rates the radiative rate $k_{radF'} = 6.7 \cdot 10^7$ s^{-1} was obtained (see section 7.3.2, p. 104). From the knowledge of the values $k_{radF'}$, a and b (using eq. 6.12) the non-radiative rates $k_{nr1} = 5.4 \cdot 10^8$ s^{-1} and $k_{nr2} = 6.5 \cdot 10^{10}$ s^{-1} were determined.

Comparison with the literature

The comparison of our results with the literature [75] shows some deviation in the values of the activation energies, the radiative and non-radiative rates in Rub crystals: The determined activation energies for the non-radiative decays of the F' (E_1 = 15 meV and E_2 = 39 meV) and the ST (E_3 = 90 meV) states are higher than the respective activation energies for the non-radiative decays of the free and the self-trapped excitonic states in the Rub crystals reported by Stöhr et al., 3 meV and 14 meV, respectively [75]. The actual value of the radiative rate $k_{radF'} = 6.7 \cdot 10^7$ s^{-1} from state F' is smaller than the radiative rate $3 \cdot 10^8$ s^{-1} reported in Ref. [75]. The value of the non-radiative rate $k_{nr2} = 6.5 \cdot 10^{10}$ s^{-1} from the state F' determined in present work is higher than the respective non-radiative rate $2 \cdot 10^8$ s^{-1} (non-radiative rate from the free excitonic state) reported by Stöhr et al. [75]

First of all, the differences in the obtained values are due to the difference in the interpretation of PL spectra of Rub crystals at low temperatures. In Ref. [75] the high energy peak in PL spectra at low temperatures was attributed to the free exciton emission as well as in our case (model 1, emission from F' state), but the lower energy peaks at 4 K were attributed to the ST state by Stöhr et al. This interpretation is in some contradiction to our interpretation of the PL spectra at lower temperatures. In particular, in our interpretation the second lower peak (peak d, see Fig. 6.2) was attributed to the same optical transition as the higher energy peak and is its vibronic side-band. The similarity in the temperature dependency of the integral intensity of the single components (b_2 and d, see Fig. 6.5) and also the identical behaviour in the time-resolved spectra of both components (see Fig. 7.2) corroborate our assumption of the same origin of the both components.

As mentioned above, we attributed the strongest component (peak c, see Fig. 6.2) of the PL spectra at high temperatures to the emission from the ST state and this is in agreement with the interpretation of the PL spectrum of Rub crystals at room temperature reported by Najafov et al. [49] Note that the position of the component c attributed to the ST emission is slightly higher on the energy scale than the position of component d (see Fig. 6.4). The difference in the energies of the two components is easy to see in the single component fit (see Fig. 6.3). In addition, Fig. 6.10 shows the peak of component d starts to be resolved only at temperatures below 60 K, and the position of the component d is lower in the energy scale than the position of component c. The emission maximum in the PL spectra at high temperatures is a result of overlapping of the emissions of the two components c and e (see Fig. 6.3). Thus, the visible PL maximum at high temperatures has a similar position as component d in the PL spectra at low temperatures (see Fig. 6.2). We assume that this similarity could be the reason for the different interpretation of the origin of component d in the PL spectra at low temperature reported by Stöhr et al. [75], with respect to our interpretation: While Stöhr et al. assigned the peak d to an emission of a ST exciton, we attributed this peak to a vibronic progression of the peak b_2, which corresponds to the free exciton emission (model 1, see section 6.6).

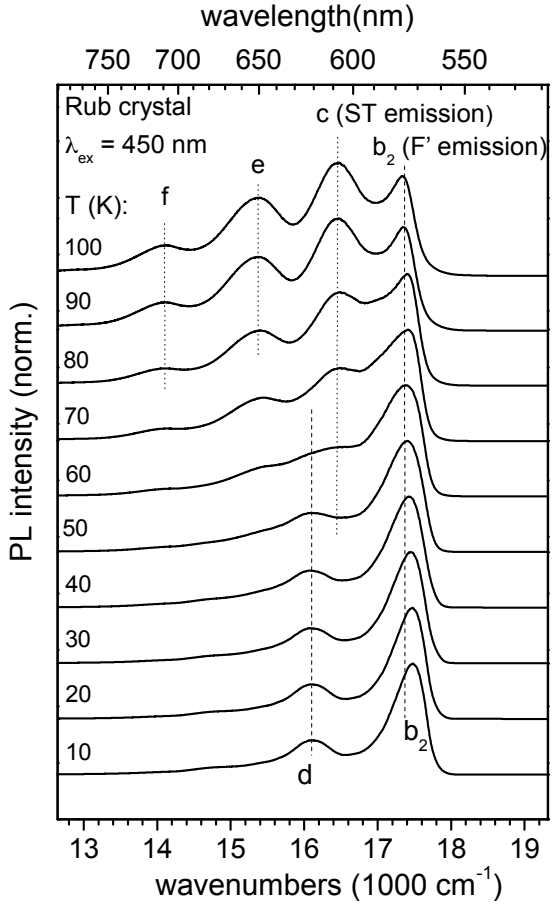

Fig. 6.10 *PL spectra of a Rub crystal at temperatures between 10 and 100 K. Component* **c** *was attributed to the ST emission. Component* b_2 *and component* **d** *were attributed to the vibronic bands of the same optical transition from the F' state. The spectra were normalized and shifted vertically against each other for clarity.*

6.7 Absorption spectra of Rub crystals

6.7.1 Dependence of the absorption spectra on the direction of the light propagation

In Rub, the absorption transition dipole moment of the S_0-S_1 transition is oriented along the short axis of the backbone of the Rub molecule. In the Rub crystal, this is the c direction, which is perpendicular to the ab plane, the most developed plane in the crystal (see Fig. 2.3, Chapter 2). Fig. 6.11 shows the orientation of the incident light propagation direction with respect to the sample orientation. When the angle between the incident light and the ab plane is equal to 90°, the electric vectors of the incident light and the transition dipole moment of the S_0-S_1 transition are perpendicular to each other and the probability for the absorption is zero (v = 90°). If the incident light is linearly polarized, the probability

of excitation is proportional to $\cos^2\nu$, i.e. the probability of excitation is maximal when the electric vector is parallel to the transition dipole moment and it is zero when they are perpendicular to each other.

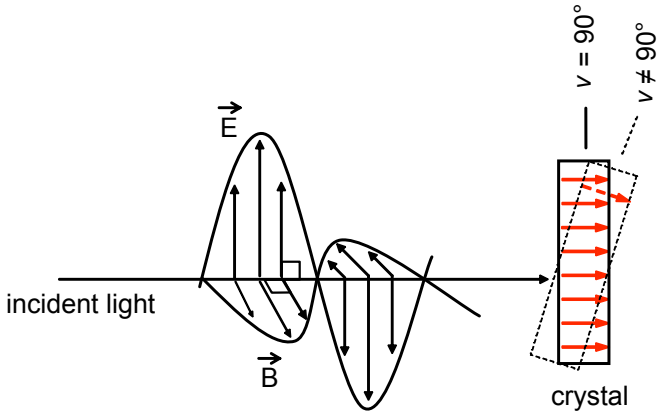

Fig. 6.11 *Schematic illustration of the direction of the incident light and the sample orientation. Relative orientation of the electrical* ***E*** *and magnetic* ***B*** *vectors of the incident light and the transition dipole moment of the S_0-S_1 transition (red arrows) of the Rub crystal. v is the angle between an electric vector of the direction of the incident light and the transition dipole moments.*

Fig. 6.2 represents the absorption spectra for the case that the ab crystal-plane is perpendicular to the optical path. The small absorption peak A at about 2.3 eV is attributed to the $S_0 \rightarrow S_1$ transition. The lowest A_u excited state give a rise to a dipole-allowed transition with c polarization. The incident light of the halogen lamp was focussed by the lens on the crystal plate (see Fig. 6.1). In that way, not only perpendicular oriented incident light reached the sample. Some light with a deviation from $v = 90°$ was also focused on the sample. This light has been absorbed by the crystal and is responsible for a weak absorption band at 2.3 eV (see Fig. 6.2). At the same time, the same interpretation about the nature of the weak low-energy absorption band in the spectra of Rub crystals has been obtained by another scientific groups [50] [61].

It is interesting that with decreasing sample temperature the peak A becomes more pronounced (see Fig. 6.2). Probably that happened due to some changes of the molecular orientation in the Rub crystal at lower temperatures. Changes in molecular orientation can appear due to a molecular dislocation during a contraction of the crystal lattice upon cooling.

At temperatures below 50 K it is possible to see that component A includes 2 components: the peak A‘ (at about 18 450 cm^{-1}) and peak A“ (at about 18 950 cm^{-1}) (see Fig. 6.12 and Tab. 6.1). As shown in Fig. 6.12, the intensity of peak A’ strongly increases upon deviations of the angle v from 90°. As it was mentioned above, the probability of the excitation of the S_0-S_1 transition is proportional to $\cos^2\nu$ for Rub crystals, and is also

increasing with deviation from angle 90°. This confirms the assumption that the peak A, in particular A', belongs to the S_0-S_1 absorption.

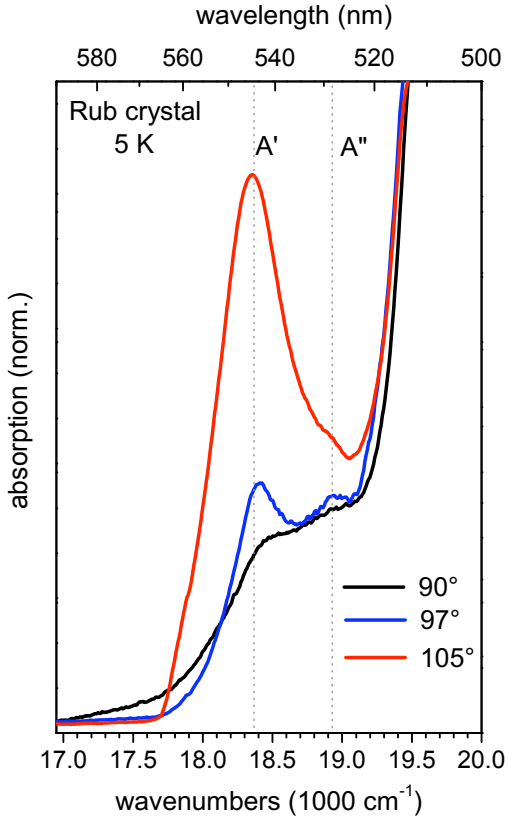

Fig. 6.12 *Absorption spectra of a Rub crystal at 5 K for three different angles.*

Davydov splitting

The Rub crystal has four molecules per elementary cell. However, due to the parallel orientation of the transition dipole moments for the S_0-S_1 transition in a Rub crystal, the component A' in absorption spectra do not show a Davydov splitting (see Fig. 6.13).

The absorption spectra show a relatively strong band at 2.49 eV, followed by weaker bands at 2.66 eV, 2.85 eV and about 3.03 eV (see Fig. 6.16), separated by 0.18 eV. In the literature, the vibronic progression, which is formed from peaks B, C, and D was attributed to the S_0-S_2 excitonic transition with LN polarization [61], where L is the long backbone axis of Rub molecule and N is axis perpendicular to the LM plane (see inset, Fig. 6.13 (c)). As Fig. 6.13 shows, two Davydov components with a small splitting (of about 230 cm^{-1} at 300 K and about 150 cm^{-1} at 5 K) were observed in the vibronic progressions of the main peaks B, C, and D.

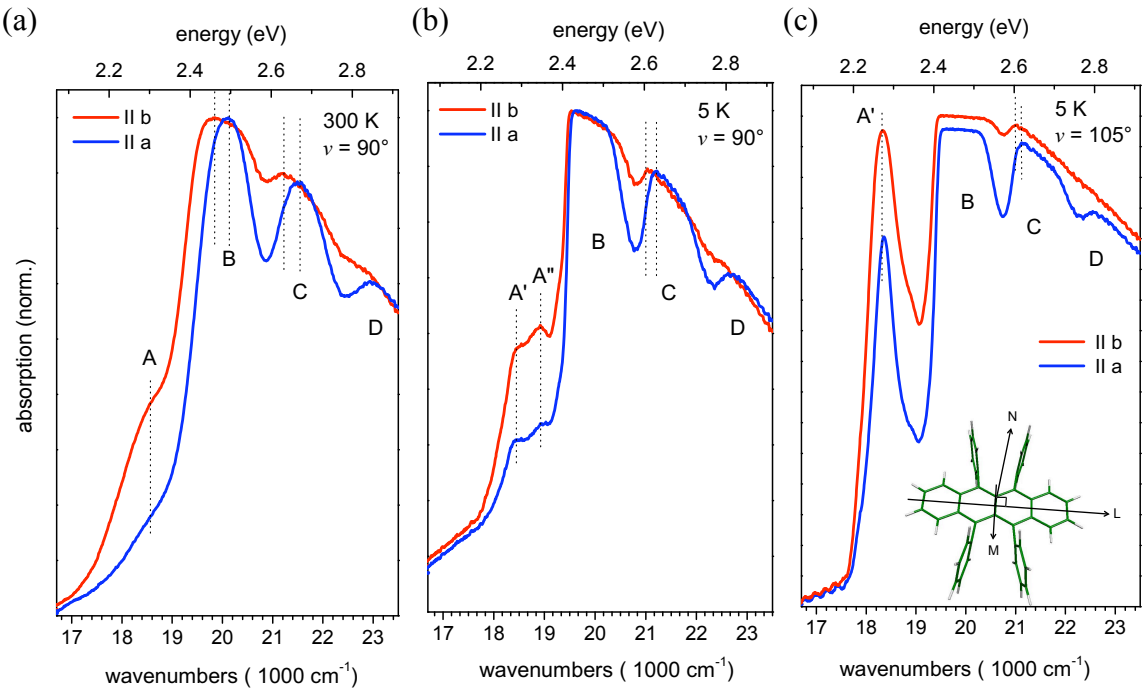

Fig. 6.13 *Polarized absorption spectra of a Rub crystal: (a) at 300 K (ν = 90°), (b) at 5 K (ν = 90°) and (c) 5 K (ν = 105°). Blue curves and red curves correspond to the a- and b-polarized light. The directions of the polarization were determined by comparison of the room temperature spectrum of the present experiment with the polarized absorption spectra of a Rub crystal from Ref. [6] (see Fig. 6.21 (b)). The polarization filter was positioned in front of the entrance slit of the spectrometer. (a) and (b) spectra were normalized at the maximum of absorption (peak* **B***) for clarity. (c) spectra were not normalized. The b-polarized absorption spectrum shows the absorption (see eq. 6.1)* $A_{B\ at\ 300\ K} = 1.32$ *at maximum* **B** *(at 300 K). The a-polarized absorption spectrum shows the absorption (see eq. 6.1)* $A_{B\ at\ 300\ K} = 1.27$ *at maximum* **B** *(at 300 K). The absorption values at maxima for the spectra at 5 K is not reported due to they inaccuracy as result of the full absorption of the incident light in the wavelength area, where the absorption is maximal (see details, p. 60). The inset in the Fig. (c) shows the sketch the direction of the M, L and N axes of the molecule.*

As mentioned in the figure caption of Fig. 6.13, the b-polarized absorption spectrum at 300 K shows the absorption $A_{B\ at\ 300\ K} = 1.32$ at maximum B and the a-polarized absorption spectrum shows the absorption $A_{B\ at\ 300\ K} = 1.27$ at maximum B. The higher absorption is realized in the case that the light is polarized along the b-axis. We assume that this is qualitatively consistent with the molecular packing in the Rub crystal (see Fig. 2.3), because one might expect a stronger overlap of the electronic π-orbitales along the b-axis. In comparison to the a-polarized absorption spectra, the b-polarized absorption spectra show the visible arising of peak **A** (see Fig. 6.13 (a)) and the arising of peaks **A'** and **A'** (see Fig. 6.13 (b) and (c)). Peak **A** (and **A'**) is attributed to the S_0-S_1 transition, which is polarized along the c-axis (normal to the ab plane). It is not affected by the b- (or a-) polarized light. The difference in the absorption values of the vibronic band **A** by b- and a-polarized light is explained by the stronger overlapping of the vibronic band **A** and the

vibronic band B for the b-polarized light. Fig. 6.13 shows that the vibronic band B for the b-polarized light is shifted to the lower energies. This shift increases the overlapping of the vibronic bands A and B for the b-polarized light, with respect to the absorption spectra for the a-polarized light. Hence the absorption spectra show the visible arising of peak A for the b-polarized light.

6.7.2 Temperature influence on the absorption spectra

It was observed that the position of the lowest-energy-peak in the absorption spectra for $v = 105°$ shifts to a lower energy upon cooling (see Figs. 6.14 (a) and (b)). It shifts gradually to lower energies in the temperature interval from 300 K to 10 K (see Fig. 6.14 (b)).

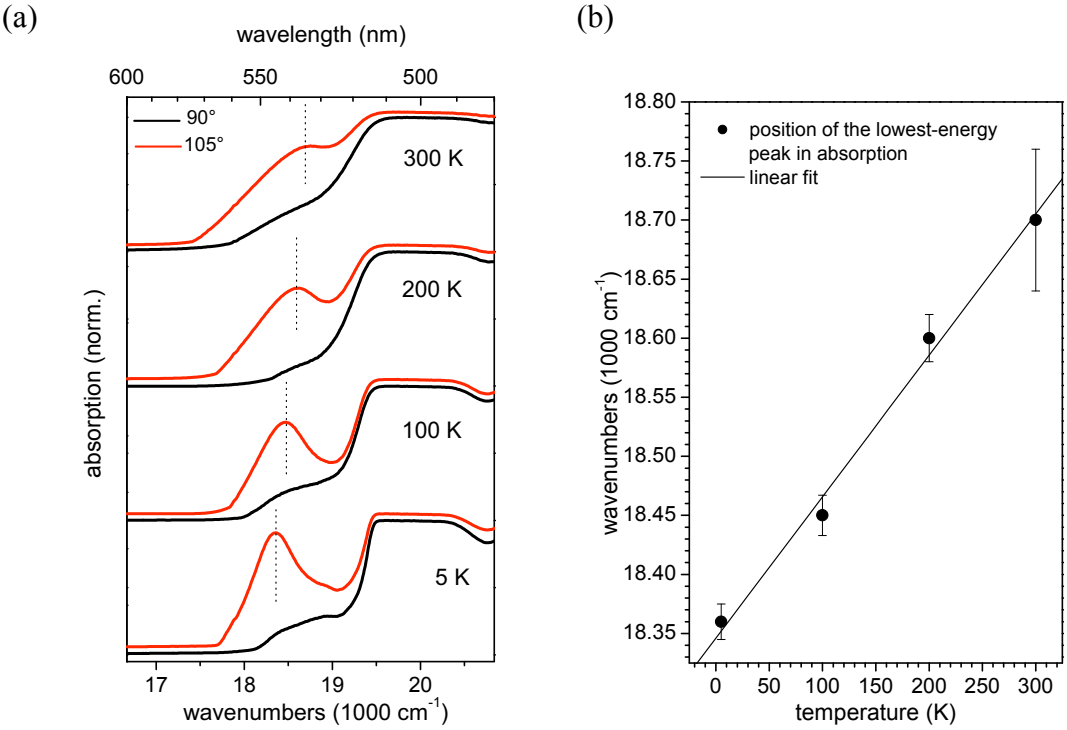

Fig. 6.14 *(a) Absorption spectra of a Rub crystal for two different angles at different temperatures: 5 K, 100 K, 200 K and 300 K. The spectra were normalized and shifted vertically against each other for clarity. (b) The positions of the lowest-energy peak in absorption for different temperatures (black circles), black line is linear fit.*

To exclude the distortion in themeasured line position due to the overlapping of the lines, the absorption spectra for $v = 90°$ (corresponding to a probability of the absorption for the S_0-S_1 transition equal to zero) have been subtracted from the absorption spectra at $v = 115°$. The author assumes that the resulting spectra correspond only to the absorption of the S_0-S_1 transition (see Fig. 6.15 (a)) and are not influenced by overlapping of other components including in vibronic progressions As Fig. 6.15 shows, the maxima of the resulting

spectra shift to the lower energies upon cooling. This shift is not trivial to explain. It was supposed that the changes have some relation to the changes in molecular conformations at different temperatures. This is confirmed by experimental results published by Jurchescu [54], which show that the crystal structure determination reveals a 2.157 % volume thermal expansion of the Rub crystal between 100 and 300 K. The thermal expansion is anisotropic for the three crystallographic directions (a = 0.410 %, b = 0.320 %, c = 1.562 %) and occurs predominantly along the weakest bonding c axis.

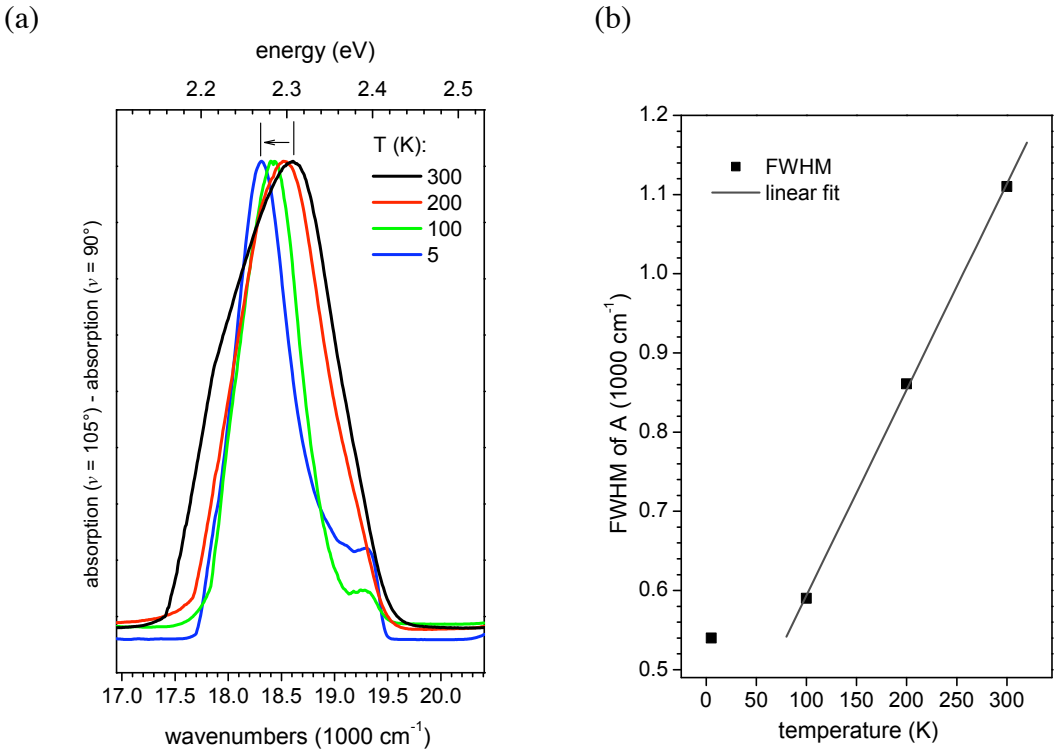

Fig. 6.15 *(a) Absorption spectra of component A' of a Rub crystal at different temperatures. The spectra were obtained by subtraction of the spectrum, which was measured at angle ν = 90° from the spectrum, which was measured at angle ν = 105° (from Fig. 6.12 (a)). This was done in order to exclude the distortion due to the overlapping of the absorption of component A' with that of component B and to get a correct form of the absorption spectrum due to the S_0-S_1 transition. All spectra were normalized. (b) The influence of the temperature on the FWHM in the absorption spectrum of component A' for a Rub crystal. The black squares are the measured values. The black line is the linear fit.*

Another effect which influences the visible shift in direction of lower energy upon cooling is the partial overlap of the absorption caused by the S_0-S_1 transition and the absorption by high-energy transitions. This is at least one of the processes which results in the visible red shift of the maximum of the S_0-S_1 transition. In addition, Fig. 6.15 (b) confirms that overlapping of single components of vibronic progressions decreases because one finds a decrease of the broadening of the line upon cooling. The full width at half of maximum (FWHM) of the absorption peak A' decreases upon cooling from 1010 cm^{-1} (at

300 K) to 500 cm^{-1} (at 5 K). Fig. 6.15 (b) shows a linear relationship between the FWHM of component A' and temperature in the temperature interval from 300 K to 100 K.

6.8 Photoluminescence excitation spectra of Rub crystals

Absorption spectra yield information about energetical properties of all excited states. PLE spectra reflect only information about the excitation into the states in to which emission eventually occurs. Comparing the excitation spectrum to the absorption spectrum could help to understand the excitation relaxation mechanism. Therefore the PLE experiments for different crystal temperatures were performed. Fig. 6.16 shows the excitation spectra together with the absorption and PL spectra of a Rub crystal at 300 K (high temperature) and at 50 K (low temperature). The PLE spectra show the progression with several maxima. At high temperature the lowest-energy-peak is at about 18 600 cm^{-1} (A_{PLE}). At low temperature the lowest-energy-peak includes two single components: a clear notable component A'_{PLE} at about 18 450 cm^{-1} and a hardly notable component A''_{PLE} at about 18 960 cm^{-1}. At higher energies additional two clear notable (B_{PLE} and D_{PLE}) and one hardly notable (C_{PLE}) maxima are observed. The energy values of the maxima of the absorption and excitation spectra are summarized in Tabs. 6.1 and 6.2.

It is important to direct the attention to the differences in the PLE and the absorption spectra (see Fig. 6.16). As mentioned above, the absorption peak, marked by letter A (and A'), corresponding to the S_0-S_1 transition, was only slightly pronounced for the case that the crystal plane is perpendicular to the optical path due to photoselection rules (see section 6.7.1). In the PLE spectrum, the lowest-energy peak A_{PLE}, is clearly pronounced and was attributed to the S_0-S_1 transition. This peak is the highest intensity peak in the PLE spectra. The positions of the lowest-energy peak in the absorption spectra and the PLE spectra coincide (see Tabs. 6.1 and 6.2), which confirms our assumption about the S_0-S_1 nature of the peak A_{PLE} (and A'_{PLE}).

Furthermore, the positions of higher-energies peaks B_{PLE}, C_{PLE} and D_{PLE} in PLE spectra do not coincide with the peaks B, C and D in the absorption spectra and are shifted in the direction of lower energies (see Fig. 6.16, Tabs. 6.1 and 6.2). These differences mean that in Rub crystals the excitation relaxation path is different from the absorption path. After absorption of the incident light the excited molecules lose the excitation by the intrinsic de-excitation processes and/or emission from molecular excited state or trapping states. However, the PLE and absorption spectra of Rub in solution are almost identical (see Fig. 6.17) above 400 nm. This means that in Rub solution the light absorption brings the molecules into excited molecular states from which the emission follows directly.

It should also be noted that the shape of the PLE and PL spectra of different Rub crystals was subject to small changes. The positions of the maxima remain the same, but the ratio of the intensities and the shape of them changes from sample to sample (see

Figs. 6.18 and 6.19). These differences we attributed to the different quality of the investigated crystals.

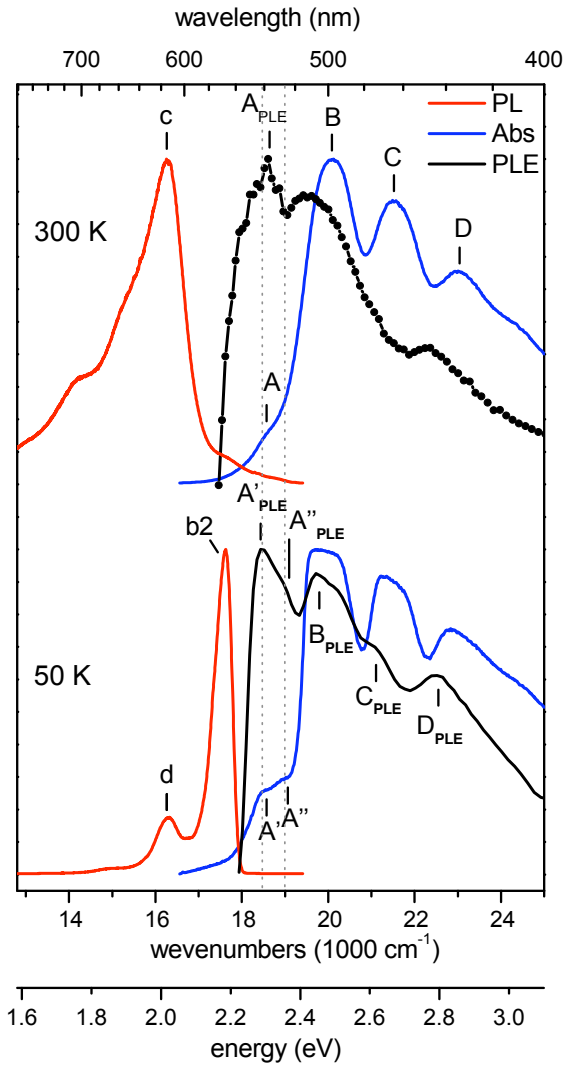

Fig. 6.16 *Absorption spectra (blue lines), cw PL spectra (red lines), and PLE spectra (black lines) of Rub single crystals. The spectra were taken at 300 K (top) and at 50 K (bottom). The spectra were normalized and shifted vertically against each other for clarity. The PLE spectrum at 300 K was monitored at 610±1.25 nm. The PLE spectrum at 50 K was monitored at 570±1.25 nm.*

For comparison of the PLE spectra of different emitting species (free exciton and self-trapped exciton) at 300 K, two PLE spectra monitored at 570 nm (17 543 cm^{-1}) and at 610 nm (16 393 cm^{-1}) are presented in Fig. 6.19 (blue and red curves, correspondingly). Unfortunately, it was not possible to record a PL spectrum without partial overlapping of the strong excitation light from the Xe lamp (bright white line in Fig. 6.20 (a)) and the weak PL emission of the crystal at 570 nm. Therefore, it was not possible to observe the PLE spectrum for energies below 19 330 cm^{-1}, because the intensity of the incident excited light is much higher than the PL emission at 570 nm in this spectral area. Consequently,

the strong rise of the PLE spectra monitored at 570 nm for energies below 19 330 cm^{-1} (517 nm) is attributed to the excitation light from the Xe lamp. It should be noted that the comparison of the PLE spectra detected at 570 nm and 610 nm (in the wavelength range where they can be compared, e.g. above 19 330 cm^{-1}) at 300 K do not show a remarkable difference in their shapes (see Fig. 6.19, crystal A). In addition, the PLE spectra monitored at different wavelengths at low temperatures have been successfully measured and are identical.

Abs	A (cm^{-1})		B (cm^{-1})	C (cm^{-1})	D (cm^{-1})
	A' (cm^{-1})	A'' (cm^{-1})			
HT	18 550 ± 200 (90°)		20 080 ± 30	21 500 ± 30	23 000 ± 50
	18 800 ± 100 (105°)				
LT	18 450 ± 100 (90°)	18 950 ± 100 (90°)	19 800 ± 100	21 330 ± 100	22 810 ± 50
	18 350 ± 30 (105°)				

Tab. 6.1 *Positions of experimentally determined peaks in the absorption spectrum at 300 K (HT) and at 50 K (LT). The values of peaks A, A' and A'' were extracted from the measurements, where the incident light and the crystal plate were perpendicular to each other (90°) or the angle between the incident light and crystal plate was equal to 105 °. The positions of the peak B, C and D were determined at 90°.*

PLE	A_{PLE} (cm^{-1})		B_{PLE} (cm^{-1})	C_{PLE} (cm^{-1})	D_{PLE} (cm^{-1})
	A'_{PLE} (cm^{-1})	A''_{PLE} (cm^{-1})			
HT	18 600 ± 100		19 550 ± 80		22 320 ± 80
LT	18 450 ± 30	18 960 ± 100	19 750 ± 50	21 150 ± 80	22 520 ± 50

Tab. 6.2 *Positions of experimentally determined peaks in the PLE spectrum at 300 K (HT) and at 50 K (LT) Spectra were measured at v=90°.*

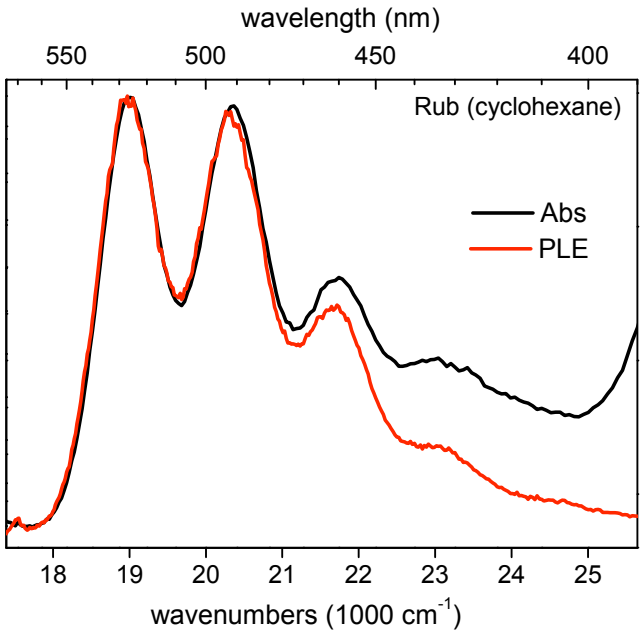

Fig. 6.17 *Comparison of PLE and absorption spectra of Rub in cyclohexane at room temperature. The PLE spectrum was monitored at 554.5 nm. The strong increase of the absorption spectrum below 400 nm is due to the S_0-S_2 transition. The spectra were normalized.*

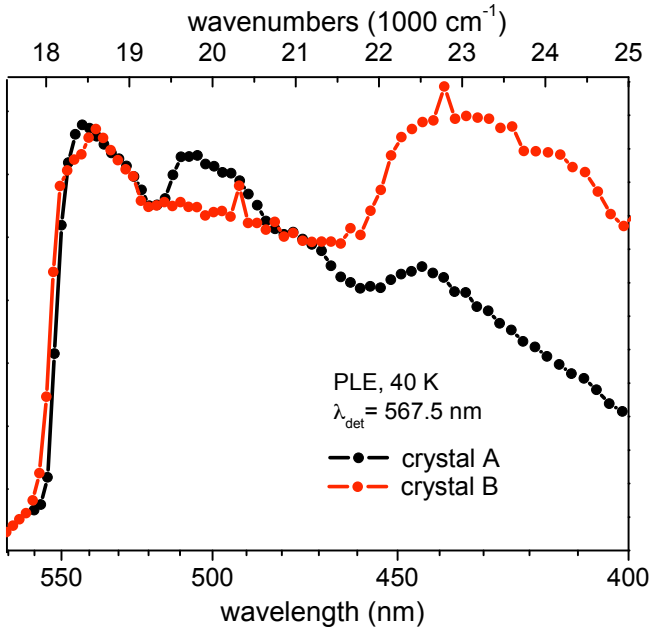

Fig. 6.18 *PLE spectra (detected at 567.5 nm) of two Rub crystals at 40 K. The shape of PLE spectrum of different Rub crystals undergoes small changes. The spectra were normalized.*

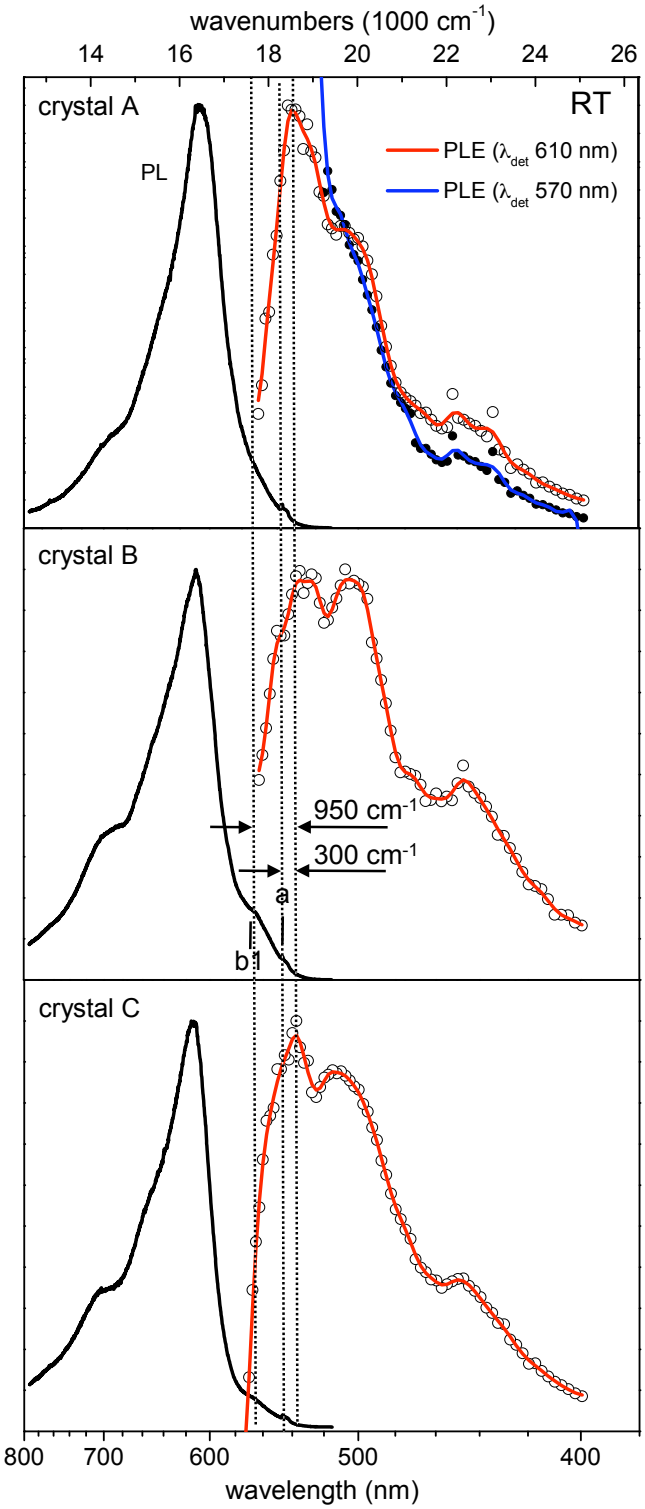

Fig. 6.19 *PL (black lines) and PLE spectra (detected at 610 nm - red lines and detected at 570 nm - blue line) of different Rub crystals. The shape of the PL spectrum and the PLE spectrum of different Rub crystals undergoes small changes. The comparison of PLE spectra monitored at 570 nm (blue line) and 610 nm (red line) do not show any difference in the wavelength range where they can be compared. All spectra were measured at 300 K. The spectra were normalized.*

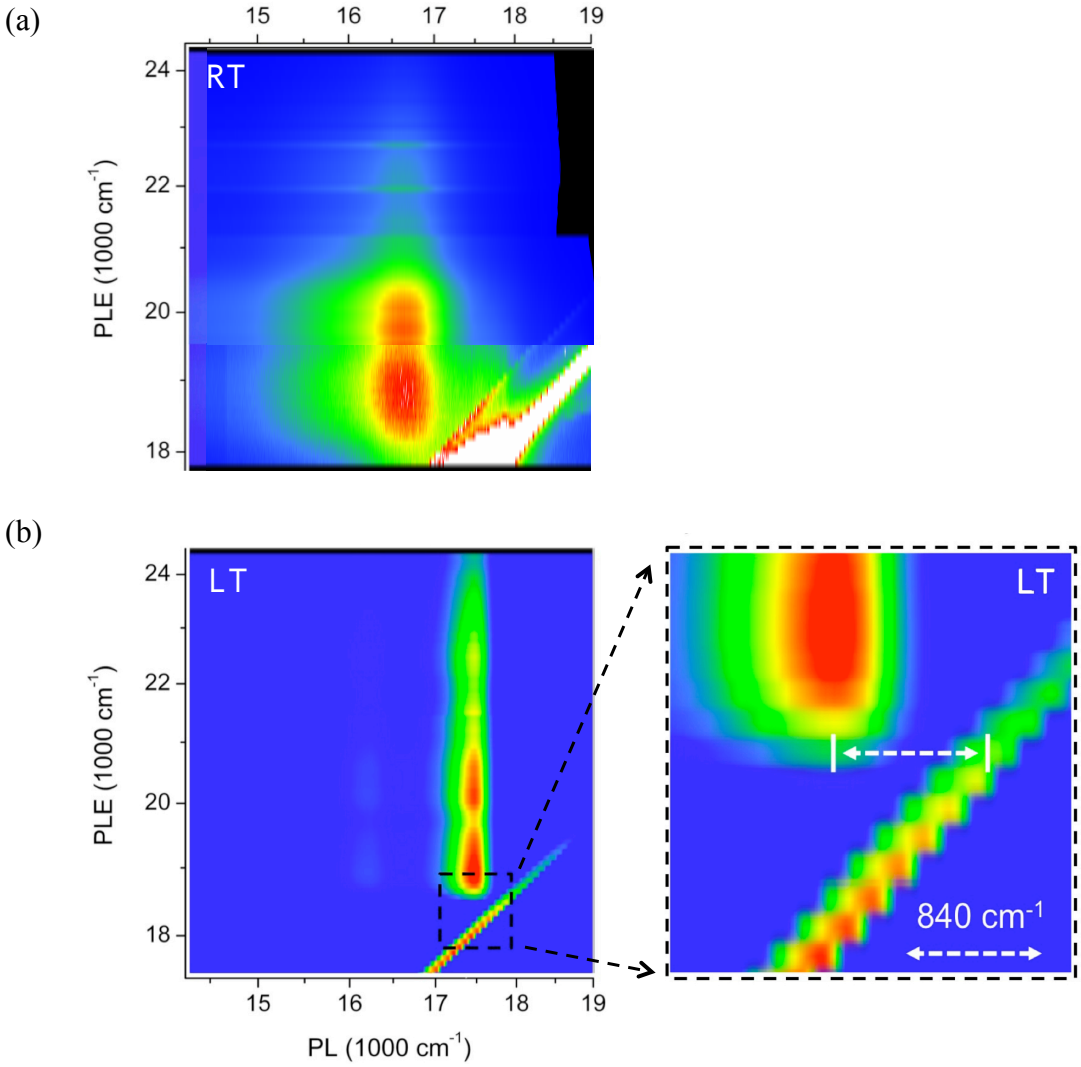

Fig. 6.20 *2-dimensional images representing the PLE experiments performed on a Rub crystal at room temperature - RT (a) and 50 K - LT (b). The horizontal cut of the pictures representing the PL spectrum. The vertical cut representing the PLE spectrum. The wavelength of the excitation light was scanned with a step width of 2.5 nm (diagonal line in the right corner). A zoom-in of the black square marked in the picture (b) is shown on the right hand side of the image. The colours define the PL (and the PLE) intensity. Blue, green, yellow, red, and white colours represent an increasing of the PL intensities, correspondingly. The energetical gap between the PL spectra and the excitation energy at LT is 840 cm^{-1}.*

In addition to the cw measurements, the time-resolved PLE spectrum (μs-PLE) obtained by monitoring the PL at 1 μs after pulsed excitation have been measured by Najafov et al. [49] (see Fig. 6.21 (a), curve with the open circles). An important result is the contrast of the μs-PLE spectrum (see Fig. 6.21 (a)) to the cw PLE spectra. The μs-PLE has the highest intensity maximum at about 17 700 cm^{-1} (565 nm), which is the position of highest-energy maximum in PL spectrum, which was attributed to the free exciton band in the PL spectrum. In addition, the μs-PLE spectrum shows an anticorrela-

tion to the absorption spectra. Najafov explained the observed anticorrelation with the assignement of the 570 nm emission band to free excitons. Since the total number of absorbed photons is constant, the two effects compete: less free excitons are created when more photons are lost to excitations of vibronic levels. The observation that the μs-PLE spectra detected at 570 nm and at 620 nm are the same means that molecular excitons decay radiatively on the microsecond time scale. They are predominantly created by a transition from a free exciton state [49].

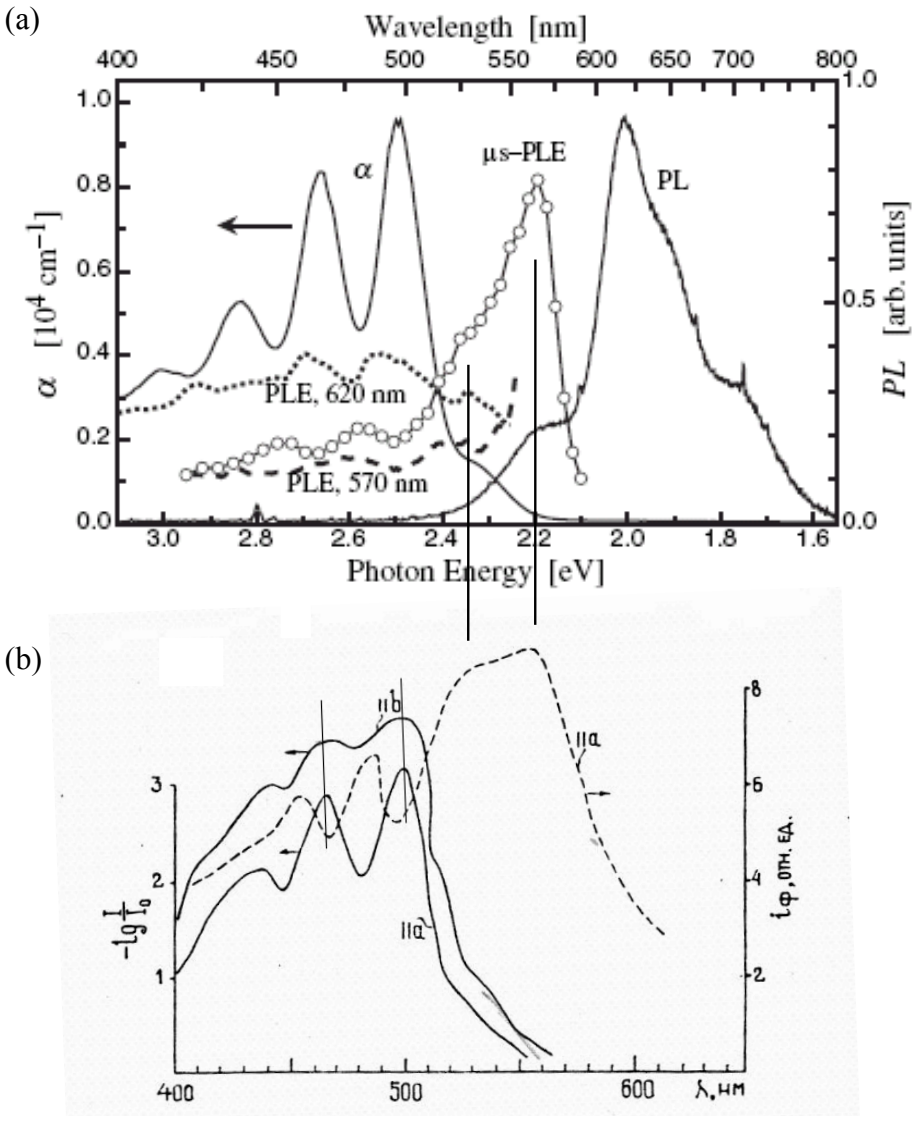

Fig. 6.21 *(a) PL, absorption a, cw PLE and μs-PLE spectra of a Rub crystal at room temperature. Reproduced from [49]. The cw PLE spectra were detected at 620 nm (dotted line) and 570 nm (dashed line). The μs-PLE was induced by transient b-polarized light (open circles). (b) Absorption spectra with orientation of the electrical E vectors of the incident light parallel to a-axis (IIa) and parallel to b-axis (IIb) of a Rub crystal at room temperature (compact lines). Photoconduction spectrum of a Rub crystal (dashed line). Reproduced from [6].*

Fig. 6.21 (a) shows a mirrorlike relationship between the PL emission and the μs-PLE spectrum. The mirrorlike relationship between the PL and the absorption (and the excitation) spectrum is typical for a transition between S_0 and S_1 states. For aromatic molecules, which exhibit vibrational bands, the energy spacing between the vibrational levels and the Franck-Condon factors (that determine the relative intensities of the vibronic bands) are similar in the ground and first excited state. The mirrorlike relationship corroborates the assumption that luminescence on the microsecond time scale is predominantly resulting from the S_1-S_0 transition [49].

Although the cw PLE spectrum detected at 610 nm from the present investigations are similar to the cw PLE spectrum detected at 620 nm reported by Najafov [49], the cw PLE spectra detected at 570 nm are not the same (see Figs. 6.19 and 6.21 (a)). This difference could be due to the low PL signals at 570 nm, which produce some inaccuracy in the form of PLE spectrum.

The cw PLE signal detected at 570 nm reported in the literature [49] was measured for a longer wavelength region (up to 550 nm, see Fig. 6.21 (a)). As was mentioned above, PLE spectra in our experiment were possible to measure only up to 517 nm because of the overlapping of the excitation light with the PL spectrum. Therefore, the comparison of the spectra at longer wavelength regions was not possible.

The comparison of Figs. 6.21 (a) and (b) shows that the μs-PLE spectrum is very similar to the spectrum of the photoconductivity (dashed line in Fig. 6.21 (b)) reported by Bulgarovslaya et al. [6]. Anticorrelation of the absorption and photoconduction spectra has been observed in polycrystalline Tc films as well [69]. It was interpreted as a result of different processes (e.g. recombination processes, injection effect) [69].

Interestingly, the PLE spectra and absorption spectra do not undergo strong temperature-depended changes, although the PL spectra at 300 K and at 50 K clearly differ from each other (see Fig. 6.16).

6.9 The gap between excitation energy and luminescence

One interesting feature of the PL characteristic at low temperatures has been observed. Fig. 6.20 (b) shows the existence of a clearly pronounced (840 cm^{-1}) energetical gap between the photoluminescence energy and the excitation energy at lower temperatures. As Fig. 6.20 (a) shows, it is difficult to recognize, if there is an energetical gap between exitation energy and the luminescence at room temperature or not due to the small crystal emission at room temperature and the relative strong and bright excitation light. Here it should be noted that a Rub solution at room temperature shows no gap between the excitation energy and the luminescence (see Fig. 6.22).

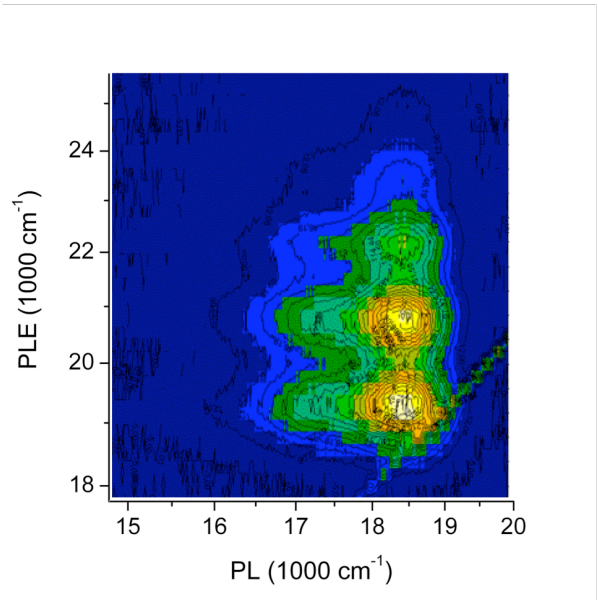

Fig. 6.22 *2-dimensional picture representing the PLE experiment performed on Rub in cyclohexane at room temperature. The experimental results do not show an energetical gap between the PL spectra and the excitation energy.*

Two different explanations of the energetical gap in the spectra of Rub crystals at lower temperatures should be discussed. In the first model (model 1, see section 6.6), the gap could be explained by the assumption of the formation of H-aggregates in the crystal (see Fig. 6.23). In the second model (model 2, see section 6.6), it is considered that it is not possible to excite species directly to the energetical level F', from which the PL emission (at 570 nm, component b_2 in PL spectra) is observed at low temperatures. Prior to the PL emission at 570 nm, the species must be excited to the higher energetic level with a following recombination to the energetical level F' (see Fig. 6.9, model 2).

6.9.1 H- and J-aggregate formation

The model of a relaxation mechanism in the system under the assumption of H-aggregate formation is shown in Fig. 6.23. The crystal structure determines the exciton band structure E (k), where k is the wavevector. The excitation of molecules always takes place at the centre of Brillouin zone, at the Γ-point (k = 0). The transition dipoles are parallel in a centre (k = 0) and antiparallel at the edge (k = π/a) of the Brillouin zone [70]. In the H-aggregates case, the antiparallel orientation of the transition dipole moments is energetically preferable. In this case, the energy of the edge of the Brillouin zone is energetically lower than in the centre of it. Thus, excitons relax to the edge of the Brillouin zone (k = π/a) during their lifetime. For emission from the edge of the Brillouin zone, the combination of the transition dipole moments of nearby molecules is out-of-phase. As a result the corresponding total transition dipole moment vanishes and H-aggregates are generally considered as poor emitters [70]. In the J-aggregates case, the parallel orientation of transition dipole moments is more preferable. Therefore, the energy at the centre of

the Brillouin zone is energetically lower than at the edge. Thus, in J-aggregates case the exciton emission takes place at the Γ-point. The transition dipole moments are in phase for nearby excitons. The phase coupling of transition dipole moments in J-aggregates could result in superrradiance [72] [73].

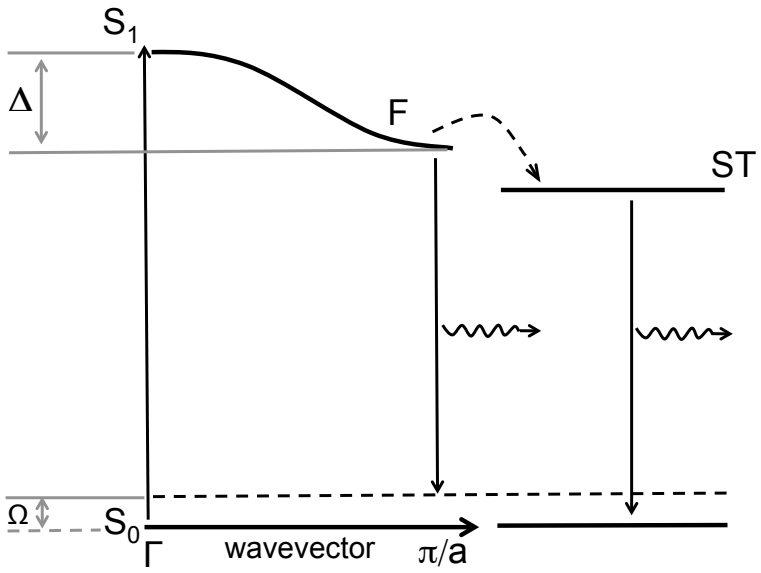

Fig. 6.23 *Schematic diagram of exciton relaxation under the assumption of an H-aggregate formation. S_0 - ground state, S_1 - first excited state, F - free exciton band, ST - self-trapped state, Γ-point - centre of the Brillouin zone, $k = \pi/a$ - edge of the Brillouin zone, Δ - energy modulation between Γ-point and edge of the Brillouin zone. Ω - vibration energy of the ground state.*

6.9.2 Calculated exciton bands structure for Rub crystal

In order to understand the band exciton structure in Rub crystals, the calculation of the excitonic band structure in the ab-plane of the Rub crystal was performed by R. Scholz [71] (see Fig. 6.24, full and dashed lines, respectively). Only dipole-dipole interactions within one single ab-plane are included, i.e. only between basic molecules residing in this plane, but ignoring the small interactions with the basis molecules in the adjacent ab-planes.

Fig. 6.24 shows two exciton bands, corresponding to two molecules in the 2-dimensional unit cell of the ab-plane. At the Γ-point, only the upper band exhibits oscillator strength, and the radiative decay is hence allowed. The upper band exhibits a negative band mass, as expected from the parallel orientation of the dipoles ("H-aggregates"). In H-aggregates, the minimum of the dispersion is at the edge of the Brillouin zone, where the transition dipole moments are in an out-of-phase relation. The 0-0 transition from the edge of the Brillouin zone is dipole forbidden. The transition is only possible to the electronic ground state with n vibrational phonons ($n > 0$) to carry

away the excess momentum. H-aggregates formation explains the very small free exciton emission in Rub crystals at room temperature.

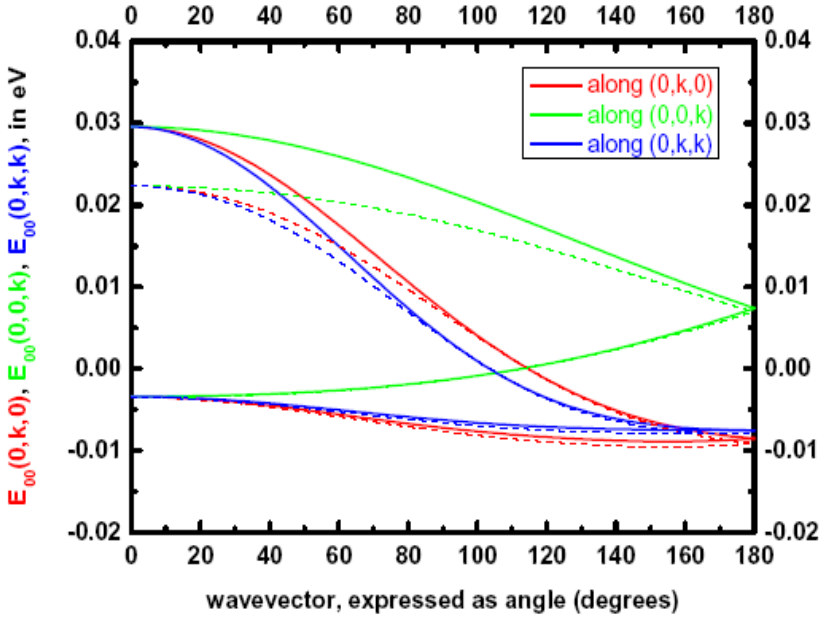

Fig. 6.24 *Calculated exciton bands structure in first perturbation theory in Rub crystal for the S_1-S_0 transition (solid lines). Reproduced from [71]. Calculated second order perturbation from the highest dispersion branches, so that the dispersion (E_{00}) is pushed down everywhere (dashed lines). Only dipole-dipole interactions in a single (ab)-plane are included, i.e. only between molecules residing in this plane, but ignoring the small interactions with the molecules in the adjacent planes. Upper dispersion branch: dipole-allowed at Γ-point, it carries the entire dipolar coupling strength, can be visualized by orientation of two contributing dipoles as two arrows pointing into the same direction. Lower dispersion branch: dipole-forbidden at the Γ-point, carries no dipolar coupling strength, can be visualised by the orientation of two contributing dipoles as two arrows pointing into opposite directions.*

Note, for a calculation with two molecules, the lower dispersion branch is quite flat in the direction (0,k,0), with an overall modulation of about only 6 meV. This indicates that the regions where the lowest dispersion branch can be populated at finite temperature might be quite different from the situation close to T = 0 K. For a temperature around kT = 6 meV or T = 70 K, thermalized excitons could be excited for any wavevector (0,k,0). This might be relevant for the temperature dependence of the PL.

No dispersion minimum has been found close to the Γ-point. Maybe the interaction between the basis molecules residing in this ab plane and the basis molecules in the adjacent ab-planes would be strong enough to generate such a minimum, but at the present stage this is rather speculative.

The energy modulation between the Γ-point and the edge of the Brillouin zone of the upper band is about 40 meV ($\Delta = 320\ cm^{-1}$) for the directions (0,k,0) and (0,k,k) (see Fig. 6.24). This value is in a good agreement with the value for the energetical gap (300 cm^{-1}, see Fig. 6.19) between the energy of the lowest-energy PLE peak and the energy of the highest-energy PL peak (peak a) at 300 K. The same value of calculated energy modulation between the Γ-point and the edge of the Brillouin zone and the observed gap between the energy of the lowest-energy PLE peak and the energy of the highest-energy PL peak at 300 K collaborates the H-aggregate formation in Rub crystal.

Low temperatures

The existence of an energetic gap between the excitation energy and the luminescence corroborates our assumption of the H-aggregate formation at low temperatures. This energetic gap in the case of H-aggregate formation is the energy modulation between the Γ-point and the edge of the Brillouin zone of the exciton band (Δ, see Fig. 6.23). The calculated value ($\Delta = 320\ cm^{-1}$) of the gap is much smaller than the gap observed in the experiment (840 cm^{-1}) (see Fig. 6.20 (b)).

It should be noted that the very strong luminescence at low temperatures (about 6 500 times higher in comparison to room temperature) rather corresponds to the assumption of a J-aggregate formation. If this is the case, then the nature of the energetic gap is still to be discussed.

The evidence of a superradiant behaviour was obtained for an organic semiconductor (quaterthiophene) whose molecules were arranged in a H-aggregate fashion [73] [74]. Spano [74] reported that rodlike molecules can form a sort of quasi bidimensional H-aggregation scheme, in which the charge carrier conduction is generally good, because of the large π-π interactions and which display the typical optical properties of the J-aggregate.

As shown, the properties of Rub crystals, such as the high energetical gap and the very strong emission, at low temperatures are not trivial to explain. Therefore additional experimental investigations, e.g. investigations of time-resolved properties of PL and also theoretical investigation could be helpful for the understanding of the nature of the excitation relaxation mechanism in Rub crystals.

6.10 Conclusions

For the first time the temperature dependency of cw PL in comparison with cw PLE and absorption spectra of Rub crystals have been studied. It was shown that the fluorescence spectrum of Rub single crystals shows a strong reversible variation with temperature. The spectral changes are accompanied by a very strong (x 6 500 times) increase of the PL intensity at low temperatures in comparison to the one at room tempera-

ture. At the same time, the absorption and cw PLE spectrum undergo only small changes during cooling.

Two simplified theoretical model of the excitation relaxation mechanism in Rub single crystals were proposed in the frame of the present study and have been used for the explanation of the experimentally observed temperature evolution of the PL spectra for the first time. The difference between the models concerns the interpretation of the low temperature emission at 570 nm. In model 1 the emission at 570 nm reproduces the free exciton emission. In model 2 the emission at 570 nm reproduces a de-excitation processes from a kind of trapped state. The emission peak at 610 nm is attributed to a kind of self-trapped state [49] in both models. It was shown that both models are capable to describe the temperature depended properties in the precision of our spectroscopic experiments. To characterize the underlying excitation relaxation mechanism, the temperature depended competition between the emission at 570 nm and the emission at 610 nm were analysed by model fits to the experimental data. The calculated curves are in very good agreement with the experimental data. From the fit the activation energies and decay rates were determined.

In addition, the PL characteristic shows the existence of an energetical gap (840 cm^{-1}) between the PL energy and the excitation energy at low temperatures. Such a high gap cannot be explained only by the H-aggregate formation in the crystal.

It was shown that the optical properties of Rub crystals are not trivially to explain only on the basis of cw data. Therefore, it was decided to perform time-resolved PL study on Rub crystals to get more detailed information about the excitation relaxation mechanism.

7 Time-resolved PL spectroscopy of Rub single crystals

7.1 Introduction

As reported in the previous chapter, the fluorescence spectra of Rub single crystals show an interesting temperature dependence, in particular strong changes in the shape of the PL spectra and a strong increase of the luminescence intensity at low temperatures. The nature of these changes is difficult to understand using only optical data performed under continuous illumination. Time-resolved (tr) measurements should hence give more detailed information on the emission processes and help to interpret the excitation relaxation mechanism in Rub crystals, which is discussed in the recent literature [49] [50] [63] [75].

In particular, three open questions concerning the tr PL measurements were considered:

1. Is there a significant difference between the lifetimes of the room temperature and the low temperature photoluminescence?

2. Is there evidence for superradiance at low temperatures?

3. Is there any difference in the photoluminecsence time decay for different wavelengths?

The present chapter will offer answers to some of these questions. First, it is necessary to mention several recently reported investigations, which include tr measurements for Rub as well. The analysis of the tr PL data for self-organized pyramidal structures on the (001) Rub crystal surface was reported by Stöhr et al. [75]. The reported lifetimes of the PL band at 17 660 cm^{-1} (566 nm) show a similar temperature depended behaviour as the PL band at 17 600 cm^{-1} (568 nm) of Rub single crystal obtained in the present work. However, the reported decay time (τ = 4 ns) of the emission at low temperature is about 2.5 times smaller [75] as the decay time in the present work ($\tau_{F'}$ = 10 ns) (see Fig. 7.6). In addition, Najafov et al. [49] [63] found that the large photoconductivity of Rub single crystals that is induced by short light pulses is produced by carriers released after an average time from a “reservoir state”. The authors developed a model, which explains the delayed excitation of charge carriers after short-pulse excitation. But the origin of the “reservoir state” is still under discussion.

7.2 Experiment

The Rub single crystals were handled in air after growth. Selected crystals were fixed on a glass plate. Some of them were fixed with a minimal drop of grease. Some of the crystals clung to the glass by themselves due to electrostatic interaction between the materials. The glass plate was fixed in the sample holder (made of electrolytic copper) and installed into the cryostat. The cryostat was maintained under high vacuum during the optical measurements. PL spectra were measured in the tr mode and, for comparison, also in the continuous wave (cw) mode. The tr PL measurements were taken for the following five temperatures while the sample was warmed up: 6 K, 50 K, 100 K, 150 K, and 260 K.

For the optical excitation, frequency doubled pulses with 80 MHz repetition rate from a Ti-Sapphire laser were used. The excitation wavelength could be varied, as well as the excitation power. The spot size diameter was about 100 μm. Spectral changes were also studied under the variation of the excitation power. Time-resolved data were recorded by a 0.25 m monochromator with a synchroscan streak camera and a CCD camera. The maximal possible time window covered in tr measurements was 2 ns. The repetition rate of the excitation pulse was 12.5 ns. From the two-dimensional data sets (e.g. see Figs. 7.1 (a) and (b)), taken as a function of wavelength and time, tr PL spectra (see Fig. 7.2) and decay curves (see Figs. 7.3-7.5) were extracted.

Time-integrated data were recorded by a 0.3 m monochromator with a CCD camera. The nominal spectral resolution of the tr PL spectra was smaller than the one of the cw PL spectra. This explains the slightly narrow shape of the "b" line in the cw spectra in comparison to the tr spectra in Figs. 7.2 (c) and (d). The tr measurements of the two Rub crystals (A and B) were performed in cooperation with PD Dr. R. F. Mahrt and Dr. T. Stöferle at IBM Research Laboratory, Rüschlikon, Switzerland.

7.3 Time-resolved PL spectra. Low power excitation case

7.3.1 PL spectra at different temperatures

2D steak camera PL images taken at 260 K and at 6 K are shown in Fig. 7.1 (a) and (b), respectively. The horizontal profile represents the PL spectrum as a function of the wavelength. The vertical profile represents the emission decay time spectrum. The moment of the optical excitation pulse was marked as the time 0 ps. Time-resolved PL spectra, which are represented above 0 ps are the spectra at the end of the cycle.

The 2D data show that the lifetime of the PL emission is different for high and low temperatures. The image at 260 K shows two emission relaxation decays - a short one and a long one. Short time emission has a much higher intensity compared to the long time one. The image at 6 K shows only the long time emission relaxation decay.

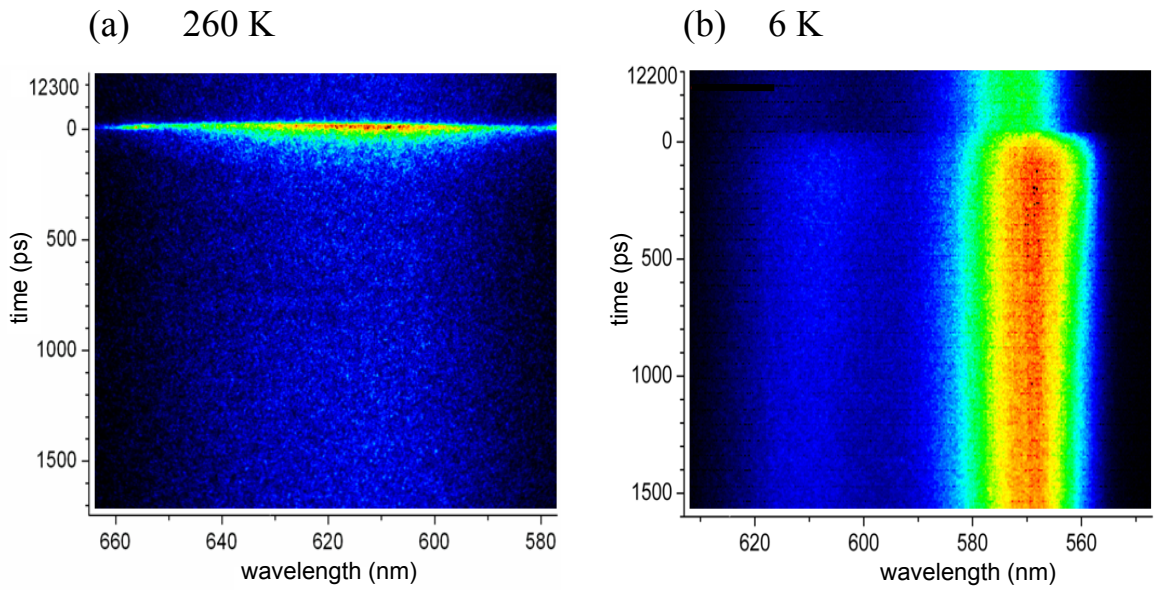

Fig. 7.1 *(a) 2D steak camera PL image of a Rub crystal taken at 260 K (λ_{ex} = 545 nm). The excitation power is 1.04 W/cm^2 (b) 2D steak camera PL image taken at 6 K (λ_{ex} = 440 nm). The excitation power is 0.78 W/cm^2. The horizontal profile represents the PL spectrum as a function of wavelength. The vertical profile represents decay spectrum. The time 0 ps was set to the moment of the optical excitation pulse. The maximal time window covered in the measurements was 2 ns. The repetition rate was 12.5 ns. The tr PL spectra, above 0 ps are the spectra at the end of the repetition cycle of the detection. Blue, white blue, green, yellow and red colours represent an increasing of the PL intensities, correspondingly.*

The tr PL spectra integrated over the different time intervals after the pulse were extracted from the 2D data sets. In order to compare them, extracted PL spectra integrated over the first 50 ps (blue curves) and integrated over the last 50 ps of the pulse (red curves) are presented together with the cw PL spectra (black curves) (see Fig. 7.2).

(a) 260 K spectra

As seen in Fig 7.2 (a), the PL spectrum integrated over the first 50 ps after the pulse and the PL spectrum integrated over the last 50 ps of the repetition cycle are very similar to the cw spectrum at 260 K. It is important to note that the PL spectrum integrated over the first 50 ps after the pulse is very similar to the spectra integrated over first few ps. Even during the excitation pulse, a broad luminescence spectrum is observed. Thus, the excitation redistribution on the emitted energy levels occurs on a time scale shorter than the time resolution of our experiment. Similar ultrafast spectral relaxation has been observed in π-conjugated polymers [76] and in smaller organic molecules [77].

The shape of the cw spectrum and the spectrum integrated over the last 50 ps have slightly higher intensities for wavelengths above 610 nm in comparison to the spectrum integrated over the first ps. Probably that is a result of energy relaxation. The small peak (at about 635 nm) in the spectra integrated over the last 50 ps might occur due to an artefact of

the smooth of the spectra integrated over the very low emission intensity in the end of the repetition rate. Therefore this peak was not considered further.

The limited statistics of the measured tr PL spectra at temperatures between 260 K and 100 K is explained by the low PL intensities over the first and the last 50 ps of the repetition cycle and by the low number of spectra accumulated to get the reported spectra. To protect the CCD camera from the strong laser light (at 545 nm), only 10 experimental spectra were included in the accumulation. Note, the shapes of the tr spectra integrated over longer time intervals than 50 ps are the same as those of spectra integrated over 50 ps only which are reported in Fig. 7.2. Therefore this statistics represent quite satisfactory experimental data.

(b) 150 K spectra and (c) 100 K spectra

As presented in Fig. 7.2, the intensity of the peak b (b_1 at high temperatures and b_2 at low temperatures) strongly increases with cooling. Different evolutions of the different parts of the PL spectra in time are observed from the tr spectra integrated at different post pulse delay times. As seen in Fig 7.2 (b), (c), the spectra integrated over the first 50 ps (blue curve) and the last 50 ps of the repetition rate of the pulse (red curve) are different. The emission represented by peak b_2 is stronger than the emission represented by peak c in the PL spectra integrated over the first 50 ps after the pulse (see blue lines). However peak b_2 is not visible or only visible as a small shoulder in the PL spectra integrated over the last 50 ps of the repetition rate (see red lines). Emission represented by peak c is stronger than the emission represented by peak b_2 over the last 50 ps. This means that the emission represented by peak b_2 has a shorter decay as the emission represented by peak c. This indicates that these luminescent species have a different nature. This result is in good agreement with our assumption about the different nature of peaks b_2 and c (models 1 and 2, section 6.6).

The lifetime of the peak b_2 increases during the cooling. This possible to see from the comparison of the tr spectra measured in time over the last 50 ps of the repetition cycle (red curves, Fig 7.2 (b), (c)) at 150 and at 100 K. The emission of peak b_2 is not visible at 150 K. But the emission is still notable after a delay of 12.45 ns at 100 K.

The comparison of the cw PL spectra with the tr PL spectra integrated over the first 50 ps at established temperatures shows some differences in the ratio of intensities of the emission peaks. At 150 K, the intensity of the peak b_2 is lower in the cw spectra than in the tr spectra. At 100 K, they have the equal height. The origin of the increase of the emission of peak b_2 during the cooling was discussed in section 6.6.

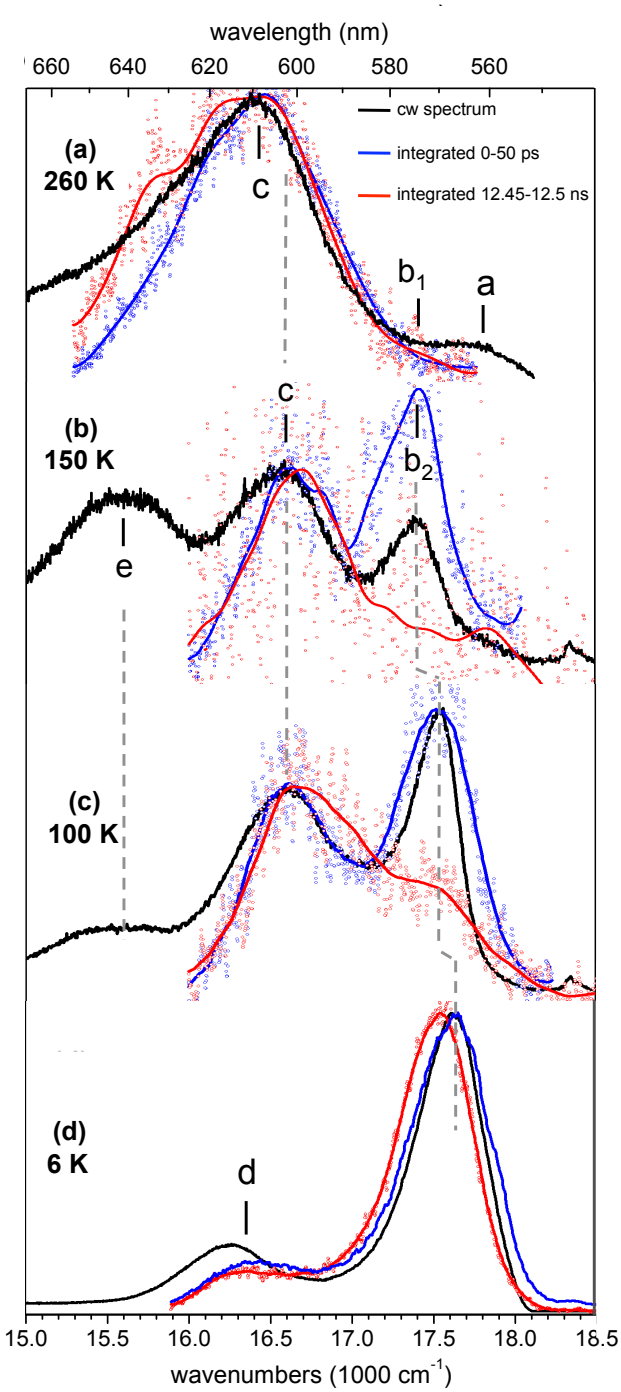

Fig. 7.2 *PL spectra of a Rub crystal at four different temperatures. Open circles represent tr experimental data. 10 spectra were accumulated to create these data sets, respectively (see details about statistics on p. 96). Continuous red and blue lines are smoothed data (50 points smoothing in Origin7). Blue lines - spectra integrated over the first 50 ps, red lines - spectra integrated over the last 50 ps of the repetition cycle, black lines - cw spectra. The time to measure one cw spectrum was 10 seconds. All spectra were normalized at the maximum of the intensity and shifted vertically against each other for clarity.* λ_{ex} *= 545 nm for (a), (b), (c), see small shoulder in cw spectra (b) and (c).* λ_{ex} *= 450 nm for (d). The labelling of the peaks is consistent with that of earlier chapter (see section 6.3).*

(d) 6 K spectra

As can be seen in Fig. 7.2 (d), the spectra integrated in time over the first and last 50 ps of the repetition cycle are very similar. This indicates the presence of only one luminescence species at low temperatures. As it was noted above, peak b_2 has been identified as the emission from the F' state. Therefore peak d is attributed to the not-resolved vibronic progression of the F' $\rightarrow$ S_0 transition.

The tr spectra show a red shift (about 100 cm^{-1}) in the positions of both peaks b_2 and d during the first 12.5 ns (see Fig. 7.2 (d), blue and red curves). This shift is related to some dynamical relaxation processes, which occur after the pulse (see Fig. 7.3).

The cw spectrum shows the same position of peak b_2 as in the tr spectra over the first 50 ps (see Fig. 7.2 (d)). It shows a small red shift of peak d in comparison to the tr spectrum. This shift can be explained by a slow relaxation of excitation to an energetically lower trap state.

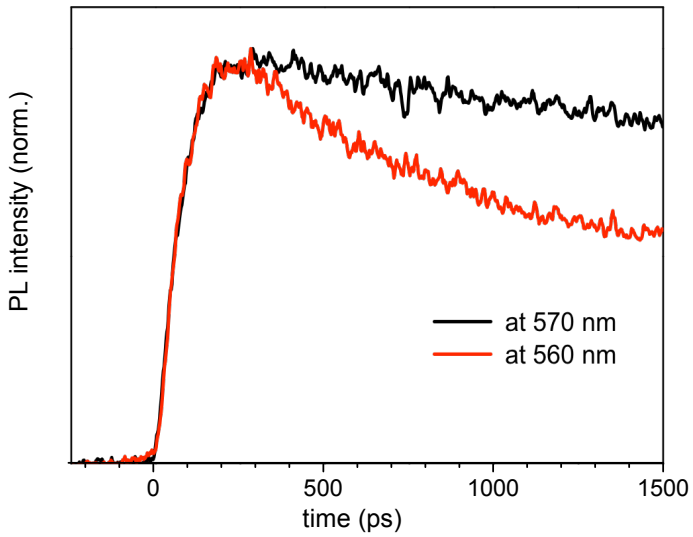

Fig. 7.3 *Decay curves of the PL intensity of a Rub crystal for different energies at 6 K. The back and red curves were extracted from emission spectra integrated over 570 ± 5 nm and 560 ± 5 nm respectively. PL intensities were normalized.*

It is important to remark that, unfortunately, the tr data set at 260 K includes a spectral area only up to 17 800 cm^{-1}. This wavelength region does not overlap with the area of the peak a (cw spectra, Fig. 7.2). The comparison of the time decay of peak a and b_1 could be helpful in understanding their nature: namely, if these peaks have a similar nature and would support the free exciton emission (model 1), or have a different nature and are supporting the free exciton emission and trapped states. Therefore further experiments, which will include the spectral area higher as 17 800 cm^{-1}, would be necessary and helpful.

It should be noted that the temperature depended cw PL spectra taken at the IBM Research Laboratory (see Fig. 7.2) and in our laboratory (see Fig. 6.2) are identical with a small deviation of the spectral shape at 150 K and 100 K. Particular, the spectrum taken at the IBM at 150 K is more consistent with the spectrum taking in our laboratory at 110 K. And the spectrum taken at the IBM at 100 K is more consistent with the spectrum taking in our laboratory at 70 K (see Fig. 6.10). The spectra at 260 K and at 6 K measured in both laboratories are identical with each over.

7.3.2 Time decay curves of the PL intensity. Experiment. Model. Fits

Fig. 7.4 shows the experimental decay curves of the integrated fluorescence intensity of the Rub single crystals at four different temperatures: (a) 260 K monitored at 610 nm (peak c); (b) 150 K, (c) 100 K, and (d) 6 K monitored at 570 nm (peak b_2). Black circles are the experimental data, the red curves are fits. As Fig. 7.4 shows, cooling of the sample leads to an increase in the luminescence decay time.

It should be noted that the increase of the radiative lifetime of the free exciton state (situation of model 1) with cooling is not typical for organic crystals [78] [52]. Matsui concluded that, if the exciton lifetime in a molecular crystal decreases as a temperature increases, the lifetime is dominated by traps [79].

Generally, an increase of temperature results in a decrease of the PL efficiency η and the corresponding lifetime τ of an excited state. This is because the non-radiative processes are related to thermal excitations [68]. The PL efficiency is given by

$$\eta = \frac{k_{rad}}{k_{rad} + k_{nonrad}} = k_{rad}\tau . \tag{7.1}$$

The cooling from 300 K to 6 K multiplies the time constant τ of the F' state by a factor of about 100 (see Tabs. 7.1 and 7.2). This explains the increase of the photoluminescence by a factor 6 500 only partly. From eq. 7.1 follows that the radiative decay rate k_{rad} should increase as well.

It is necessary to notice that a difference in the emission decay times at different wavelengths of a sample at the same temperature was not found. For low temperatures data this is predictable under the assumption of the same nature of all visible peaks in PL spectra at low temperatures - namely the vibronic progression of the F' $\rightarrow$ S_0 transition.

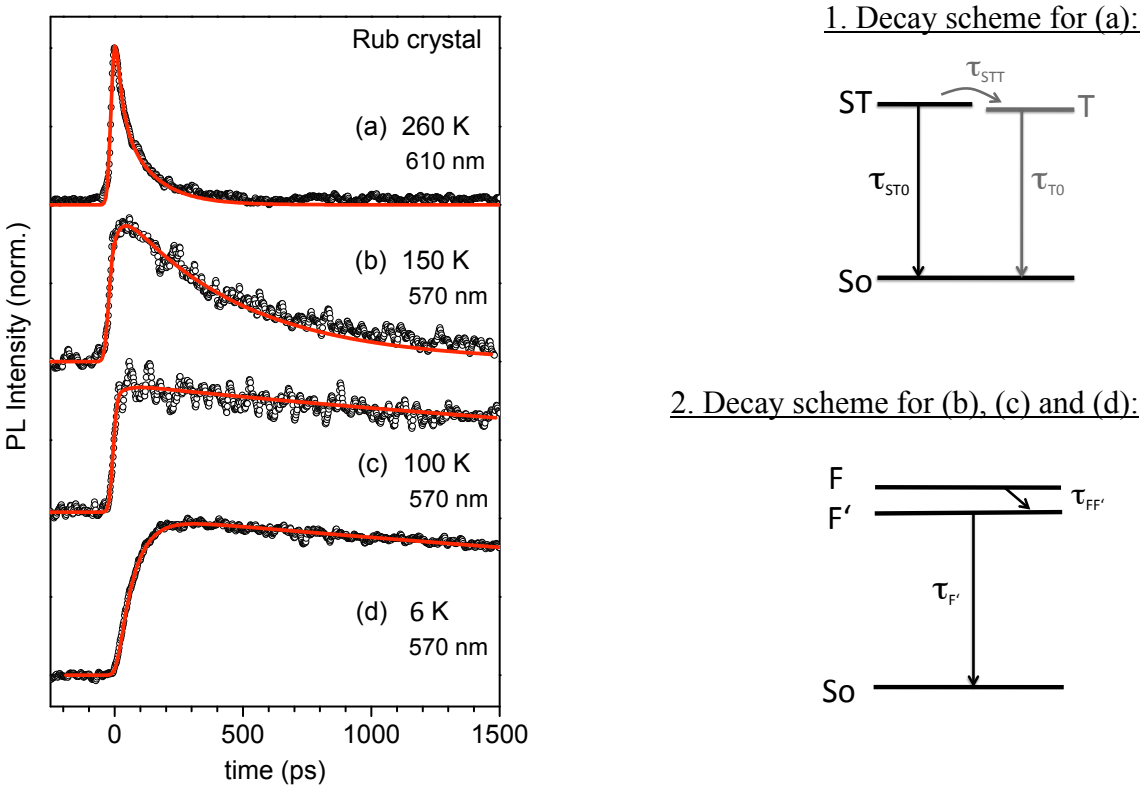

Fig. 7.4 *Black circles represent decay curves of the integrated fluorescence intensity of a Rub crystal at four different temperatures: (a) 260 K integrated over 610 ± 5 nm and (b) 150 K, (c) 100 K, (d) 6 K integrated over 570 ± 5 nm. Red curves are fits by eq. 7.2 for (a) and by eq. 7.4 for (b). (c), (d). The schematic diagram of the excitation-relaxation from the ST state (at 610 nm) at high temperatures is shown on the right hand side of the image: 1. decay scheme for (a). The excitation-relaxations from the F' state (at 570 nm) at low temperatures are shown in the 2. decay scheme for (b), (c) and (d).*

At high temperature (260 K), the difference in the decay curves is to be expected, under the assumption of the different nature of the peak b_1 and c. However as Fig. 7.5 shows, there is no visible difference in decay curves detected at 610 nm and 570 nm at 260 K. That could be explained by the similar decay time for both transitions or by the low statistics of experimental data due to the very low intensity of the emission at 570 nm.

Fits

1. High temperatures

As mentioned above, the time-resolved image at 260 K shows two emissive relaxation decays: a short-time one and a long-time one (see Fig. 7.1 (a)). Two different PL decays are explained by the existence of two luminescence species. The author attributes the short living decay (610 nm, maximum of emission at high temperatures) to the self-trapped (ST) exciton emission and the long living component (see Fig. 7.1(a)) to an additional trap state (T), which energetically slightly lower than the ST state and which is

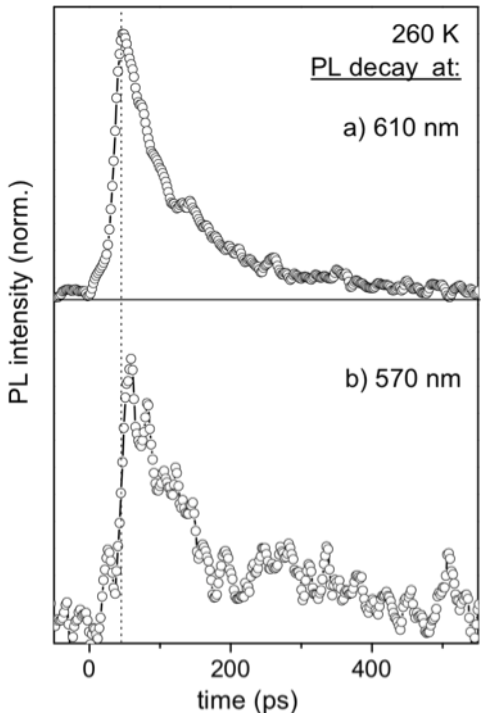

Fig. 7.5 *Comparison of decay curves of the PL intensity of a Rub crystal for different wavelength at 260 K. The curves a) and b) are extracted from the emission spectra at 610 ± 5nm (ST state) and 570 ± 5 nm (F' state), respectively. The PL intensities were normalized.*

filled by energy relaxation from the ST state. The simplified deexcitation decay scheme from ST state (610 nm) for high temperatures is shown on the right hand side of Fig. 7.4. The decay curve of the integrated intensity (including emission from ST) is shown in Fig. 7.4 (a) (black circles). The integrated intensity as a function of time can well be fitted by an exponential luminescent decay (eq. 7.2) as shown in Fig. 7.4 ((a), red curve). Note that the emission from the T state cannot be included in the fit due its very long lifetime in comparison to the maximal possible time-window in the tr measurements. So, the emission from the T state has been ignored and has been added as a constant in the fitting procedure. Only the ST state has been included in the fitting of the decay curve of the integrated fluorescence intensity. As such the fitting model is a simplification by neglecting the feeding process of the ST state from the $F^{(')}$ state and by neglecting the emission from the T state. The model is described by the following time dependence of the luminescence intensity of the ST state:

$$I(t) = A_{ST} \exp\left(-t/\tau_{ST}\right). \tag{7.2}$$

The state ST decays with decay time constant τ_{ST} which includes the radiative and non-radiative decay into the ground state S_0, with a time constant τ_{ST0} and a feeding of the T state with a time constant τ_{STT} (eq. 7.3).

$$1/\tau_{ST} = 1/\tau_{ST0} + 1/\tau_{STT}. \tag{7.3}$$

The amplitude A_{ST} was taken as a free fitting parameter. The convolution by a Gaussian was used to describe the instrument response function. The parameters extracted from the fitting procedure using eq. 7.2 are reported in Tab. 7.1.

T (K)	$k_{ST}(sec^{-1})$	τ_{ST}(sec)	A_{ST}	R^2	c
260	$(1.19\pm0.04)x10^{10}$	$8.30x10^{-11}$	0.6	0.954	18

Tab. 7.1 *Decay time constant τ_{ST}, decay rate k_{ST} ($1/\tau_{ST}$), amplitude A_{ST}. The parameter R^2 shows a value describing the quality of the fit (Origin 7), c is the FWHM of the Gaussian function.*

2. Low temperatures

The decay curves of the integrated fluorescence intensity of Rub crystal for low temperatures are shown in Fig. 7.4 ((b), (c) and (d), black circles). Model 2 (see p. 69) was chosen to describe the decay curves of the PL intensity due to the clearly observed slow increase of the PL intensity in time with a maximum at about 200 ps after the excitation pulse at 6 K. This observation is explained by a non-direct excitation of the emitted state (F'), where the luminescence of F' builds up due to feeding from the state F. The decay scheme for the low temperature cases is presented in Fig. 7.4 (right side, bottom). The scheme shows an energetical gap between the excited state and the emitting state. This model is in agreement with the PLE results, which show this gap between excitation and emission spectra at low temperatures (see Figs. 6.20 (b)).

The low temperature model can be described by the following time dependence for the luminescence intensity [52]:

$$I(t) = A_{F'}\left[\exp(-t/\tau_{F'}) - \exp(-t/\tau_{FF'})\right]. \tag{7.4}$$

The first term $A_{F'}\exp(-t/\tau_{F'})$ describes the luminescence decay from the F' state with a time constant $\tau_{F'}$, the second term $-A\exp(-t/\tau_{FF'})$ describes feeding of the F' state with a time constant $\tau_{FF'}$. The state F' decays with the decay time constant $\tau_{F'}$, which includes the radiative ($\tau_{radF'}$) and non-radiative (τ_{nr2}) decays into the ground state (S_0) and a feeding of the ST state (τ_{nr1}):

$$1/\tau_{F'} = 1/\tau_{radF'} + 1/\tau_{nr1} + 1/\tau_{nr2}. \tag{7.5}$$

As shown in Fig. 7.4 (b), (c) und (d) (red lines), the integrated intensity as a function of time can well be fitted by eq. 7.4. This indicates the validity of the model. As for the high

temperature case, a convolution by a Gaussian to describe the experimental broadening has been used again. The amplitude $A_{F'}$ has been taking as a free fitting parameter. The parameters extracted from the fit using eq. 7.4 are reported in Tab. 7.2.

T (K)	$k_{FF'}$ (s^{-1})	$\tau_{FF'}$ (s)	$k_{F'}$ (s^{-1})	$\tau_{F'}$(s)	$A_{F'}$	R^2	c
6	$(1.82\pm0.03)\times10^{11}$	5.49×10^{-12}	$(1.00\pm0.03)\times10^{8}$	1.00×10^{-8}	0.48	0.993	27
50	$(3.7\pm0.2)\times10^{11}$	2.70×10^{-12}	$(1.11\pm0.04)\times10^{8}$	9.09×10^{-9}	0.46	0.987	27
100	$(6.46\pm0.47)\times10^{11}$	1.55×10^{-12}	$(2.10\pm0.06)\times10^{8}$	4.76×10^{-9}	0.41	0.975	27
150	$(6.64\pm0.35)\times10^{11}$	1.51×10^{-12}	$(1.56\pm0.008)\times10^{9}$	6.41×10^{-10}	0.5	0.969	27

Tab. 7.2 *Experimental decay time constants $\tau_{FF'}$ and $\tau_{F'}$, decay rates $k_{FF'}$ $(1/\tau_{FF'})$ and $k_{F'}$ $(1/\tau_{F'})$, amplitude $A_{F'}$. The parameter R^2 describes the quality of the fit (Origin 7), c is the FWHM of the Gaussian function.*

Fig. 7.6 shows the increase of decay time constant $\tau_{F'}$ and non-radiative decay time constant $\tau_{FF'}$ for decreasing sample temperature. Fig 7.7 shows the temperature-dependent decay rates $k_{F'}$ $(1/\tau_{F'})$ (black circles). Low temperatures values (from 6 K till 150 K) were determined by fitting the decay curves using eq. 7.4. The high temperature value (260 K) was determined by fitting the decay curve using eq. 7.2.

The temperature-dependent decay rate $k_{F'}$ can be described by the following equation including a radiative decay and two non-radiative decay channels [75]:

$$k_{F'}(T) = \frac{1}{\tau_{F'}(T)} = k_{nr1}\exp\left(-\frac{E_1}{k_B T}\right) + k_{nr2}\exp\left(-\frac{E_2}{k_B T}\right) + k_{radF'}. \qquad (7.6)$$

Using eq. 6.12, $k_{F'}(T)$ can be rewritten as:

$$k_{F'}(T) = \frac{1}{\tau_{F'}(T)} = ak_{radF'}\exp\left(-\frac{E_1}{k_B T}\right) + bk_{radF'}\exp\left(-\frac{E_2}{k_B T}\right) + k_{radF'}. \qquad (7.7)$$

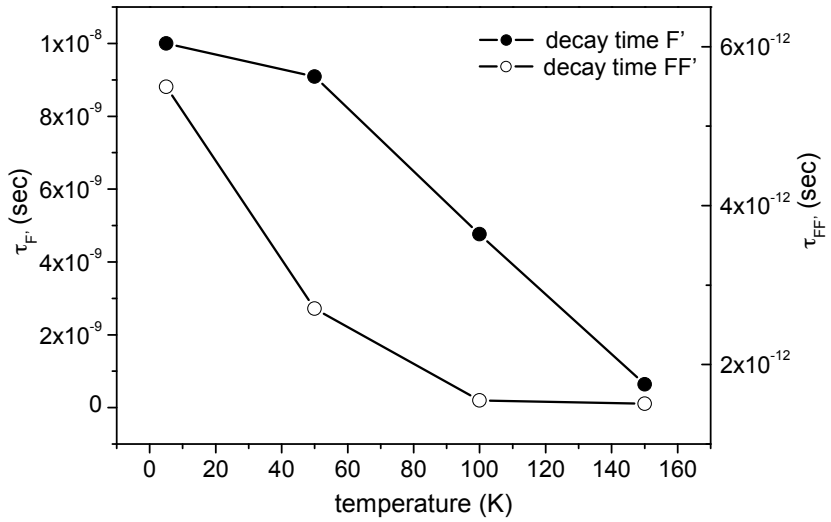

Fig. 7.6 *Temperature-dependent decay time constants $\tau_{FF'}$ and $\tau_{F'}$ have been determined from the fits by eq. 7.4 to the time dependent integrated intensity.*

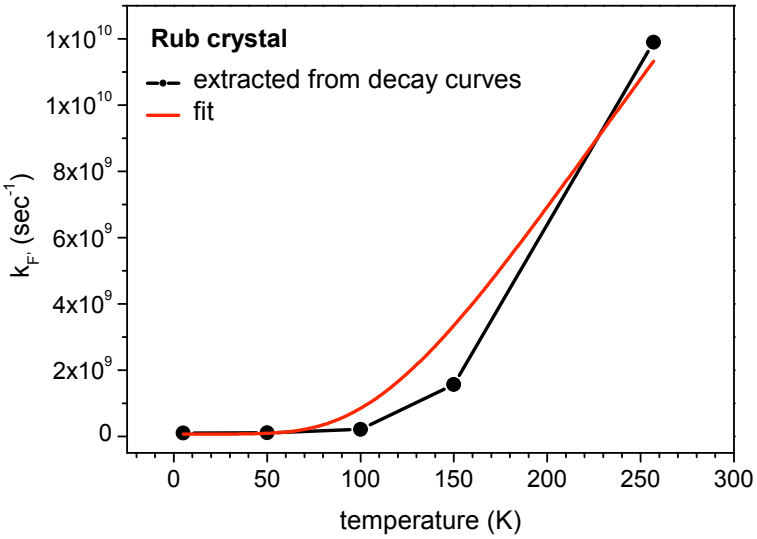

Fig. 7.7 *Temperature-dependent decay rates $k_{F'}$. The black circles are decay rates extracted from decay curves of the integrated fluorescence intensities. The red line is a fit.*

Temperature-dependent decay rates $k_{F'}$ extracted from the experimental data (see Fig. 7.7, black circles) were fitted by eq. 7.7 using the constants (*a*, *b*, *c*, E_1 and E_2, see p. 72) which in turn were determined from the fit of Fig. 6.7 and Fig. 6.8 by eq. 6.10 and eq. 6.11. This fit is presented in Fig. 7.7 by the red line. From the fit the radiative rate $k_{radF'} = 6.7 \cdot 10^7\ s^{-1}$ was determined. As shown in Fig. 7.7, the decay rates extracted from the PL decay curves and the fit have a similar behaviour and increase with the increase of the temperature. The decay rates extracted from the PL decay curves and the fit are in a very good agreement at temperatures below 50 K. At higher temperatures (100 K and 150 K), the values of the calculated decay rates are a slightly higher than the experimental

values. Intuitively, this can be explained by an increase of the number of, e.g. non-radiative recombinations, which have not been taken into account by the models for simplification.

7.4 PL spectra at high excitation power

In this section the influence of the input power on the emission spectra of Rub crystals at low temperatures (6 K) are reported. Interesting spectral changes at high excitation power are observed. This section discusses their possible origins. The PL cw and tr spectra were measured for the case that the ab plane of the crystals is perpendicular to the incident light.

7.4.1 cw experimental data

The shape of PL spectrum does not change upon variation of excitation powers for the laser excitation intensity below 89 mW/cm^2. As shown in Fig. 7.8, the additional sharp peaks in the PL spectrum appear at excitation intensities above 89 mW/cm^2. The increase of the excitation power leads to an increase of the intensity of sharp peaks (see Fig. 7.8).

Fig. 7.9 shows the evolution of the PL spectra of the same Rub crystal upon the increase of the excitation power with better spectral resolution (grating 1800 lines/mm). The spectra are measured at the different position of the same crystal in comparison to the one in Fig. 7.8. From the better spectral resolution, it is possible to see that several additional sharp lines appear at an excitation power above 89 mW/cm^2. In addition, the number of new lines increases with the increase of the excitation power. For 165 mW/cm^2, the spectrum shows only one clear, pronounced sharp line (at 17 810 cm^{-1}). Follow up increase of the excitation power leads to an increase of the number of additional sharp lines. The line positions do not change with the variation of power.

Fig. 7.10 shows the PL spectra at different positions of the same Rub crystal. The positions of the some lines coincide. But, due to the observation of those lines, which do not belong to both spectra, it can be concluded that the observed emission does not represent the real energies of the Rub molecules and is the result of the lasing (see section 7.4.3). An analogical situation is observed by the comparison of the positions of sharp lines of the different crystals (see Fig. 7.11). The positions of some lines coincide, but some of them are different.

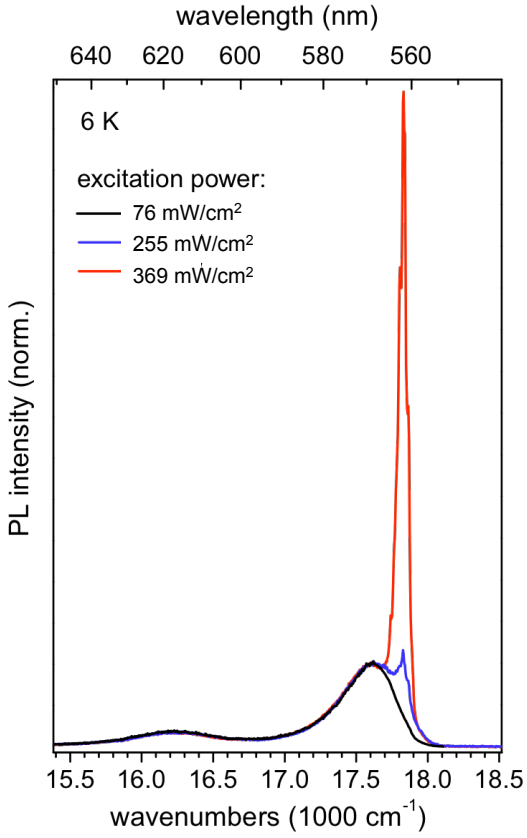

Fig. 7.8 *The cw PL spectra of a Rub crystal (crystal A) at 6 K for the same position at different excitation powers. The black line is the PL spectrum at an excitation power 76 mW/cm^2 (without long pass filter). The blue line is PL spectrum at an excitation power 255 mW/cm^2 (with long pass filter, transition > 490 nm, to protect detector from laser emission). The red line represents the PL spectrum at excitation power 369 mW/cm^2 (with a long pass filter). λ_{ex} = 450 nm. The spectra were normalized at the maximum position for low powers (570 nm). The grating had 300 lines/mm.*

7.4.2 Time-resolved experimental data

The tr data show several interesting phenomena. First of all, although the excitation wavelength was 450 nm, there are two horizontal lines at about 555 nm and one line at about 520 nm in two-dimensional emission spectra (see Figs. 7.12 (a) and (b)). These lines were attributed to the laser lines. The origin of the "satellites" is associated with nonlinear optical effects in Ti-Sapphire laser, but is still not absolutely clear at the moment. The position of earliest satellite at 555 nm was set as time 0 ps. The second satellite came with delay in 55 ps (see Fig. 7.13 (b)). Both lines have the same short FWHM on the time scale, which is equal to 15 ps.

Furthermore, the two-dimensional images show several vertical sharp lines which appear with some delay after the laser pump (see Figs. 7.12 (a) and (b)). These lines are identical to the sharp lines in cw spectra, which appear at high excitation power (see

Fig. 7.11, crystal B). From the comparison of two-dimensional pictures for 92 mW/cm^2 and 115 mW/cm^2 (see Figs. 7.12 (a) and (b)) it is possible to see that the time delay dependents on the excitation power. The vertical cuts of these two-dimensional pictures represent the time evolutions of the PL spectra for two different excitation powers (see Figs. 7.13 (b) and (d)). As shown in Fig. 7.13 (c), the time delay decreases from 229 ps to 62 ps with an increase of the excitation power from 92 mW/cm^2 to 153 mW/cm^2. Additionally, Figs. 7.13 (b) and (d)) show a symmetry in the time evolution of the PL spectra of the delayed emission. This is a sign of an equilibrium in the population and depopulation processes of the emitting energy level. The FWHM of vertical lines (in time scale) decreases with an increase of the excitation power (Fig. 7.13 (c), open circles).

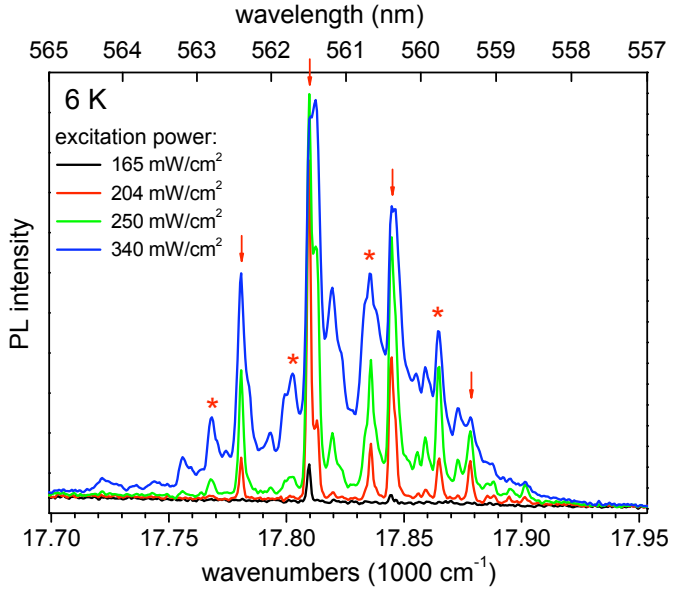

Fig. 7.9 *PL spectra of a Rub crystal at different excitation powers and at the same position of the crystal (crystal A, the position of the crystal is different in comparison to one in Fig. 7.8) at 6 K. λ_{ex} = 450 nm. Grating has 1800 lines/mm. The two groups of the equidistant lines are marked by red arrows and stars.*

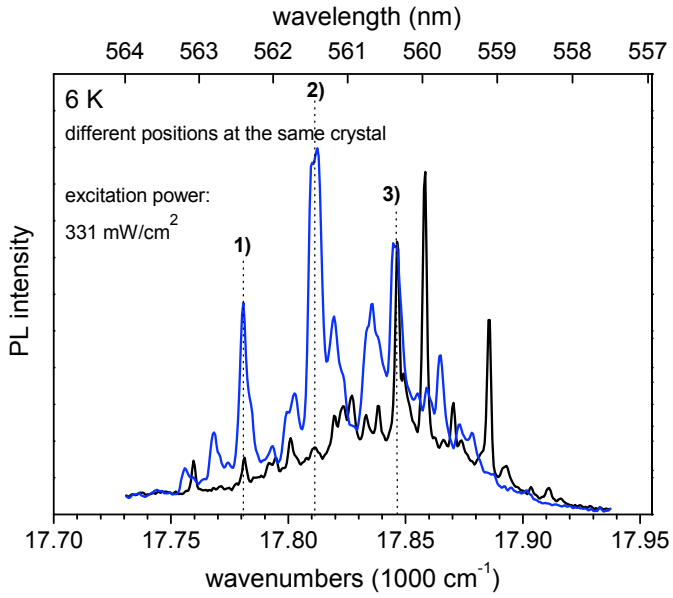

Fig. 7.10 *PL spectra of a Rub crystal at different positions on the crystal (crystal A). λ_{ex} = 450 nm. The grating had 1800 lines/mm. The positions of some lines are the same for different positions at the crystal: peak 1) at 17 781 cm^{-1}, peak 2) at 17 811 cm^{-1} and peak 3) at 17 845 cm^{-1}. The frequency spacing $\Delta\nu_1$ between peak 1), 2) and 3) is about 30 cm^{-1}.*

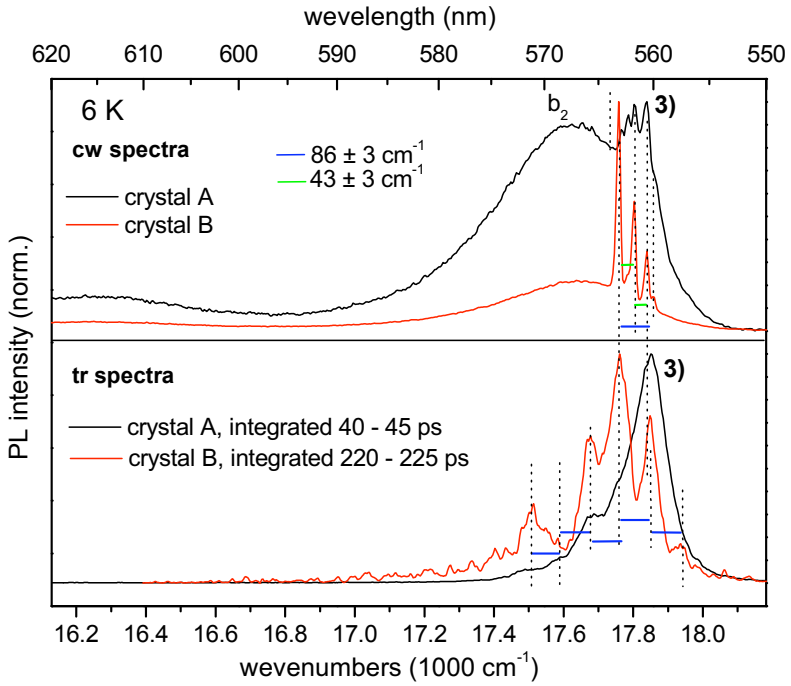

Fig. 7.11 *PL cw and tr spectra of Rub crystals at 6 K. Excitation power was 255 mW/cm^2 (with long pass filter) for the spectrum of the crystal A. Excitation power was 92 mW/cm^2 for the spectrum of the crystal B (without long pass filter). λ_{ex} = 450 nm. Both spectra are normalized. The positions of some lines are the same for the crystal A and B. The peak 3) at 17 845 cm^{-1} is the same as in Fig. 7.10.*

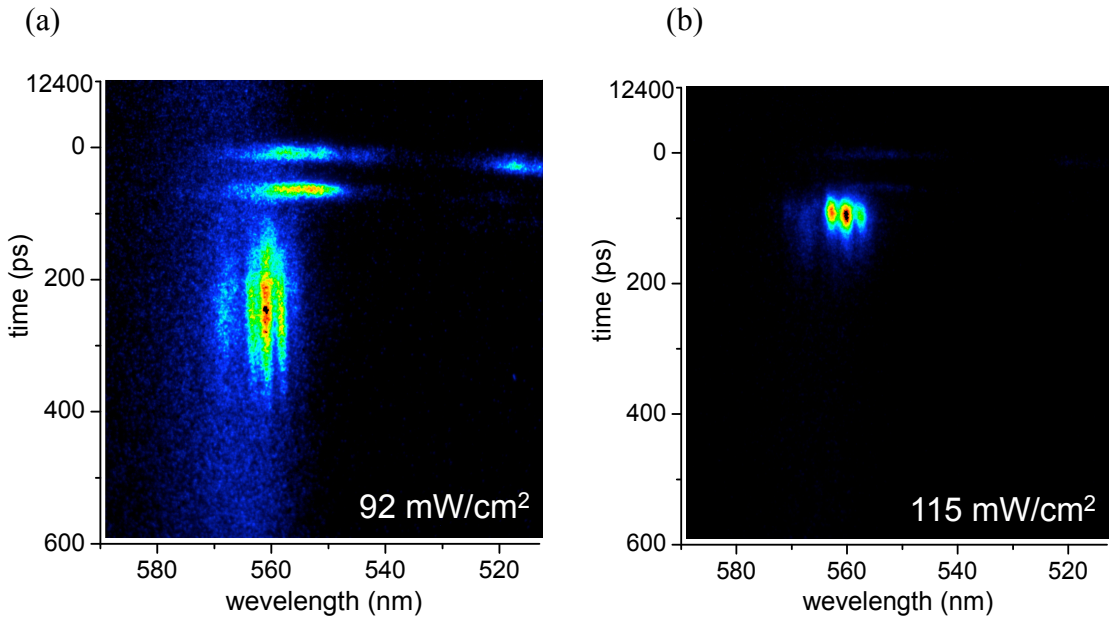

Fig. 7.12 *2D steak camera PL images taken at 6 K: (a) Excitation power was 92 mW/cm^2, (b) Excitation power was 115 mW/cm^2. λ_{ex} = 450 nm. Crystal B. For further analysis the position of earliest "satellite" was set as time 0 ps.*

7.4.3 Discussion of the experimental data

What is the origin of the additional sharp peaks in the PL spectrum in the high power excitation case? This is the most interesting question. In this section the author discusses the possible origin of this observation. There are at least two possible points of view in the interpretation of these results. The observed lines could appear due to optical pumped spontaneous emission or due to the lasing in Rub crystals. Because the nature of the lines is under discussion, the possible interpretations based on both assumptions will be presented.

Spontaneous emission?

In case of amplified spontaneous emission, the positions of the lines should be the same for different spots on the crystal and for different Rub crystals as well. As Figs. 7.10 and 7.11 show, the positions of some lines coincide, but some of them are different. That might be a sign that the observed emission does not represent the real energies of Rub molecules. In the case of an amplified spontaneous emission, the observed delay in the luminescence (see Fig. 7.12) means that after the excitation of a higher energy level the energy relaxation to a lower level is followed by delayed luminescence from it.

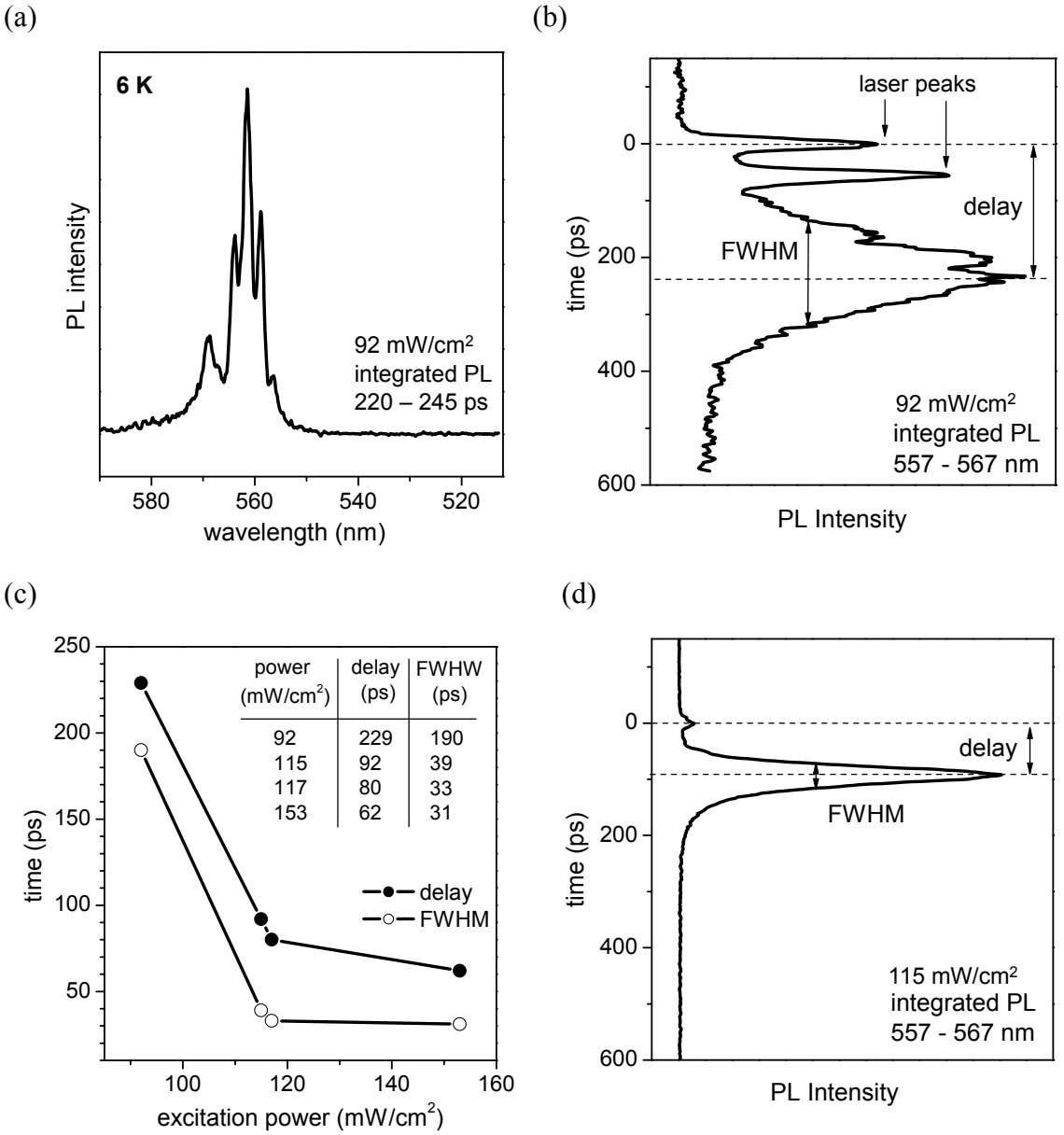

Fig. 7.13 *(a) Integrated PL spectrum over time 220-245 ps after the laser pulse, obtained from a horizontal cut of Fig. 7.12 (a), excitation power 92 mW/cm^2. (b) and (d) The time evolution of the PL spectra, integrated over wavelength region 557-567 nm, obtained from a vertical cut of Fig. 7.12 (a) (excitation power 92 mW/cm^2) and Fig. 7.12 (b) (excitation power 115 mW/cm^2), correspondently. (c) Dependence of emission delay (filled circles) and the FWHM in the time decay curve on the excitation power (open circles).* λ_{ex} *= 450 nm. Crystal B.*

Lasing?

In the case of lasing, the sharp lines represent resonator modes and thickness of the crystal corresponding to a cavity (resonator) length. The energetical positions of these lines (resonator modes) are given by eq. 7.8 [80]:

$$v_q = q/2Ln, \tag{7.8}$$

where ν_q are the wavenumbers, q is an integer number, n is the refractive index of the crystal, L is the length of the resonator.

The difference between neighbouring standing waves $\Delta\nu$ (in wavenumbers) is given by eq. 7.9:

$$\Delta v = v_q - v_{q-1} = \frac{q}{2Ln} - \frac{q-1}{2Ln} = \frac{1}{2Ln}. \tag{7.9}$$

As Fig. 7.10 and Fig. 7.11 show, the spectra do consist of some equidistant lines (Δv_1 = 30 cm^{-1}, Δv_2 = 43 cm^{-1}, Δv_3 = 86 cm^{-1}). The differences in $\Delta\nu$ in the spectrum of the same crystal (Δv_2 and Δv_3) could be explained by defects of the crystal itself. The thickness of a not perfect crystal might differ. And therefore the observed lines are the result of the lasing with different cavity length, due to the collection of the luminescence signals from parts of the crystal with different thicknesses. If the $\Delta\nu$ and n are known, it is easy to calculate the thickness of a crystal from eq. 7.9. The refractive index along the main crystallographic axes c (see Fig. 2.3 (a)) is equal to 2.02 (n_c = 2.02) [81]. The calculated thicknesses of the crystals using values Δv_1, Δv_2 and Δv_3 are L_1 = 0.08 mm, L_2 = 0.06 mm and L_3 = 0.03 mm, correspondently. These values seem to correspond well to the reality, but unfortunately, the crystal thickness has been not measured. Therefore it is not possible to verify the calculation directly.

In addition, the radiative time of lines decreases with an increase of excitation power (Fig. 7.13 (c), open circles). The origin of this power dependence is not clear yet.

7.5 Conclusions

The significant difference between the decay time constants at the high temperatures ($\tau_{at\,260K}$ = 8.3·10^{-11} s) and at the low temperatures ($\tau_{at\,6K}$=1.0·10^{-8} s) was observed. The increase of the decay time with decreasing temperature of the sample partly explains the high PL yield at low temperatures. By model fits to the experimental data the radiative decay rate ($k_{radF'}$ = 6.7·10^7 s^{-1}) and non-radiative (k_{nr1} = 5.4·10^8 s^{-1} and k_{nr2} = 6.5·10^{10} s^{-1}) decay rates from the F' state were determined. Comparing the adjusted decay rates indicates that the non-radiative recombinations are the dominant decay paths. The strong increase of the luminescence by cooling is mainly explained by a decrease of the high non-radiative decay rates.

For the first time it was observed that the intense optical excitation of Rub crystal at 6 K produces sharp lines (e.g., at 17 845 cm^{-1}, 17 811 cm^{-1} and 17 781 cm^{-1}) above the PL

maximum from F' state. The positions of some of those lines are equidistant and similar for different crystals. It is assumed that the intense optical excitation of Rub crystals produces lasing and those sharp lines are interpreted as resonator modes of the Rub crystals. The peak at 17 845 cm^{-1} was observed in the PL spectra measured at different positions of the same crystal and for different crystals as well (see Fig. 7.10 and 7.11, peak 3). Therefore, this peak was attributed to the free exciton emission.

Finally, the observation of the sharp lines with energies above the F' state corroborates our assumption that the F' state is a state below the free exciton state and is some kind of trap exciton state.

8 Summary and conclusions

The aim of this thesis was to study the optical properties of rubrene (Rub). Recently Rub got into scientific focus as a material with a promising potential for future device applications due to the surprisingly high charge carrier mobility in Rub single crystal organic field effect transistors and the ability of Rub to show strong fluorescence as a dopant in organic light emitting diodes. In particular, the origin of the high mobility has been discussed in the literature. However, the incomplete understanding of the optical properties of this material inspired the present study.

A detailed analysis of the optical characteristics of Rub was carried out by using angle resolved absorption spectroscopy, excitation fluorescence spectroscopy, time-integrated and time-resolved fluorescence spectroscopy, and theoretical modelling. The general results of this study are separated into two groups related to the investigated objects: Rub in solution (I) and Rub single crystals (II).

I. Rub in solution

A comparison of photoluminescence and absorption spectra of two prototype fluorescence molecules Rub and tetracene (Tc) in solution has been performed. This comparison was interesting because Tc is an organic molecule with well known optical properties and has the same 'fluorescent backbone' as Rub. This results in similarities in their optical spectra. However, noticeable differences have been observed during the present investigations as well. The differences in the spectra of both molecules have been attributed to the twisting of the backbone of Rub as well as to the electronic effects of its additional phenyl groups. In particular, the optical spectroscopy of Rub and Tc solutions reveals that the $S_0 \rightarrow S_1$ transition in Rub is red shifted with respect to Tc, and that Rub exhibits a considerably larger Stokes shift and less resolved vibrational progressions. The nature of the red shift is not trivial to explain. On the one hand, the backbone of Rub is twisted, whereas it is planar for Tc. As a result, the conjugation in the π system is smaller for Rub than for Tc, which is expected to cause a spectral blue shift. On the other hand, the additional phenyl groups have an inductive effect which is expected to cause a red spectral shift.

To understand the nature of the differences in spectra of both molecules, the present experimental study has been supported by a theoretical study performed by the theoretical chemistry group from University of Bonn [11]. The principal results of this investigation can be formulated as follows:

The energy of the lowest unoccupied molecular orbital (LUMO) decreases upon twisting of the Tc backbone. However, the lowering of the energy of the LUMO is nearly

compensated by its increase upon adding of the phenyl groups. That means, that the LUMO energies of Tc and Rub nearly coincide, and the experimentally observed ~2000 cm^{-1} red-shift of the spectra of Rub versus Tc is thus mainly due to inductive destabilization of the highest occupied molecular orbital (increase in energy) upon the attachment of the phenyl groups to the Tc backbone.

The large variation of the Stokes shift for Tc (80 cm^{-1}) and Rub (820 cm^{-1}) originates mainly from the vibronic activity of low frequency modes which is obtained by the twisting of the backbone in Rub and which must be absent for Tc. Less resolved vibronic peaks in the case of Rub are due to a larger number of active modes of vibrations due to the additional phenyl groups.

II. Rub single crystals

The main goal of the optical investigation of Rub single crystal was the understanding of its excitation relaxation mechanism. A detailed study of the temperature depended optical characteristics of Rub single crystals has been performed here for the first time. Interestingly, the investigations of the fluorescence spectrum of Rub single crystals as a function of temperature shows a significant spectral variation with a temperature. The spectral changes are accompanied by a very strong (x 6500) increase of the luminescence intensity at low temperatures in comparison to that at room temperature. Time-resolved measurements show a strong increase of the photoluminescence decay time upon cooling. In particular, the decay time is 80 ps at 260 K and 10 ns at 6 K.

In the temperature range above 200 K, the emission maximum occurs at wavenumbers close to 16 270 cm^{-1} and is assigned to a self-trapped (ST) exciton. The weak shoulder of the photoluminescence (PL) spectrum at an energy close to 17 840 cm^{-1} is attributed to the free exciton emission. The calculation of the excitonic band structure shows H-aggregate formation. This leads to emission from the edge of the Brillouin zone where the transition dipole moments are in an out-of-phase relation. H-aggregates formation gives a low luminescence yield, which explains the very small free exciton emission in spectra of Rub crystals at room temperature.

At temperatures below 150 K, the maximum emission was found at wavenumbers close to 17 610 cm^{-1} and it strongly increases with cooling. The emission at low tempertatures has been attributed to a de-excitation processes from a kind of trapped state (F'). This state can be attributed to a defect formation or a self-trapping. Important findings corroborate the assumption of a defect nature of this transition which is observed in the measurements of PL spectra as a function of the excitation wavelengths: The existence of an energetical gap (840 cm^{-1}) between the photoluminescence energy and the excitation energy at low temperatures was observed. Such a large gap cannot be explained only by the formation of H-aggregates in the crystal, since the calculated energy difference between the Γ-point and the edge of the Brillouin zone is only about 320 cm^{-1}. Thereby, prior to the emission at 17 610 cm^{-1}, the species must be excited to the free exciton

state ($S_0 \rightarrow S_1$). The luminescence of the F' state builds up due to a fast feeding from the S_1 state, and a subsequently decay with a slow time constant. From time-resolved luminescence spectra taken as a function of temperature, an increase of the time constant of the feeding of state F' and an increase of the lifetime of excited state F' is identified. In detail, the feeding time constant $\tau_{FF'}$ at 5 K is found to be larger by a factor of 3 with respect to the feeding time constant at 150 K. The fluorescence decay time $\tau_{F'}$ at 5 K is found to be larger by a factor of 15 with respect to the fluorescence decay time constant at 150 K.

Time-resolved PL experiments with intense optical excitation show quite unexpected results. Excitation power dependent measurements at 5 K show that the intense optical excitation (above 90 mW/cm^2) of Rub crystal has produced sharp lines above the PL maximum from the F' state. It is assumed that the intense optical excitation of Rub crystal produced the lasing and that those sharp lines represent resonator modes of the crystal. The difference between some neighbouring lines is equal to 30 cm^{-1} and corresponds to the resonator cavity of a length of 0.08 mm. Time-resolved PL measurements show that the sharp lines appear with some delay after the laser pump. This delay and the radiative time of the lines exponentially decreases with the increase of excitation power. The origin of this power dependence is not clear. However, an important outcome from the case of intense optical excitation is that the observation of the sharp lines with energies above the F' state corroborates the assumption that the F' state is a state below the free exciton state. The peak at 17 845 cm^{-1} was observed in PL spectra measured at different positions of the same crystal and for different crystals as well and was attributed to the free exciton emission.

In order to describe the temperature evolution of luminescence properties of Rub crystals, a model based on the assumption that the Rub crystal is a system with strong exciton-phonon interaction was developed. In such a system with strong exciton-phonon interaction, the self-trapped state is below the free exciton state and there is a barrier between potential curves of free and self-trapped states. The excitation relaxation mechanism at high temperatures is dominated by non-radiative recombinations and the emission from self-trapped state. At high temperatures, the exciton - after excitation ($S_0 \rightarrow S_1$ transition) - directly relaxes to the ST state, or first relaxes to the F' state and subsequently relaxes to the ST state by overcoming the energy barriers. As the temperature is reduced, the direct self-trapping rate decreases. Additionally, at low temperatures, the thermal energy is not high enough anymore to activate excitons to cross the potential barrier between the F' and the ST state. In this case, the excitons from the free exciton state S_1 relax to the trapped state F' with following emission. To characterise the underlying excitation relaxation mechanism, the temperature dependent competition between the F' emission and the self-trapped emission were analysed by model fits to the experimental data. From the fits, the following activation energies were determined: E_1= 15 meV (activation energy necessary to overcome the potential barrier between the F'

and the ST state), $E_2 = 39$ meV (activation energy for the non-radiative decay from the F' state), $E_3 = 90$ meV (activation energy for the non-radiative decay from the ST state). From the model fit of the temperature-dependent PL decay the radiative rate from the F' state $k_{radF'} = 6.7x10^7\ s^{-1}$ was obtained. Comparing the adjusted radiative decay rate $k_{radF'}$ and the non-radiative decay rates ($k_{nr1} = 5.4 \cdot 10^8\ s^{-1}$ and $k_{nr2} = 6.5 \cdot 10^{10}\ s^{-1}$) from the F' state indicates that the non-radiative recombinations are the dominant decay paths. The strong increase of the luminescence from the F' state upon cooling is mainly explained by a decrease of the high non-radiative decay rates. The adjusted constants satisfactorily explain the temperature-dependencies of time-integrated and time-resolved PL spectra of Rub single crystals and therefore confirm the proposed model.

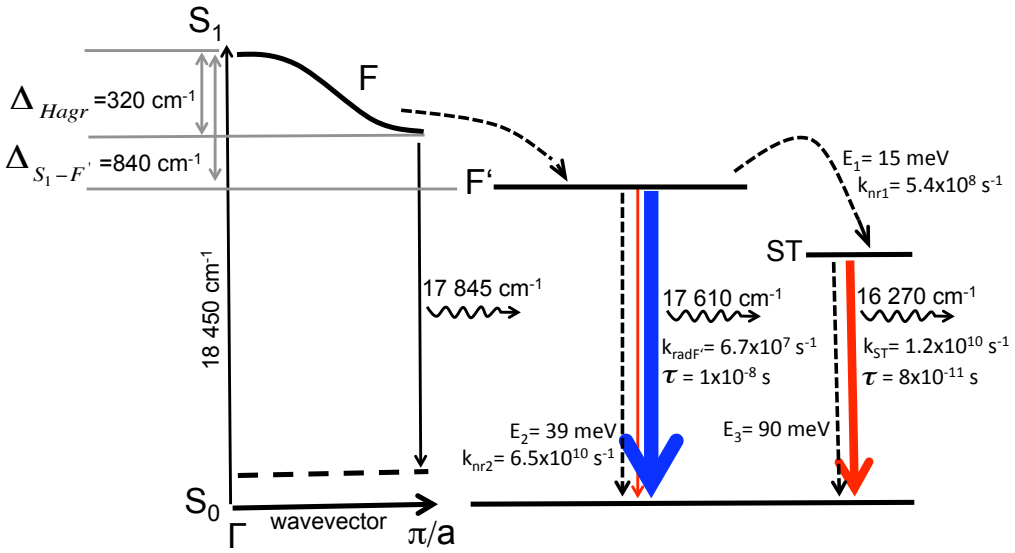

Fig. 8.1 *Schematic diagram of excitation relaxation mechanism in Rub single crystals.*

The main results of this thesis might help to understand the excitation relaxation mechanisms, which determine the luminescence of Rub and open new possibilities for material applications.

Appendix A: Spectrometer calibration

A.1 Conversion between wavelength and wavenumbers

Sometimes it is preferable to present optical spectra on the wavenumbers scale rather than on the wavelength scale. Wavelength are converted to wavenumbers simply by taking the reciprocal value. However, when the spectrum is recorded with constant wavelength resolution - as usual in spectrometers with grating monochromators - the bandpass in wavenumbers is not constant. As the wavelength increases, the bandpass in wavenumbers decreases as the square of the corresponding wavelength. For example, $\Delta\lambda = \lambda_2 - \lambda_1$ is the constant spectral resolution in wavelength, then the spectral resolution in wavenumbers is equal to

$$\Delta\bar{\nu} = \bar{\nu}_2 - \bar{\nu}_1 = \frac{1}{\lambda_2} - \frac{1}{\lambda_1} = \frac{\lambda_1 - \lambda_2}{\lambda_1\lambda_2} = \frac{\Delta\lambda}{\lambda^2}. \qquad \text{(A.1)}$$

Therefore, if the spectrum is obtained in the form of intensity per wavelength interval, then the conversion to the wavenumbers scale requires an intensity correction by multiplication of each intensity by λ^2 :

$$I_\lambda \cdot \Delta\lambda = I_{\bar{\nu}} \cdot \Delta\bar{\nu} \rightarrow I_{\bar{\nu}} = I_\lambda \cdot \frac{\Delta\lambda}{\Delta\bar{\nu}} = I_\lambda \cdot \lambda^2. \qquad \text{(A.2)}$$

Multiplication by λ^2 results in an increase of the emission of the long-wavelength side and therefore it appears as a visual shift in the spectral maximum [7].

A.2 Wavelength calibration

During the investigations, some deviation between measured wavelengths and real wavelengths in the case of spectrometer SpectraPro 2300i were found. Therefore it was necessary to calibrate the spectrometer wavelength. Usually a wavelength calibration is done with the help of a lamp with a line spectrum, for example that of a Hg or Xe pin lamp. Spectra of these lamps consist of a big amount of single, sharp lines with well known spectral positions and relative intensities in the visible wavelength region. That allows the wavelength calibration. In the present work, a Xe pin lamp was used. The measured Xe lamp spectrum with identification of the lines is presented below on Fig. A.1. A comparison of the measured wavelength positions and the real values of the Xe lines positions gives us the relationship between the measured and real wavelengths and the correlation for these two values is linear:

$$\lambda_{real}\,(\text{Å}) = 0.9102 \cdot \lambda_{measured}\,(\text{Å}) + 62.62\ (\text{Å}). \qquad \text{(A.3)}$$

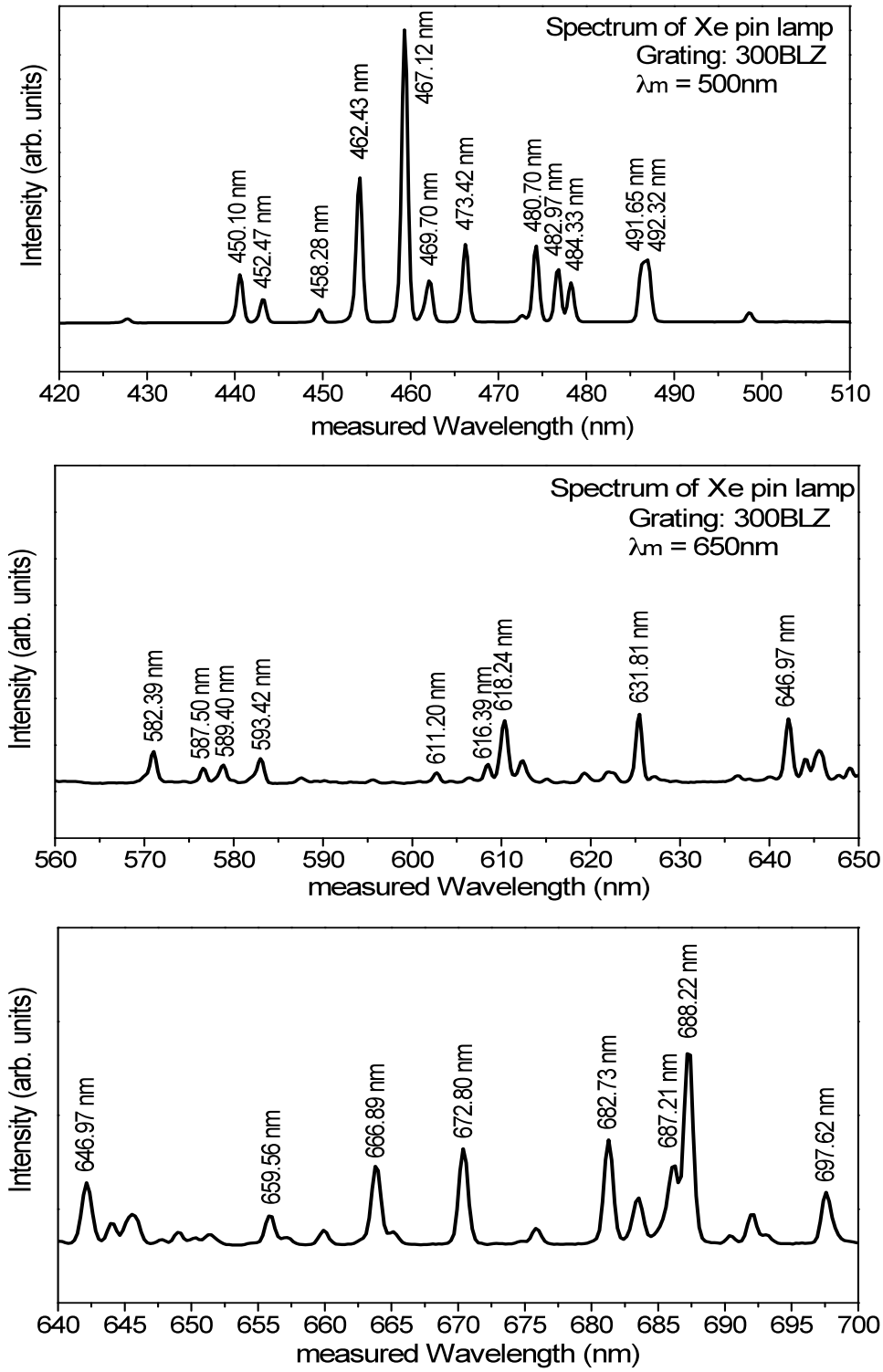

Fig. A.1 *The spectrum of a Xe pin lamp was used for wavelength calibration of the spectrometer. The presented spectrum was recorded with a 0.3 m spectrometer (SpectraPro 2300i) with a grating of 300 lines/mm, with a middle wavelength position (λm) of 500 nm (first Xe spectrum) and 650 nm (second and third Xe spectrum). The positions of Xe lines were taken from NIST database (NIST WebBook). Measured and real wavelengths are linearly dependent (see eq. A.3).*

A.3 Spectral positions of the maxima of the PL spectra in different sets of measurements

PL Rub cr.	a	b	c	d	T (K)	Ref.
cm^{-1} eV nm	17720* 2.20* 565*	17140* 2.12* 584*	16250 (16370*) 2.02 (2.03*) 616 (611*)		300	Krylova (exp. 1)
cm^{-1} eV nm		17690 2.19 565	16270 2.02 615		300	Krylova (exp. 2)
cm^{-1} eV nm			16395 2.03 610		300	Krylova (exp. 3)
cm^{-1} eV nm		17545 2.175 570	16130 2.00 620		300	Najafov [49]
cm^{-1} eV nm		17520 2.17 570.8		16160 2.00 619	5	Krylova (exp. 1)
cm^{-1} eV nm		17610 2.18 568		16270 2.02 615	50	Krylova (exp. 2)
cm^{-1} eV nm		17600 2.18 568		16250 2.01 616	5	Krylova (exp. 3)
cm^{-1} eV nm		17545 2.18 570		16130 2.00 620	5	Mitrofanov [50]
cm^{-1} eV nm		17660 2.19 566		16292 2.02 614	4	Stöhr [75]

Tab. A.1 *Positions of experimentally determined peaks in the PL spectra in different experimental sets and in the literature. Components a, b, c, d are the peaks in the PL spectra in the present work. Stars (*) mark the positions of the components from the single component fit (see section 6.4). exp. 1 - the experimental set of cw PL measurements for different temperatures of the Rub crystals (see Fig. 6.2), exp. 2 - the experimental set of PLE measurements (see Fig. 6.16). exp. 3 - the experimental set of tr PL measurements (see Fig. 7.2).*

A.4 Sensitivity of a detector

The sensitivity of the detection system is wavelength dependent. Therefore, in order to get the correct shape of optical spectra and to calculate the absolute intensity of spectra, it is necessary to know the efficiency of the detector in the investigated spectral range. Usually, if the position of the sample and the optical parts are not changeable, the sensitivity curve is available from the manufacturer of the detector, as in the case of Perkin Elmer LS 55 fluorescence spectrometer, which was used for solutions experiments in this work. Fig. A.2 shows the sensitivity curve of the photomultiplier of the system. The system is equipped with standard photomultiplier, which is sensitive in the 200 to 650 nm range.

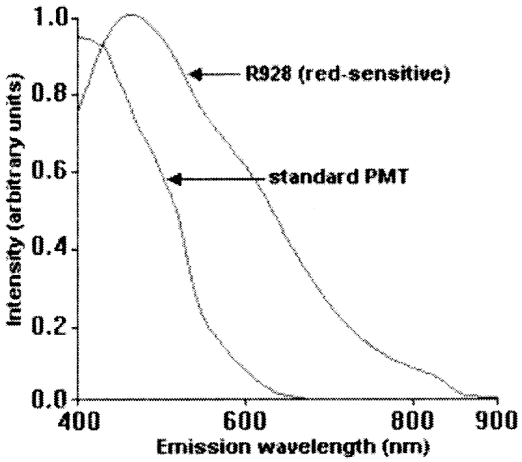

Fig. A.2 *Sensitivity curve of the photomultiplier* [82].

In cases than the sensitivity of the detector is unknown, the correction factor can be obtained from the spectrum of a calibrated light source, e.g. a standard tungsten lamp. The spectrum can be approximated by the spectrum of the black body radiation. The relation between the temperature of the black body radiation, which is proportional to the current through the lamp, and the black body radiance can be found in the book [83]. The calibration of the detection system includes several steps:

1) The intensity of the standard lamp I(λ) is measured by detector.
2) The sensitivity of the detection system S(λ) is calculated by division the measured intensity of the lamp I(λ) by the known output of the lamp L(λ):
   $S(\lambda) = I(\lambda)/L(\lambda)$
3) The corrected spectrum is obtained by multiplying the measured spectra by the calculated sensitivity of detection system S(λ).

It should be noted, that the output of a calibrated lamp might change due to aging.

In addition, absorption and luminescence spectra of Rub films and crystals were recorded with a 0.3 m-spectrometer (SpectraPro 2300i) equipped with a liquied-nitrogen-cooled the CCD camera. All measurements were done for a constant temperature of CCD camera (-100 C°), because the sensitivity of the detector strongly depends on the CCD camera temperature and the room temperature as well.

Appendix B: Abbreviations

Abs	absorption
BHLYP	Becke half-and-half exchange functional and the Lee–Yang–Parr correlation functional
BP86	Becke's exchange with Perdew's gradient-corrected functional
cw	continuous-wave
DFT	density function theory
FWHM	full width at half maximum
HOMO	highest occupied molecular orbital
Hg	mercury
IMDHO	independent mode, displaced harmonic oscillator
LUMO	lowest unoccupied molecular orbital
MO	molecular orbital
PL	photoluminescence
PLE	photoluminescence excitation
PM	photomultiplier
QMS	quadrupole mass spectrometer
rR	resonance Raman
Rub	rubrene
SPA-LEED	spot profile analysis low energy electron diffraction
Tc	tetracene
TD-DFT	time-dependent density function theory
TPD	temperature programmed desorption
tr	time-resolved
TZVP	triple zeta valence plus polarization
UHV	ultra high vacuum
UV	ultraviolet
VIS	visible
Xe	xenon

References

[1] V. Podzdorov, E. Menard, A. Borissov, V. Kiryukhin, J. A. Rogers, M. E. Gershenson, *Phys. Rev. Lett., 93,* 086602, **2004**.

[2] H. Mattoussi, H. Murata, C. D. Merritt, Y. Iizumi, J. Kido, Z. H. Kafafi, *J. Appl. Phys., 86*, 2642, **1999**.

[3] Z. Zhi-lin, J. Xue-yien, X. Shao-hong, T. Nagotomo, O. Omoto, *J. Phys. D, 31*, 32, **1998**.

[4] H.-G. Löhmannsröben, *J. Appl. Phys. B, 47*, 195, **1988**.

[5] B. M. Rumeantcev, V. I. Lesin, E. L. Frankevich, *Zh. Fiz. Khim*., *53*, 1504, **1979**.

[6] I. Bulgarovskaya, V. Vozzhennikov, S. Aleksandrov, V. Belsky, *Latv. PSR Zinat. Akad. Vestis, Fiz. Teh. Zinat., 4*, 53, **1983**.

[7] A. Langner, PhD thesis, University of Bonn, **2005**.

[8] D. E. Henn, W. G. Williams, D. J. Gibbons, *J. Appl. Cryst., 4*, 256, **1971**.

[9] H. Hoyer, W. Peperle, *Z. Electrochem., 62*, 61, **1958**.

[10] E. Müller, O. Bayer*, Methoden der Organischen Chemie*, *Vol. 5/2b,* Houben-Weyl, Stuttgart, **1981**.

[11] T. Petrenko, O. Krylova, F. Neese, M. Sokolowski, *New J. Phys., 11*, 015001, **2009**.

[12] D. Käfer, L. Ruppel, G. Witter, C. Wöll, *Phys. Rev. Lett., 95*, 66602, **2005**.

[13] D. Käfer, G. Witte, *Phys. Chem. Chem. Phys., 7*, 2850, **2005**.

[14] J. A. Miwa, F. Cicoira, S. Bedwani, J. Lipton-Duffin, D. F. Perepichka, A. Rochefort, F. Rosei, *J. Phys. Chem. C, 112*, 10214, **2008**.

[15] M.-C. Blüm, E. Ćavar, M. Pivetta, F. Patthey, W.-D. Schneider, *Angew. Chem. Int. Ed., 44*, 5334, **2005**.

[16] V. C. Sundar, J. Zaumseil, V. Podzorov, E. Menard, R. L. Willett, T. Someya, M. E. Gershenson, J. A. Rogers, *Science, 303,* 1664, **2004**.

[17] R. A. Laudise, C. Kloc, P. G. Simpkins, T. Siegrist, *J. Cryst. Growth, 187*, 449, **1998**.

[18] T. Minato, H. Aoki, H. Fukidome, T. Wagner, K. Itaya, *App. Phys. Lett., 95*, 093302, **2009**.

[19] G. S. Bales, A. C. Redfield, A. Zangwill, *Phys. Rev. Lett., 62*, 77, **1989**.

[20] M. Campione, R. Ruggerone, S. Tavazzi, M. Moret, *J. Mater. Chem., 15*, 2437, **2005**.

[21] http://www.merck-chemicals.com, Merck KGaA.

[22] M. Voigt, Diploma thesis, University of Bonn, **2001**.

[23] A. Langner, Y. Su, M. Sokolowski, *Phys. Rev. B*, *74*, 045428, **2006**.

[24] U. Bardi, A. Atrei, G. Rovida, *Surf. Sci., 239*, L511 **1990**.

[25] U. Bardi, A. Atrei, G. Rovida, *Surf. Sci., 268*, 87, **1992**.

[26] S. Degen, A. Krupski, M. Kralj, A. Langner, C. Becker, M. Sokolowski, K. Wandelt, *Surf. Sci. Lett., 576*, L57, **2005**.

[27] M. Müller, Diploma thesis, University of Bonn, **2007**.

[28] H. Y. Kim, T. G. Bjorklund, S.-H. Lim, C. J. Bardeen, *Langmuir, 19*, 3941, **2003**.

[29] C. K. Chan, G. B. Page, *J. Chem. Phys., 79*, 5234, **1983**.

[30] E. J. Heller, *J. Chem. Phys., 68*, 2066, **1978**.

[31] T. Petrenko, F. Neese, *J. Chem. Phys., 127*, 164319, **2007**.

[32] A. B. Myers, R. A. Mathies, D. J. Tannor, E. J. Heller, *J. Chem. Phys., 77*, 3857, **1982**.

[33] T. Petrenko, K. Ray, K. Wieghardt, F. Neese, *J. Am. Chem. Soc., 128*, 4422, **2006**.

[34] F. Neese, ORCA program package, University of Bonn, **2007**.

[35] R. M. Hochstrasser, M. Ritchie, *Trans. Faraday Soc., 52*, 1363, **1956**.

[36] D. R. Maulding, B. G. Roberts, *J. Org. Chem., 34*, 1734, **1969**.

[37] C. Burgdorf, S. Ehrhardt, H.-G. Löhmannsröben, *J. Phys. Chem., 95*, 4246, **1991**.

[38] J. B. Birks, *Photophysics of Aromatic Molecules,* Wiley-Interscience, London, **1970**.

[39] I. B. Berlman, *Handbook of Fluorescence Spectra of Aromatic Molecules, 2nd-ed.*, Academic Press, New York, **1971**.

[40] P. W. Atkins, *Physical Chemistry*, 3*rd-ed.*, Oxford University Press, Oxford, **1987**.

[41] R. Lehnig, A. Slenczka, *J. Chem. Phys*., *122*, 244317, **2005**.

[42] M. Dierksen, S. Grimme, *J. Phys. Chem. A, 108*, 10225, **2004**.

[43] T. Petrenko, private communication, **2008**.

[44] A. Nitzan, M. A. Ratner, *Science, 300*, 1384, **2003**.

[45] W. Gebauer, M. Sokolowski, E. Umbach, *Chem. Phys., 227*, 33, **1998**.

[46] Z.-C. Dong, X.-L. Guo, A. S. Trifonov, P. S. Dorozhkin, K. Miki, K. Kimura, S. Yokoyama, S. Mashiko, *Phys. Rev. Lett., 92*, 086801, **2004**.

[47] W. Gebauer, A. Langner, M. Schneider, M. Sokolowski, E. Umbach, *Phys. Rev. B., 69*, 125420, **2004**.

[48] M. Schneider, E. Umbach, A. Langner, M. Sokolowski, *J. Lumi.*, *110*, 275, **2004**.

[49] H. Najafov, I. Biaggio, V. Podzorov, M. F. Calhoun, M. E. Gershenson, *Phys. Rev. Lett.*, *96*, 056604, **2006**.

[50] O. Mitrofanov, D. V. Lang, C. Kloc, J. M. Wikberg, S. Sigrist, *Phys. Rev. Lett.*, *97*, 166601, **2006**.

[51] S.-W. Park, J. M. Hwang, J.-M. Choi, D. K. Hwang, M. S. Oh, J. H. Kim, S. Im, *Appl. Phys. Lett.*, *90*, 153512, **2007**.

[52] M. Voigt, A. Langner, P. Schouwink, J. M. Lupton, R. F. Mahrt, M. Sokolowski, *J. Chem. Phys., 127*, 114705, **2007**.

[53] M. Müller , A. Langner, O. Krylova, E. Le Moal, M. Sokolowski, *Appl. Phys. B., 105*, 67, **2011**.

[54] O. D. Jurchescu, A. Meetsma, T. T. M. Palstra, *Acta Cryst. B, 62*, 330, **2006**.

[55] R. R. Chance, A. Prock, R. Silbey, in *Advances in Chemical Physics* (Eds.: I. Prigogine and S. A. Rice), Wiley, New York, *37,* **1978**.

[56] S.-H. Lim, T. G. Bjorklund, F. C. Spano, C. J. Bardeen, *Phys. Rev. Lett.*, *92*, 107402, **2004**.

[57] R. Hesse, W. Hofberger, H. Bässler, *Chem. Phys.*, *49*, 201, **1980**.

[58] R. Jankowiak, K. D. Rockwitz, H. Bässler, *J. Phys. Chem.*, *87*, 552, **1983**.

[59] J. Lodder, S. Iven, in *Laboratory report*, University of Bonn, **2008**.

[60] G. J. Laurent, N. T. Ha-Duong, R. Meallet-Renault, R. B. Pansu, in *Nanophotonics: Integrating Photochemistry, Optics, and Nano/Bio Materials Studies* (Eds.: H. Masuhara, S. Kawata), Elsevier, Osaka, **2004**.

[61] S. Tavazzi, A. Borghesi, A. Papagni, P. Spearman, L. Silvestri, A. Yassar, A. Camposeo, M. Polo, D. Pisignano, *Phys. Rev. B*, *75*, 245416, **2007**.

[62] N. Sai, M. L. Tiago, J. R. Chelikowsky, F. A. Reboredo, *Phys. Rev. B*, *77*, 161306, **2008**.

[63] H. Najafov, B. Lyu, I. Biaggio, V. Podzdorov, *Phys. Rev. B*, *77*, 125202, **2008**.

[64] M. Müller, Spectra2 program package, University of Bonn, **2009**.

[65] A. Matsui, *J. Opt. Soc. Am. B*, *7*, 1615, **1990**.

[66] A. Matsui, *Pure & Appl. Chem.*, *67 N° 3*, 429, **1995**.

[67] P. Irkhin, A. Ryasnyanskiy, M. Koehler, I. Biaggio, *Phys. Rev. B*, *86*, 085143, **2012**.

[68] B. Valeur, *Molecular Fluorescence*, WILEY-VCH, Weinheim, **2002**.

[69] R. Signerski, J. Kalinowski, *Thin Solid Films*, *75*, 151, **1981**.

[70] A. S. Davydov, *Usp. Fiz. Nauk, 82*, 393, **1964**.

[71] R. Scholz, *calculations of exciton bands structure,* private communication, **2008**.

[72] A. S. Davydov, *Theory of Molecular Excitons*, Plenum Press, New York, **1971**.

[73] F. Meinardi, M. Germinara, A. Sassella, R. Bonifacio, R. Tubino, *Phys. Rev. Lett., 91*, 247401, **2003**.

[74] F. C. Spano, *Chem. Phys. Lett.*, *331*, 7, **2000**.

[75] R. J. Stöhr, G. J. Beirne, P. Michler, R. Scholz, J. Wrachtrup, J. Pflaum, *Appl. Phys. Lett., 96*, 231902, **2010**.

[76] R. Kersting, U. Lemmer, R. F. Mahrt, K. Leo, H. Kurz, H. Bässler, E. O. Göbel, *Phys. Rev. Lett., 70*, 3820, **1993**.

[77] A. M. Weiner, E. P. Ippen, *Chem. Phys. Lett.*, *114*, 456, **1985**.

[78] J. Feldmann, G. Peter, E. O. Göbel, P. Dawson, K. Moore, C. T. Foxon, R. J. Elliott, *Phys. Rev. Lett.*, *59*, 2337, **1987**.

[79] A. Matsui, K. Mizuno, N. Tamai, I. Yamazaki, *Chem. Phys.*, *113*, 111, **1987**.

[80] A. E. Siegman, *Lasers*, University Science Books, Sausalito, California, **1986**.

[81] M. El Helou, O. Madenbach, G. Witte, *Crystal Growth & Design, 10*, 3496, **2010**.

[82] *Manuel of Perkin Elmer LS 55 spectrometer*, Perkin Elmer, **2005**.

[83] H. R. Griem, *Plasma Spectroscopy*, McGraw-Hill Book Company, New York, **1964**.

Erklärung

An Eides statt versichere ich, dass ich die Dissertation „Optical investigations on rubrene in the condensed state“ selbst und ohne jede unerlaubte Hilfe angefertigt habe, dass diese oder eine ähnliche Arbeit noch keiner anderen Stelle als Dissertation eingereicht worden ist und dass sie an den nachstehenden Stellen auszugsweise veröffentlicht worden ist:

- T. Petrenko, O. Krylova, F. Neese, M. Sokolowski, *New J. Phys., 11*, 015001, **2009**.
- M. Müller , A. Langner, O. Krylova, E. Le Moal, M. Sokolowski, *Appl. Phys. B.*, *105*, 67, **2011.**

Bonn, 08. November 2012

Olga Krylova

Acknowledgements

First and foremost I would like to express my deep and sincere gratitude to my supervisor, Prof. Dr. M. Sokolowski for the opportunity of doing research in his group, for his permanent attention and great support throughout this work.

I am deeply grateful to Prof. Dr. J. Pflaum from the Institute of Physics, University of Würzburg for his agreement to act as a co-referee for my thesis. I also wish to express my warm and sincere thanks to Prof. Dr. J. Pflaum and his workgroup for preparing the high quality Rub crystals, which I used in the optical investigations.

I owe my sincere gratitude to Dr. T. Petrenko and Prof. F. Neese from the Max Planck Institute for Bioinorganic Chemistry for their theoretical support in the interpretation of the experimental data.

My warm thanks go to PD Dr. R. Scholz from Technical University Munich for the calculations of exciton band structure in Rub crystals and for the interesting discussions concerning our results.

I wish to express my warm and sincere thanks to PD Dr. R. F. Mahrt and Dr. T. Stöferle from IBM Research Laboratory, Rüschlikon, Switzerland, who kindly gave me the opportunity to perform the time resolved study on Rub crystals and films in their laboratory. I would like to thank them for their detailed and constructive comments.

I owe my loving thanks to my husband Relja, my daughter Mia and my son Gavrilo. Without their encouragement and understanding it would have been impossible for me to finish this work. My special gratitude goes to my mother Irina, my mother-in-law Bojana, my father-in-law Kosta, my Aunt Svetlana K. and my friend Svetlana M. for their continuous support and love.

My great and deep thanks go to my friend Dr. J. Gutschank for his kind and careful proof-reading of my thesis and important comments.

Special thanks to my colleague Dr. E. Le Moal. I am very grateful for his outstanding friendship, interesting discussions and light-hearted moments we shared.

During this work I have collaborated with many colleagues. I wish to extend my warmest thanks to all those who have helped me with my work, especially to Dr. M. Müller who assisted me during the time-resolved measurements at IBM in Zürich and the PLE measurements in Bonn and Dr. A. Langner who introduced me to the experiment with the Argon laser. Furthermore, the students D. Berg, S. Iven, and J. Lodder, who assisted me during my work, must be mentioned.

I also wish to thank the technician D. Gauer for his kindly help and valuable advices during the work with the UHV-equipments.

Thanks must be extended to K. Hintzen. He was always very friendly and helpful as expert in computers.

I would like to thank A. Kleine from secretariat, for all the small but important things.

I wish to thank the teams of the mechanical and electrical workshops. Their expertise on all the nitty gritty has been very helpful for good experiments.

I am grateful to the DFG for the financial support in the frame of Research Unit 557 “Light Confinement and Control with Structured Dielectrics and Metals”.